A Novel Detection Method for Determining a Surgeon's Fatigue and Hand Tremor

Paul Stephen Slack

Engineering Systems and Management

ASTON UNIVERSITY

Doctor of Philosophy

September 2007

A novel detection method for determining a surgeon's muscular fatigue and hand tremor

Paul Stephen Slack

Engineering Systems and Management

ASTON UNIVERSITY

Doctor of Philosophy

September 2007

The thesis presents new methodology and algorithms that can be used to analyze and measure the hand tremor and fatigue of surgeons while performing surgery. This will assist them in deriving useful information about their fatigue levels, and make them aware of the changes in their tool point accuracies. This thesis proposes that muscular changes of surgeons, which occur throughout a day of operating, can be monitored using Electromyography (EMG) signals. The multi-channel EMG signals are measured at different muscles in the upper arm of surgeons. The dependence of EMG signals has been examined to test the hypothesis that EMG signals are coupled with and dependent on each other. The results demonstrated that EMG signals collected from different channels while mimicking an operating posture are independent. Consequently, single channel fatigue analysis has been performed.

Conventional fatigue analysis is by examining the mean frequency shift of the power spectra of the EMG signals measured at muscles. Due to the decreases in contraction level, and changes in the variation from fast to slow twitching muscles, it is suggested that a complexity analysis can be used as an alternate fatigue index. The thesis presents the new methodology of using Shannon entropy from a dynamically embedded signal as an alternate fatigue index. The experiments confirmed that a signals complexity decreases when the mean frequency of the power spectrum

decreases in conventional fatigue analysis methods. The robustness of the two methods based on different data analysis window sizes was assessed, and it was demonstrated that the complexity method's was fractionally better than conventional methods.

In measuring hand tremor, a new method for determining the maximum tremor amplitude using Principal Component Analysis (PCA) and a new technique to detrend acceleration signals using Empirical Mode Decomposition algorithm were introduced. This tremor determination method is more representative for surgeons and it is suggested as an alternative fatigue measure. This was combined with the complexity analysis method, and applied to surgically captured data to determine if operating has an effect on a surgeon's fatigue and tremor levels. It was found that surgical tremor and fatigue are developed throughout a day of operating, and that this could be determined based solely on their initial values.

Finally, several Nonlinear AutoRegressive with eXogenous inputs (NARX) neural networks were evaluated, by separately using Mean Frequency (MF) and Complexity (H) fatigue indices to predict the maximum tremor amplitude. This involved comparing two and eight channel configurations of Bayesian Regularization and Resilient Backpropagation trained networks. It was demonstrated that the BRN trained eight channel MF, and H networks achieved prediction errors of less than 5%. The results suggest that it is possible to monitor surgeon tremor variations during surgery from their EMG fatigue measurements.

Keywords: Complexity Analysis, Maximum Tremor Amplitude, Artificial Neural Network

Acknowledgments

First of all, I would like to thank Dr. Xianghong Ma for her patience, direction, and giving me the opportunity to explore my ideas, while ensuring that I was following a reasonable path. I wish to thank Prof Peter Brett for his insightful comments and motivational talks. I would also like to acknowledge support from the EPSRC for the funding of the project, and the surgeons and theatre staff at the Queen Elizabeth Hospital Birmingham, UK, and the University Hospital of North Staffordshire, UK that participated in the collection of the data.

I would like to thank some of my colleagues and friends for their assistance and support during my time at Aston University. Firstly, to Erik Casagrande, for providing hours of interesting discussions and his expertise in signal processing. Secondly, to Dr Mark Prince (Fingers), Dr Mark Elliott (Billy), and Charles, for providing not only the needed distractions during the days, but also excellent advice and innovation. Thirdly, to Chris Coulson, for the boxes of Krispy Kreme Doughnuts, and his interesting views on the research from a surgical perspective. I extend thanks to all my friends on and off the PG and RT Rota, my colleagues in the Biomedical Engineering Research Group at Aston, and the Woodcock Sports Centre for providing me with a stress release during those times of need.

In addition, I would like to acknowledge every single person who mentioned, nagged, bugged, and even pressured me into finishing this thesis. Your words probably went unappreciated at the time but please know that they really did help. My parents have been the most significant people in my life so far, and this part of my life was no exception. Without your support, persistence, and love, I would not be where I am today. Finally, I would like to express my sincere thanks to Diane, for being there when I needed her. Your words and actions are inspiring to me.

Declaration

This thesis is the result of my own original work. The following publications were derived from this work:

Reviewed Journal Articles

- Slack, P.S., Ma, X., Determination of Muscle Fatigue using Dynamically Embedded Signals, Proceedings of the Institution of Mechanical Engineers, Part H, to appear in *Journal of Engineering in Medicine.*
- Slack, P.S., Ma, X., Tremor Amplitude Determination for Use in Clinical Applications, Measurement Science and Technology, 2007. 18(1):p3471-3478.

Reviewed Conference Proceedings

- Slack, P.S, Ma, X., Determination of Muscle Fatigue using Dynamically Embedded Signals, DETC2007-34287, *MSNDC-1 Musculoskeletal Biomechanics and Bioassistive Devices, Las Vegas, September 2007.*
- Slack, P.S., Ma, X., Time dependency assessment of muscular fatigue index and hand tremor under operating conditions, appeared in *IEEE Engineering in Medicine and Biology Society,* 2007.

Journal Articles Under Review

- Slack, P.S, Coulson, C.J., Ma, X., Pracy, P., Parmar, S., The effect of operating time on surgeon's hand tremor, in review, *European Archives of Oto-Rhino-Laryngology and Head & Neck.*
- Slack, P.S, Coulson, C.J., Ma, X., Webster, K., Proops, D.W., The effect of operating time on surgeon's muscular fatigue, in review, *Annals of the Royal College of Surgeons of England.*

List of Abbreviations

ANN:	Artificial Neural Network
BCG:	Ballistocardiogram
BRN:	Bayesian Regularization
BSS:	Blind Source Separation
DCS:	Dynamical Cumulative Sum
DE:	Dynamical Embedded
EEG:	Electroencephalography
EMD:	Empirical Mode Decomposition
EMG:	Electromyography
EOF:	Empirical Orthogonal Function
FMRI:	Functional Magnetic Resonance Imaging
GNG:	Growth Neural Gas
H:	Entropy
HHT:	Hilbert Huang Transform
ICA:	Independent Component Analysis
IMF:	Intrinsic Mode Function
KL:	Karhunen-Loeve
MDF:	Median Frequency
MF:	Mean Frequency
MRI:	Magnetic Resonance Imaging
MSE:	Mean Sum of the Square Error
MTM:	Multi Taper Method
NARX:	Nonlinear Autoregressive with Exogenous Inputs
PCA:	Principal Component Analysis
POD:	Proper Orthogonal Decomposition
POM:	Proper Orthogonal Mode
PSD:	Power Spectral Density
RMS:	Root Mean Square
RMSE:	Root Mean Sum of the Square Error
RP:	Resilient Backpropagation
SSA:	Singular Spectrum Analysis
WA:	Wavelet Analysis
WT:	Wavelet Transform

Contents

List of Figures

List of Tables

1

Introduction

1.1 Motivation

In this day and age, the safety of both patients and surgeons during surgical procedures is of great importance. There exist concerns within today's health care systems relating to increases in the number of performed surgical procedures, the surgeons tremor during these procedures, and requirements for reductions in operating times. All of these concerns warrant the need for advances in the surgical field. Therefore improvements in ergonomics, surgical methods, reduction in the length of operation, and the surgeon's precision during an operation will enhance the safety of any operation, whilst ensuring that the trauma to both patient and surgeon remains at a minimum.

Technological advances in visualization, intraoperative monitoring, and instrumentation have already improved our understanding of the human body. Smart sensing techniques for the measurement, modeling, and the control mechanisms at the different scales of cells, tissues, and body have also been shown to vastly improve the accuracy of surgical procedures. Information was derived from these techniques to control surgical tools and to diagnose directly specific properties of tissues and cells. This has been demonstrated by Rothbaum *et al* [1] where robotic assistance vastly improved the performance for micropick fenestration in a surgical model of stapedotomy. Information is derived from these techniques to control surgical tools and to diagnose directly specific properties of tissues and cells. During most surgical procedures, the surgeon is working towards and beyond the limit of their dexterity and

perception. Consequently, there is a need for developing tools that can assist surgeons derive useful information about their fatigue levels, their movements, and the tool points. The final objective would be to improve the level of control, the surgical precision, the tactile sensitivity, and the overall efficiency of surgical procedures. These developed tools could ultimately be adapted to determine the point at which a surgeon should be relieved during a procedure, or to filter out undesired noise or disturbances within surgical equipment that has been caused by involuntary tremor.

1.1.1 Fatigue and Tremor Development

Over the length of surgical procedures, fatigue sets in and finger and hand tremors increase. Fatigue is considered to be one of the body's protection mechanism that ensures injury is kept to a minimum [2]. In addition, physiological tremors, which include postural and isometric tremors (4-12 Hz), become more prominent [3, 4]. The development of these tremors concerns both surgeons and the patients alike, as they can negatively affect a surgeon's fine finger precision, and can adversely affect the ability of the surgeon to perform accurately during an operation.

Although current systems can detect changes in fatigue levels by examining spectral variances within the Electromygraphic (EMG) signals, none have been utilized for monitoring these levels during surgery. In addition, none of the current systems provide any knowledge of a surgeon's hand steadiness. Consequently, this thesis will further the understanding of both these parameters, so that they can be adopted into a surgical monitoring system.

1.2 Objectives

The principal objective of the research is to derive and evaluate an automated identification method that can be generically applied to detect and evaluate the state of body functions by acquiring multiple Electromyographic and acceleration signals in the time-space domain.

The research is based on the hypothesis that the body system presents highly non-linear complexity and that the body functions are coupled with each other. From the non-linear coupling dynamics between processes and tissues of the body, system parameters can be derived to detect and predict the onset of fatigue and hand steadiness deterioration during lengthy microsurgical procedures.

The hypothesis is that a change in state from non-fatigued to fatigued, leads to an increase in a surgeon's hand tremor. Ultimately, this could lead to a potential decrease in the surgeon's performance. Therefore, the ultimate objective of the thesis is to design a prediction system that can monitor the level of an individuals fatigue and hand tremor based on their EMG measurements. The system could be ultimately adapted to real-time, and assist surgical staff in determining a potential decline in a surgeon's performance. This could potentially reduce patient injuries and reduce operation durations.

The specific objectives are:

a) Study the dependency of EMG signals as the various muscles work together to perform a specific action.

b) Develop and perform a robustness analysis of a novel fatigue detection method.

c) Demonstrate that fatigue leads to an increase in hand tremor during surgical procedures, and develop an innovative algorithm which determines the tremor amplitude.

d) Develop a tremor amplitude prediction method using EMG signals.

1.3 Technical Background

Electromyography has proven itself to be an invaluable tool for the analysis of muscle activity, be it force amplitude or the prediction of fatigue during repetitive tasks [5, 6]. It has also been demonstrated as an efficient non-invasive tool of monitoring changes in body functions, such as with pregnancy and parturition monitoring [7].

As the muscles of interest fatigue, the Mean Frequency (MF) and Median Frequency (MDF) of EMG signal's spectral density function decrease [8, 9]. EMG signals are dependent on the number of muscle fibers, on the muscle group, the force required to move a particular object, and the variance in signals from one individual to the next. This makes it very difficult to predict over time how much the signals will differ. The fatigue analysis, however, examines trends in the signal and not the amplitude. Therefore, it can determine with some certainty a development towards fatiguing muscles. Consequently, EMG fatigue analysis could be used during surgical procedures to determine how the fatigue develops, and if and when a surgeon has reached the limit of their ability.

Because of the coupling of muscular activity, it is assumed there is some coupling between the different EMG signals as a surgical action is mimicked or performed. If this were true, then a multivariate fatigue analysis could be performed on the data. Doing so would reduce computational time by not having to apply the methods to

individual channels. This area is addressed in the thesis with the independence analysis of the EMG channels.

On top of the existing MF methods, it is suggested that perhaps complexity within the EMG signals could be used as a fatigue index, and that it could be determined by examining a system's dynamics. As most algorithms rely on the signal stationarity, choosing an improper window sizes could introduce errors within the results. Therefore, developing an algorithm that offers more robustness over different window sizes would be particularly advantageous over existing MF methods. This thesis will concentrate an initial effort towards the complexity algorithms development, and compare its robustness with the conventional MF method.

1.4 Thesis Organization

In Chapter 2, the current literature that has led to the developments within the proposed area of research will be examined. It begins by outlining the biology behind muscular fatigue relating to surgery, and the methods for detecting such changes from the body's normal state. The decoupling methods are then reviewed, which leads to a method for distinguishing the independence of EMG signals, and the development of a novel fatigue index. Subsequently, tremor measurement is introduced as an alternative fatigue indicator and the literature relating to its development is examined. Finally, the two fatigue measurements are combined and the literature relating to predictive systems involving neural networks are reviewed.

The first task of thesis involves examining the independence of the EMG signals by conducting a series of tests using Independent Component Analysis (ICA). Chapter 3 clarifies the EMG signals dependency status, and the ultimate reason for developing the fatigue detection methods of Chapter 4. It examines the independence of multiple

captured EMG signals using Independent Component Analysis, and the correlation between different channels while perform a specific task.

In Chapter 4, a new methodology to determine a fatigue index is developed using complexity from a dynamically embedded system, and the instantaneous frequency from Hilbert Huang Transform (HHT). The method is applied to an experiment in which individuals mimic a typical surgical action, and EMG signals are captured from specific muscles. The fatigue indices are analyzed for a variety of time window sizes, and a robustness comparison is performed between the new and existing methods.

A surgeon's hand steadiness is also a concern during an operation, as failure to maintain a certain level could result in patient injury, or an increase in an operations length. This thesis addresses the concern associated with a surgeon's hand tremor by adopting a new parameter which is more easily understood than the conventional fatigue indices. Chapter 5 introduces a novel method for detecting this tremor amplitude parameter using piezoelectric accelerometers attached to the hand. This new method uses Empirical Mode Decomposition (EMD) to remove the drift component from the signal. The new method for determining the maximum tremor amplitude is derived from the integrated displacement and Principal Component Analysis (PCA). The indices described in Chapter 4 and this new indicator are then applied to real surgical data to demonstrate the development of fatigue during a day of microsurgery, and correlated with the operation length.

In Chapter 6, the newly developed methods for detecting tremor amplitude and fatigue, have been combined within a Artificial Neural Network (ANN) to develop a performance prediction methodology which can be applied to monitor the deterioration of surgeon's accuracy and precision throughout a day of surgery. Several Nonlinear AutoRegressive with eXogenous inputs (NARX) neural networks are proposed and analyzed, using the experimental data from Chapter 4. This involved comparing two

and eight channel configurations of Bayesian Regularization and Resilient Backpropagation trained networks, and separately using Mean Frequency (MF) and Complexity (H) fatigue indices to predict the maximum tremor amplitude. Consequently, the prediction errors between the predicted and the actual data have been compared for the suggested neural network alternatives.

Finally, in Chapter 7, conclusions are drawn from the results of the thesis, and suggestions are made as to how the research methods can be integrated into a viable real time predictive system for surgery.

Throughout entire thesis, the experiments performed for the development and performance analysis of the suggested algorithms, consist of collecting data from within a controlled lab setting. The methods, once proven, have then been applied to real surgical data.

2

Literature Review

2.1 Introduction

The bulk of this thesis combines fatigue and tremor research. The information derived from these parameters can prove useful for surgeons as they perform lengthy microsurgical procedures. This chapter encompasses a literature review of the various fields of study, and assists with understanding the development of the research methods referred to in the body of the thesis.

Section 2.2 begins by providing a platform of microsurgical procedures. The notion of muscular fatigue is introduced, and the typical actions, postures, and muscles used during microsurgery are also presented. Section 2.3 ties in with Section 2.2, by further expanding on the definition of fatigue, and links it to its measurement using Electromyography (EMG). Consequently, the review of the various studies measurement techniques leads to the development of the complexity fatigue index introduced in Chapter 4.

Before deciding whether multivariate fatigue analysis is possible, however, it is necessary to investigate the coupling and independence between multiple EMG channels. The methods that have been at the forefront of signal decoupling are reviewed in Section 2.4. These paved the way for the independence analysis in Chapter 3, and the methods developed in Chapter 4.

Finally, Section 2.5 takes the fatigue analysis a step further by introducing tremor as a performance-reducing factor, and reviewing past studies that have contributed to its

measurement. The review paves the way for the novel tremor amplitude measurement algorithm presented in Chapter 5. It would be better understood by most, if we explained fatigue as a performance reducing factor, rather than an index. In addition, predicting an individual's tremor amplitude solely from their fatigue index would be also highly useful. Neural networks have demonstrated themselves as valuable predictive methods in biological systems. Consequently, they are ideally suited for the proposed application, and are reviewed in Section 2.6. The review is tied in with the research of Chapter 6, which develops a tremor amplitude prediction method using multiple fatigue measurements; the ultimate aim of this thesis.

2.2 Muscular Fatigue in Microsurgery

The duration of lengthy microsurgical procedures are very often in excess of five hours [10]. Many of these procedures are performed without a break, and usually by the same surgeon. Combined approach tympanoplasty, and the translabyrinthine approach to acoustic neuroma [11] are two examples of these types of procedures. In comparison, shorter procedures such as a cochleostomy can be repeated several times throughout the day, and frequently without breaks. The motion and actions performed by micro-surgeons during these procedures tend to be very similar: that of drilling, incision, pinching and sewing. These actions are performed under a microscope and require the micro-surgeon to have an upright posture with their shoulders as stationary as possible, as well as having their forearms parallel to the operating surface (Figure 2.1). The surgical tools are typically gripped in the palm of the hand, between index finger and thumb. The major hand muscle utilized is the Adductor Pollicis (AP), while the muscles that contribute the motion of the wrists are the Flexor Carpi Radialis (FCR) and Flexor Carpi Ulnaris (FCU). Both the FCR and the FCU flex adduct the hand at the wrist joint [12] (Figure 2.2). The stability of the arm is controlled primarily by the Deltoids and the Trapezius, while lateral movement of the forearm is controlled

primarily by the Biceps Brachii, the Latissimus Dorsi, the Pectorals, the Brachialis and the Triceps. These muscles work concurrently to ensure that the surgeon performs the operation to the desired precision, with the least amount of trauma to himself and the patient.

Figure 2.1: *Image of a micro surgeon's posture throughout a Cochleostomy procedure and the drilling of the Posterior Tympanotomi.*

Figure 2.2: *Muscle and EMG Channel identification* [12].

Similarly, over the length of the microsurgical procedures, it is believed that fatigue sets in, as any prolonged voluntary muscular contraction induces fatigue [10]. Increasing the level of these contractions leads to a reduction in the time that an individual can maintain the contraction, thereby reducing their endurance time [13]. In general, muscular fatigue is described as the point by which a specific muscle can no longer sustain a contraction. This can be misleading in practice, as this defines fatigue as a specific point, where fatigue is in fact a development stage [14]. The fast twitching Motor Units (MU) in a non- fatigued state slow down over time to produce slower twitches. In addition, physiological tremors, which include postural and isometric tremors, become more prominent [3, 4]. The development of which could potentially affect the outcome of a particular task.

2.3 Muscular Fatigue Analysis and EMG

Electromygraphic analysis has demonstrated itself as being a useful method for predicting fatigue during repetitive tasks [5, 6]. The EMG measurements are primarily captured using surface EMG, although they can be obtained using needle electrodes. The latter unfortunately cause some risks of infection, damage to muscle fibers, and are painful to the subjects [15]. Muscle fatigue is characterized by changes in intracellular action potentials and in the propagation velocity of the excitation waves along the active fibers. It is not always true that the amplitude of the EMG signal decreased with fatigue. The amplitude can also increase during the fatigue process [16]. It is generally accepted, however, that as the muscles of interest fatigue during a sustained isometric contraction, the Mean Frequency (MF) and Median Frequency (MDF) of the power spectrum of muscle activation decreases [17-19]. Interestingly this occurs even in the absence of tremor. A substantial amount of research has been performed in this field over the last twenty years. For example, Gaudreault *et al* [8] used the MDF and amplitudes from back muscle's EMG signals to evaluate the muscular fatigue and neurophysiological efficiency due to abnormalities in their muscle fibers. Although the MDF slopes were all found to be negative, suggesting fatigue, and the amplitudes slopes positive, suggesting compensation to maintain the desired contraction level, the results could not discriminate between normal and scoliotic subjects. Lariviere *et al* [9] also used EMG fatigue indices to assess the biomechanical effect of gloves on fatiguing finger flexor and extensor muscles. They discovered that although the indices indicated fatigue within the muscles, they demonstrated poor sensitivities for assessing the effects of the gloves on these muscles. It was suggested that perhaps this was because of the differences in glove materials and muscle activation levels.

It should be noted, however, that the MF shift can only be considered as a fatigue index, and not actual fatigue. The change in MF is therefore a representation of the muscle's shift towards a fatigued state. As a consequence of the fatiguing motor units,

other units within the same region that have not contributed to the signal previously become more prevalent. Not only are EMG signals dependent on the number of motor units, but on the muscle group, the force required to move a particular object, and the variance in signal amplitude from one individual to the next. Therefore, it is very difficult to predict over time the absolute magnitude of the signal changes. The fatigue analysis proposed in this thesis, however, examines trends in the signal. It can therefore determine with certainty a development towards a fatigued state.

EMG fatigue analysis has been primarily applied to shorter muscular bursts at the similar strength levels (constant percent Maximum Voluntary Contraction (%MVC)) [20-22]. The problem arises, however, when dealing with daily routine movements and muscular contractions, as the strength level of these contractions varies. Little is known as to what happens to the frequency of the muscular motor units over these longer periods. Long-term studies have been performed whereby EMG has been captured throughout a 24 hour period, and have examined parkinsonian, essential [23], and wrist tremor [24]. Christensen *et al* [25] also examined the MF change throughout the day of the deltoid, trapezius, and infraspinatus muscles in subjects operating a pillar drill.

The reduction in strength over the length of a sustained isometric contraction and the reduced variation between slow and fast twitching MUs suggest that the complexity of the EMG signals decreases as fatigue sets in. A measurement of this complexity could therefore correlate directly with muscle fatigue. Yang *et al* [26] demonstrated that the nonlinear Lempel–Ziv complexity, $C(n)$, captured from bicep's EMG signal decreased during flexion exercises at various force levels. The $C(n)$coefficient was determined by following the procedures described by Wei *et al* [27], which transforms a window of data into a sequence of binary points. They suggested that the Lempel–Ziv complexity used to analyze sEMG signals, reflected the neural activity strategy and neuromuscular function changes.

Complexity, however, is typically quantified using the non-dimensional measure of Shannon entropy. Sung *et al* [28] proposed using the measure as a diagnostic tool for lower back pain by quantifying the complexity using the outcome probability of an experiment. They did so by analyzing the correlation between successive time frames within the EMG signals with the Hurst component, and determining the Shannon entropy from these parameters. They confirmed that the complexity of a biological system is decreased with injury. Shannon entropy has also been proven useful in the prediction of epileptic seizures [29]. Although James *et al* introduced a combination of dynamical embedding [30], and Independent Component Analysis (ICA) to describe the changing dynamics of single EEG channel leading up to an epileptic seizure [29], they also suggested that both the entropy and Fisher information of the embedded system could provide useful information about its complexity. This paved the way for this thesis' proposed method for finding changes in the underlying dynamics of a fatiguing system, using only a single embedded channel.

2.4 Decoupling and Independence of the EMG Signals

It has been suggested by Kilner *et al* [31] that perhaps there exists some coupling and synchronization between motor functions while performing a specific muscular motion, however he did not provide any proof. Farina *et al* [32] suggested that because the captured MUs from two separate muscles are located at different distances from the electrodes, it would be unlikely that there would exist any cross-correlation between their EMG signals. If coupling between EMG signals exists, then a multi-channel fatigue analysis would be possible. However, decoupling the signals from one another, and proving that the EMG signals are dependent on one another, requires determining the validity of Kilner *et al* statement. There exist numerous methods of decoupling signals and statistically extracting the necessary information. Signal detection in climates has produced much of these analysis methods. This is because the science

requires the extraction of information trends from multiple signal sources, which might be collected simultaneously or over many time periods. And as with all of these methods, the patterns within the multivariate data can be analysed spatially or temporally.

The method that has been at the forefront of spatial pattern detection is the Empirical Orthogonal Function (EOF), otherwise known as Karhunen-Loeve (KL) decomposition, or PCA. This method analyses the information of spatially distributed data sets, and determines orthogonal principal directions of maximum energy by determining the covariance matrix. It has been demonstrated by Liyu *et al* [33] that feature extraction for classification can be obtained from surface EMG using singular value decomposition techniques. However, this method is restrictive when attempting to decouple EMG signals, as the orthogonal directions are calculated sequentially. In effect, all calculated orthogonal directions are found to be uncorrelated and orthogonal with respect to the first and most dominant direction. However, this can be particularly limiting, as the required signal sources might not be orthogonal to one another.

Temporal analysis methods such as Multi Taper Method (MTM), Singular Spectrum Analysis (SSA), and Wavelet Analysis (WA) have also been used to detect and isolate temporal signatures within an electromyographic time series. Khalil *et al* [34] initially demonstrated that the WA is an efficient tool in detecting the frequency components within an EMG signal. Khalil *et al* [35] furthered his research by showing that the detection of the signals can be approached using a Dynamical Cumulative Sum (DCS) followed by a Wavelet Transform (WT). However these methods only provide insight into the frequency components of a signal mixture, and offer little knowledge about underlying source signals within that mixture.

There exist other methods that can identify both the spatial and temporal structures in multivariate data sets. These include many extensions of the EOF, such as the

Extended EOF, and the Frequency Domain EOF. Another such method is ICA, which works on the principle of Blind Source Separation (BSS). It has been used extensively in the fields of speech processing [36], brain imaging [37], telecommunications [38], and stock market predictions [39]. Calhoun *et al* [37] applied spatial ICA to Functional Magnetic Resonance Imaging (FMRI) data and 144 whole-brain 3D images. They demonstrated that it was an extremely useful tool in characterizing high dimensional data in a concise manner. This has paved the way for the use of ICA in the medical field. Future work included an analysis of temporal and spatial ICA with FMRI data [40] and once again proved to be fruitful, as it was demonstrated that the data can be characterized without making specific modelling assumptions. Additionally, ICA has been used as a method of removing artifact noise in EEG data from MRI scans [41]. The ballistocardiogram (BCG) artifacts generated by the movement of EEG electrodes were removed from the data after processing the original EEG data through an ICA algorithm. Five or six of the ICs were extracted from the data and were shown to be the BCG artifact. The results clearly illustrated that ICA could be used as an efficient method of noise cancellation. More importantly, it has also been used in separating mixed biomedical signals into their source components, by relying on the fact that the signal sources are not only uncorrelated, but independent of one another. Moving-window ICA decomposition was demonstrated by Makeig *et al* [42] on electroencephalographic (EEG) measurements and was found to be useful in determining independence of activity in different brain regions.

Many studies have also examined the performance of ICA over other methods such as PCA. Manduchi *et al* compared it with PCA for modelling of synthetic and natural textures in computer vision [43], and proved that it had superior performance over PCA. Bartlett *et al* [44] applied the algorithm to facial recognition using both spatial and temporal ICA methods. Once again, when compared to PCA, both ICA methods proved to be far superior at recognizing faces across days and facial expressions.

The most important results of all the studies demonstrate that ICA is an ideal method for ensuring that mixture signals are separated into their source components. And because the method operates on the assumption that the mixture signals are independent of one another, it can be particularly useful for identifying the independence of source signals within a signal mixture. Based on this knowledge, the topic of signal independence from an EMG standpoint will therefore be examined in Chapter 3.

2.5 Fatigue, Tremor, and Surgical Performance

Fatigue is a very subjective term and therefore difficult to quantify. In addition, it can vary from individual to individual. As discussed above, fatigue from physical exertion can have an affect on the characteristics of an individual's muscular contractions, and that the preferred way to quantify a fatigue trend is to examine the shift in frequencies from captured Electromyographic (EMG) signals [16]. With this increase in fatigue, comes a decrease in fine motor control, and an increase in tremor. Numerous studies have examined the effects of tremor from factors such as age [45, 46], amitriptyline [47] caffeine, fasting, and propanolol [48-50]. Others have examined the effects of tremor from fatigue through physical and mental activity. These included Viitasalo's *et al* [51] who compared forearm tremor amplitude and frequency characteristics during different types of loading scenarios, and Morrison *et al* [52] who studied the effects of fatiguing wrist extensor muscles on postural tremor during goal directed pointing of a laser. Both demonstrated an increase in tremor after fatiguing by specific exercises. However, none of the studies have examined the effects of operating on fatigue and tremor.

Some surgical studies have examined aspects of fatigue during simulated laparoscopic surgery, which have been conducted over short periods of time, and during sustained

isometric muscular contraction levels [53]. Others have examined the effects of laparoscopic training on muscular demand [54]. These studies have examined the muscular contribution during specific surgical tasks. They have concluded that certain muscles are used more often than others and are therefore at a greater risk of fatiguing. However, they have not shown that the studied muscles had fatigued.

Surgical decision making is the most important factor determining operative success. However, once a decision has been made the performance of the surgeon comes into play. Similar to any job or task [14], it is believed that mental and muscular fatigue is developed during a day of operating. It is likely that an increase in arm fatigue causes an increase in hand tremor. This leads to a reduction in the surgeon's fine motor control, and hence a reduced precision of the surgeons hand movement. Based on the relation between fatigue and tremor, the objective of Chapter 5 is to demonstrate that an increase in a surgeon's fatigue while operating leads to an increase in the hand tremor of the surgeon's dominant hand. Ultimately this increase in tremor amplitude could translate to a reduction in performance precision and accuracy.

Tremor is a manifestation of the rhythmic involuntary movements resulting from regular oscillatory contractions of corresponding agonistic and antagonistic muscles [55]. Tremor experienced during a surgical procedure can be divided into postural, isometric, and physiologic components [3]. Postural tremor refers to the tremor exhibited by an individual attempting to maintain a body part's position against the effects of gravity. Isometric tremor refers to the tremor induced by muscle contractions against stationary objects. Physiologic tremor refers to a high frequency, low amplitude postural tremor that all normal persons exhibit. The neurally generated physiological subgroup lie in the 8-12 Hz range, and can adversely affect or hinder an individual's ability to perform a specific task [52, 56, 57]. In certain cases, it is possible to filter out the undesired tremor, thereby improving the accuracy and precision. Telerobotic control is one such discipline, where undesired vibrations are

generally filtered out from the devices to achieve the desired dynamics. On the other hand, there are still tasks such as surgical operations, which for the most part require complete human contribution. Brommeland *et al* [58] showed that parameters such as the length of time to complete, and positional information such as accuracy and precision, are regarded as being very significant when performing certain surgical tasks. It was also shown by Hsu *et al* that the length of time to complete a task and accuracy are dependent on the amount of tremor a surgeon experiences [59].

The normal operating day may involve one long operation or many short procedures. These can have differing levels of complexity requiring differing degrees of accuracy. Throughout a day of surgery, a surgeon's tremor can play an important role when completing several difficult tasks, such as performing a vascularized reconstruction after a cancer resection. These tasks tend to be performed at the end of a long surgery and require the surgeon's utmost precision. The same can be said for multiple short surgeries performed throughout the same day. The repetitive and stressful natures of the physically challenging conditions the surgeons are exposed to, can potentially affect the accuracy and the length of time to complete the procedure. These parameters might become particularly influenced by the manipulation of minute objects, where the tremor far exceeds their size. One such example is a stapedectomy. This procedure requires the creation of a 0.6mm stapedotomy through which a 0.4mm piston is inserted [60]. Hence, any form of excessive hand tremor could potentially affect a surgeon's performance, and compromise the outcome of an operation. It stands to reason that in order to keep the human accuracy at required levels, it might be desirable to monitor the surgeon's hand tremor throughout a procedure.

Most studies that have analyzed hand and arm tremor by using accelerometer data [52], however, some have used position measured from either video [59], through opto-electronic motion capture [61], or laser interferometry [56]. The disadvantage of using video is that information cannot be easily analyzed in real time, and is restricted to

measurements in two axes. Similarly, laser interferometry can only measure in one axis, is plagued by a fixed displacement axis, and is generally comprised of large equipment not suited for operating theatres. This becomes an issue if the subject's actions are not completely restrained to the desired measurement direction. On the other hand, 3-axis accelerometers offer an important advantage over the other devices. Not only can they measure the acceleration in three directions, but they are small enough to be attached directly to small biological surfaces, such as the hand. However, they have not been used for the analysis of hand tremor developed throughout the day due to fatigue.

Some studies, such as Elble *et al* [45], used accelerometers to analyze tremor, by comparing differences in the mean raw acceleration. Others, such as Morrison *et al* [52], preferred using a more accepted method of characterizing changes, by analyzing differences in the acceleration's Root Mean Square (RMS). However, examining solely the acceleration data does not necessarily provide all the desired information with regards to the movement of the hand. It would be far more useful to identify the displacement of a surgeon's hand, so that the maximum level of accuracy might be attained during an operation. Chapter 5 will therefore introduce an innovative method for determining hand displacement, while correlating the measure with fatiguing muscles.

2.6 Tremor Amplitude Prediction from EMG

The ultimate goal of this research is to combine newly developed methods detailed in this thesis for fatigue analysis and tremor amplitude determination, and develop a real time predictive measurement system that could monitor surgical performance. Neural networks have proven themselves in a variety of fields as satisfactory prediction methods. Most importantly, because of the subjective nature of biological systems,

neural networks offer an ideal benefit over other classification methods. Applications have included load position and weight predictions along a beam embedded with Fibre-Bragg sensors [62], as well as the estimation of high precision temperature measurement [63] . Although neural networks have been typically adapted to nonlinear dynamic systems, they have also been utilized with EMG and accelerometer measurements to predict specific underlying parameters of many biological systems. Some neural network EMG research has been completed in the determination of muscle fatigue [64, 65], however, most of the efforts have been directed towards the recognition of limb motion [66-69], filtering [70], and control [71]. Azzerboni *et al* proposed an unsupervised learning process, the Growth Neural Gas (GNG) algorithm to perform time-frequency analyses [65]. They were able to extract features from multiple EMG measurements as the muscle dynamics changed. They did so by characterizing the frequency content of the signal during force variations. They found that the features extracted by the network depended only on the force applied and not on the contraction time. This demonstrated that during constant force contraction cycles, the signals exhibited stationary behavior. Ultimately, it was suggested that this method could be very effective at estimating muscle fatigue during complex tasks. However, this seems to contradict previous findings by Karlson *et al*, which state that muscle fatigue is not necessarily dependent on the level of applied force [72]. Moushou *et al* proposed an alternate method for identifying muscle fatigue which relied on the wavelet coefficients [64]. By displaying the coefficients into Self Organizing Maps (SOM) neural network, they found that it was possible to detect whether an individual had fatigued. Regrettably, these studies only provided methods for predicting a fatigue index, but did not address tremor prediction during the fatiguing process.

Some studies have applied neural networks to the field of tremor classification [73, 74], and involuntary motion cancellation which could be applied to microsurgery using telerobotics or handheld instruments [75]. Jakubowski *et al* and Engin *et al* used them

to classify acceleration based tremor [73, 74]. Jakubowski *et al* [73] demonstrated that second order statistical information about the accelerometric tremor was not sufficient enough to categorize tremor. Instead, they suggested that the polyspectra of the second, third and fourth order statistics were well suited for the categorization task. With this information as input into a backpropagation based multilayer perceptron (MLP) neural network, they were able to determine the tremor signals as belonging to either parkinsonian, essential, or physiological, and with a prediction error of less than 3%. Once again, Engin *et al* [74] used a back-propagation based multilayer perceptron network to categorize healthy and the pathological type tremor for the purpose of medical diagnosis. Because of the nonstationary nature of the accelerometer signals, a wavelet-based parameter was used for an improved time-frequency resolution. In addition, they captured entropy, time, time-scale, high-order spectral domain, and entropy information from the tremor signal. They found that it was possible to categorize the tremors with up to a 91% accuracy. Neural networks have also been used for increasing precision, by canceling involuntary motion which could be applied to microsurgery using telerobotics or handheld instruments [75]. However, none of these studies have combined both EMG and accelerometer measurements to predict the outcome of an individual's tremor amplitude. Chapter 6 will attempt to fill this gap in the research.

2.7 Summary

The review has examined the research areas which have led to the development of this thesis. It has demonstrated the shortcomings of several of the methods, and built on upon others to demonstrate the necessity for the proposed research within the microsurgical field.

3

Independence Analysis of EMG

3.1 Introduction

This chapter examines the independence of EMG signals captured from muscles during a specific task. Although logically speaking, muscles performing a specific task must be interconnected or dependent on one or another, the question then arises:

"Are their EMG signals interconnected and dependent on one another as well?"

If they are indeed dependent on each other, it would make it possible to analyze the fatiguing muscles as a group rather than individually. The analysis could also provide some insight into how an individual's muscles work together. This chapter will answer this question by determining the dependency of multiple channel EMG signals during a task.

Although there are many multiple dimensional analysis methods, most of them are dependent on magnitude rather than the signal's frequency content. Because, Dimitrova *et al* demonstrated that fatigue is not dependent on the force level [16], correlation methods such as KL Decomposition or PCA would not be useful, as they rely on the determination of the eigenvalues and modes of the multiple time series. These methods would be quite useful, however, in determining which muscle is dominant, and when this occurs.

Although direct ICA would also be ineffective for analyzing fatigue, it is possible to provide insight into the signal's and ultimately, the muscle's independence using ICA. This method is somewhat an extension of PCA, and once again is dependent on the magnitude of the signals. However, what sets it apart from the others is that it can distinguish whether or not the muscles are correlated and independent. If ICA should find independent components that are different from the original signal mixtures, it would prove that the signals have some dependency on each other. On the other hand, if the independent ICA signals, or estimated source signals are found to be the same as the signal mixture, it would suggest that the signals are indeed independent of one another, and no correlation will be found between the signal channels.

3.2 Methods

3.2.1 Independence, randomness and distribution

By simply looking at the distribution of the EMG signal, it is possible to get a good understanding of its nature. The variance of the data points around the mean can provide valuable information relating to the signal's randomness, its mixture content, and its independence.

In general, if a mixture signal is comprised of multiple underlying signals, then according to the limit value theorem, it tends to have a Gaussian probability distribution. Conversely, a signal which does not have any other signals or dependencies within it, tends to have a super-gaussian distribution [76]. A distribution

is considered Super-Gaussian if $E\left[\frac{f'(x)}{x}\right]$ is strictly decreasing on $\{0,\infty\}$, where its density function is defined as

$$p(x) = E[-f(x)] \tag{3.1}$$

Graphically, this corresponds to having all of the signal's values centered around the mean, and a small variance amongst those values. Super-gaussian signals are therefore less likely to be complex or random, and are easier to predict.

Although there exists many methods for determining the randomness of a signal, the turning point test has been chosen for the analysis in this Chapter. This method counts the number of turning points within a signal to determine the randomness of a signal [15]. It has been used to measure the level of randomness of electrogastrograms [77] as well as the fluctuations within economic variables [39]. A turning point is defined as being either a localized minima or maxima. It is measured by examining the slope before and after a particular point. If the slopes change sign, then the point is considered a turning point. The sum of all turning points, U, throughout a windowed signal of length N is determined, and the process is described as random if the threshold equation is exceeded.

$$U > \frac{2}{3}(N-2) \tag{3.2}$$

Alternatively, it is possible to verify the null hypotheses that states

- H_0: The EMG signal is a random process with no trend.

The number of turning points is asymptotically normally distributed with

$$\mu_U = \frac{2(N-2)}{3}, \quad \sigma_U = \sqrt{\frac{16N-29}{90}} \tag{3.3}$$

H_0 is rejected with a α confidence level if $|z| = \frac{|U-\mu_U|}{\sigma_U} > z_{\alpha/2}$. If rejected, this confirms with a $(1-\alpha)\times 100\%$ confidence that the EMG signal has a trend and isn't a random process. It also suggests that the signals are not mixtures of other signals. However, if the hypothesis is not rejected, it confirms that the EMG signal is in fact a random process [78].

3.2.2 Signal Decoupling Multi-signal Analysis

The independence of the EMG signal can be further investigated by examining the combined array of signals, and determining whether these signals exhibit dependency on each other. As mentioned previously, ICA is a proven method of decomposing mixture signals into their original source signals. It is an extension of the PCA, or Karhunen Loeve (KL) Decomposition, whereby the independent components (ICs) of the system are independent, but not necessarily orthogonal. The angles between the two separated vector signals are determined stochastically. ICA extracts either temporally or spatially desired information from a data set by determining information that is, not only orthogonal, but independent as well. It is used for analysing large data sets, like conventional methods such as PCA and Factor Analysis (FA). Unlike PCA,

however, which is used for extracting uncorrelated signals, or new mixtures, from a set of mixtures, ICA extracts a set of independent signals, or single signals, from a set of mixtures [36]. It relies on using higher order moments of the data in order to separate the mixtures, whereas PCA only uses the second order information. Using this constraint minimizes the statistical dependence between the extracted signal sources. In addition, no prior information is required with respect to the properties of the signal sources, making ICA very advantageous. ICA allows for most of the mixture data to be represented by a moderately small amount of independent components. From a signal processing viewpoint, it represents more efficiently the data by minimizing the mutual information between the signal sources.

3.2.3 Independent Component Analysis

The basic theory behind ICA is that a set of source signals can be determined from a mixture of signals by utilizing a mixing matrix that maximizes the original signal's independence from one another.

This matrix is By definition, the marginal probability density functions (pdf), $p_x(x)$ and $p_y(y)$, of two variables x and y are said to be independent if

$$p_{xy}(x,y) = p_x(x)p_y(y) \tag{3.4}$$

where $p_{xy}(x,y)$ is the joint pdf, $p_{xy}(x,y)$.

This implies that

$$E[x^p y^q] = E[x^p][y^q] \tag{3.5}$$

, where $E[x^p y^q]$ is the central moment.

In contrast, uncorrelatedness only implies that

$$E[xy] = E[x][y] \tag{3.6}$$

where $E[xy]$ is the first moment and $p = q = 1$.

The most commonly used ICA methods for extracting original signals from mixtures are the Maximum Likelihood, Infomax, and the FastICA algorithms. The Projection Pursuit method, although not considered to be ICA, produces the same extracted signals as ICA. In contrast, however, this method does not necessarily require the extraction of M signals from M signal mixtures.

If we define an unknown pair of source signals as

$$s = (s_1, s_2)^T \tag{3.7}$$

where $s_1 = (s_1^1, s_1^2, \ldots, s_1^N)$ and $s_2 = (s_2^1, s_2^2, \ldots, s_2^N)$

Similarly if we define a pair of observed signal mixtures as

$$x = (x_1, x_2)^T \tag{3.8}$$

We can transform the source signals to the observed signals by an unknown mixing matrix A, such that

$$x = As \tag{3.9}$$

x is then transformed to a pair of extracted signals $y = (y_1, y_2)^T$ by an unmixing matrix as follows

$$y = Wx \tag{3.10}$$

The predicted source signals are determined by optimizing W using the fast ICA algorithm.

3.2.4 FastICA Algorithm

Because of the computing demands required for the previous methods, FastICA was developed. It implements a fast fixed-point algorithm for independent component analysis. This fixed-point iteration scheme is a highly efficient computational method for performing the estimation of the unmixing matrix. The computations are performed in a batch mode, where large portions of the data are used in a single step of the algorithm. It has been found in independent experiments that ICA algorithms that use this iteration scheme are several times faster than conventional gradient descent methods [79, 80]. This is because of its convergence properties. Moreover, the algorithm is advantageous because it can also be used for projection pursuit. This makes it an efficient general purpose analysis method for the estimation of independent source signals.

The weight vector, w, which maximizes the non-gaussianity of the projection $y = w^T x$ for x is calculated in an iterative process as follows:

- Initialize w to 1.
- Let $w(k) = E[x(w(k-1)^T x)^3] - 3w(k-1)$.
- Normalize the weight vector.
- $\frac{w(k)}{\|w\|} \rightarrow w(k)$
- Proceed to step 2, if the weight vector has not converged, or $\left|w(k)^T w(k-1)\right|$ is not close enough to 1.

3.2.5 Separation Quality

The measure of the ICA separation quality is defined by the performance matrix $P = WA$ [81]. As $W = A^{-1}$ by definition, P should be close to the identity matrix, indicating near perfect separation. If they are near perfectly separated (the estimated signals are the same as the signal source), and the estimated signal sources are essentially the same as the measured signals, X, indicates that the signals are already independent of one another.

Another measure of the separation performance is by calculating the performance index, PI, as follows

$$PI = \sum_{i=1}^{N} \left\{ \sum_{k=1}^{N} \frac{|p_{ik}|^2}{max_j |p_{ij}|^2} - 1 + \left(\sum_{k=1}^{N} \frac{|p_{ki}|^2}{max_j |p_{ji}|^2} \right) - 1 \right\} \tag{3.11}$$

Where p_{ij} is the $(i, j)^{th}$ element of the performance matrix P,

$max_j\, p_{ij}$ is the maximum element value of the i^{th} row of P,

$max_j\, p_{ji}$ is the maximum element value of the i^{th} column of P,

According to Potter *et al* [82], $PI = 0$ if there exists perfect separation of the signals.

3.3 Measurements

3.3.1 Subjects

Twelve healthy volunteers participated in the study: 8 males, aged 30.63 ± 4.59 (27 to 40 years old) and 4 females, aged 26.25 ± 0.50 (26 to 27 years old). The study was approved by the Aston University Ethics Committee, and each subject signed a written consent form prior to participation.

3.3.2 EMG Signal Recording

The EMG signals were collected using a Bagnioli-16 system, with a bandpass filter within the signal conditioning unit of 20-500 Hz, and preamplified with a system gain of 1000. The data was captured using the DE-2.1 electrodes, the Delsys EMGWorks Acquisition 3.1.0.5 software, and a National Instruments DAQ Card-6036E Data acquisition card sampled at a rate of 1000 Hz. The DE-2.1 electrodes are organized in a single differential configuration. It consists of two 10.0 x 1.0 mm Ag contacts separated by 10 mm. The contacts lie within a 41 x 20 x 5 mm casing. The electrodes were placed over the muscles mid-muscle region of each subject's right arm as

described in Figure 2.2. Electrodes for Channel 1 and Channel 2 were separated by 2 cm to reduce the amount of crosstalk. The data was acquired at a sampling rate of 1 kHz and 16-bit precision.

The EMG signals were analyzed without any pre-processing other than the bandpass of the signal conditioning unit (20 – 500 Hz). The raw signals were normalized and inputted directly into the FastICA calculation algorithms.

3.3.3 General Procedures

All EMG data was collected in the same manner under similar operating conditions to reduce the degree of variations between datasets. The reason for selecting the muscles in question has been explained in Section 2.2. The subjects were asked to sit upright with their arms extended and unsupported, while holding the wrist curl device (Figure 3.1). The subjects were then asked to perform ten 30 second sets of the weight extension exercises, whereby a 3 kg weight was hung from the wrist curl device. The purpose of performing the extension exercises was to mimic the posture and arm positioning of a surgeon.

Figure 3.1: *Subject performing the wrist curl exercises.*

3.4 Results and Discussion

By plotting a histogram of an original sample EMG signal, it is possible to determine the signal's distribution. Figure 3.2 plots the histogram of subject 2, CH2, repetition 6. It is clearly noticeable that the signal is supergaussian in nature. We can therefore classify it as a source signal rather than a signal mixture. Since the signal is considered a source signal, then it is conceivable that this signal is also independent.

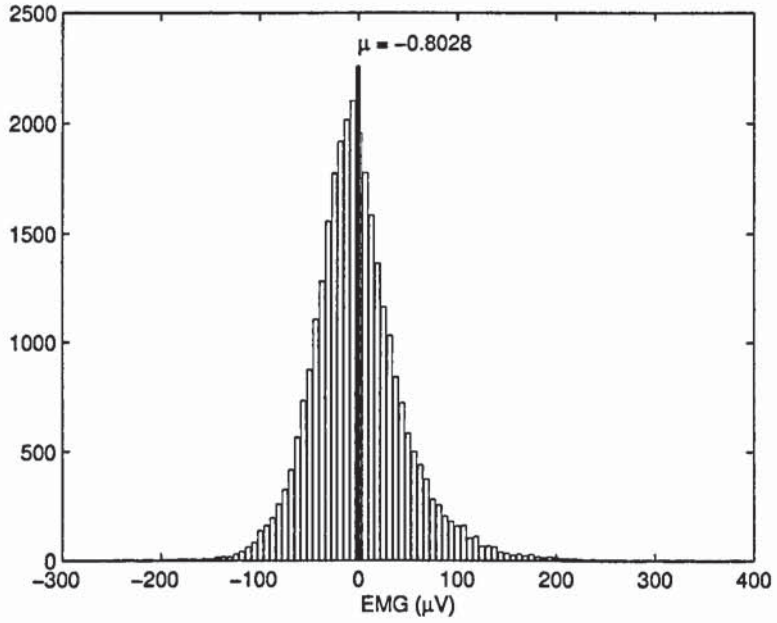

Figure 3.2: *Histogram of subject 2, CH2, repetition 6, demonstrating the super Gaussian nature of the raw EMG signal.*

Figure 3.3 shows the number of turning points using a 200 sample window, as well as the threshold value. It clearly shows that the signal lies well below be threshold for the duration of the experiment, also indicating that the signal is not random.

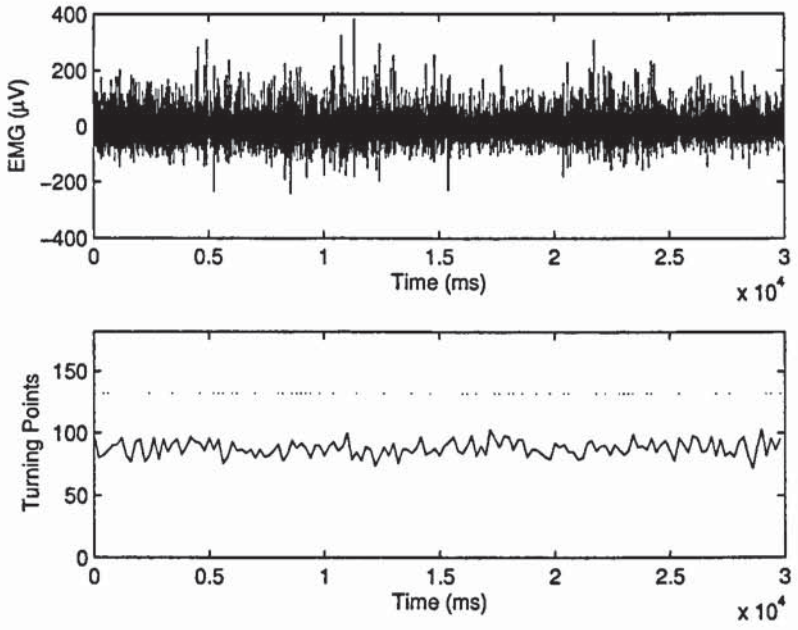

Figure 3.3: *(top) EMG signal potential of subject 2, CH2, repetition 6. (bottom) The number of turning points in the signal with threshold at 132.*

The null hypothesis is also rejected for each of the window sizes. This confirms the previous result, which suggests that the EMG signal is not random, and exhibits a trend. It also suggests that the signals are not likely to be mixtures of other signals.

3.4.1 ICA Analysis

The EMG measurements collected from the sample sets were processed through a FastICA algorithm in a preliminary attempt to decouple the muscle signal mixtures and determine the signal sources. The original mixtures (Channels 1-8) and the estimated signal sources (Channels A-H) are shown in Figure 3.4. The signal sources found after

the ICA algorithm were then compared with the mixture signals by analyzing their correlation coefficients.

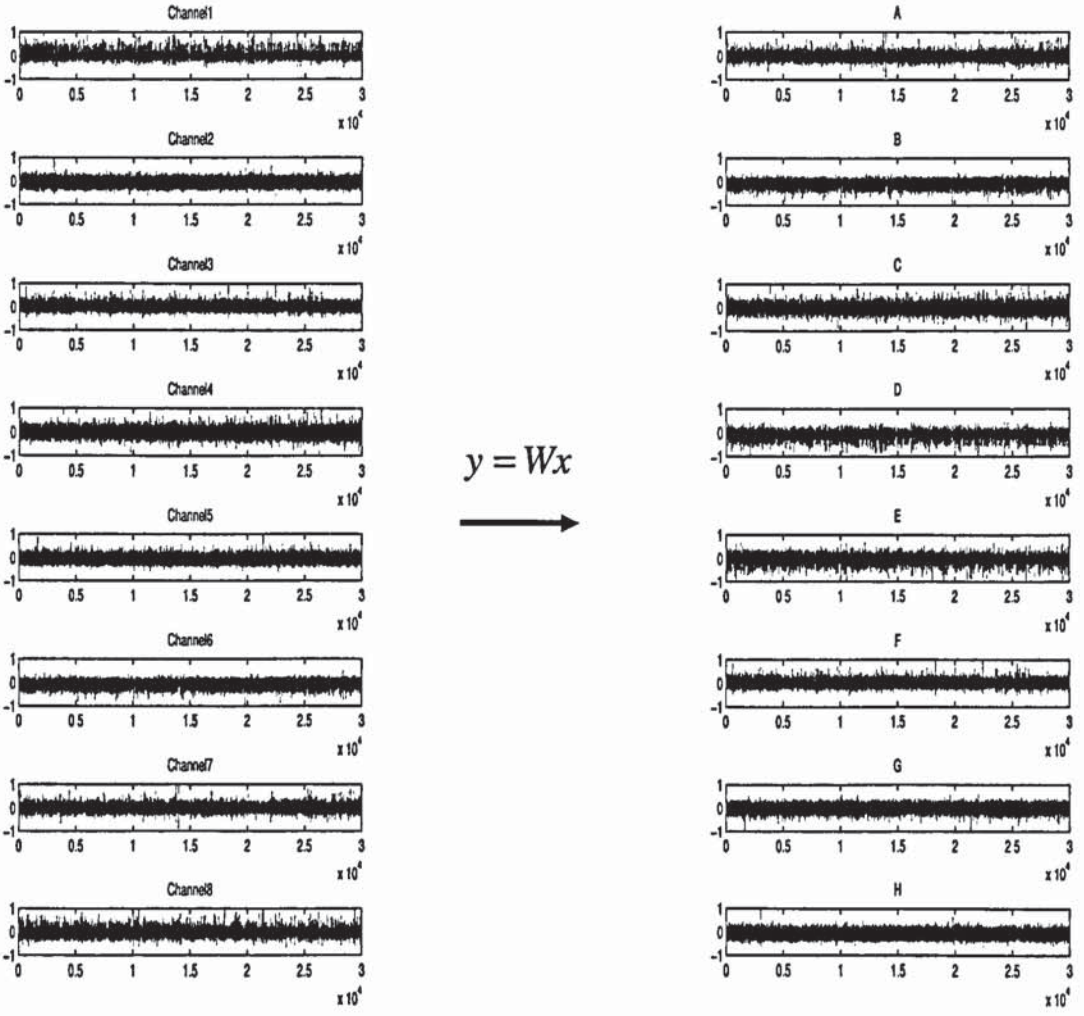

Figure 3.4: *(left) Mixed EMG signals before ICA. (right) Decoupled EMG signals after ICA for subject 2, repetition 1.*

By examining the two signal plots for before and after ICA, it is apparent that the signals before are almost exactly those of after running ICA. The only difference is that ICA does not order the signals according to their original channel. Because ICA is a form of Blind Source Separation (BSS), the independent signals derived from the algorithm do not correlate with the original channels. It visually demonstrates for instance that CH7 is strongly related to A, and CH6 is strongly related to B. The relation between the mixed and unmixed signals can also be confirmed by determining the correlation coefficients between the two. The correlation coefficient provides a reasonable representation of how close to signals are to each other. The values range from {-1,1}, where 1 indicates a strong correlation, and 0 demonstrates that the signals are orthogonal to each other, and therefore uncorrelated. As an example, the correlation coefficients between channels for subject 2 and repetition 1 are tabulated in Table 3.1. Similar to the visual results, it shows that CH7 is strongly related to A, and CH6 is strongly related to B.

		After ICA (Y)							
		A	B	C	D	E	F	G	H
Before ICA (X)	CH1	-0.0249	-0.0110	0.0148	**-0.9871**	0.0075	0.1262	-0.0137	0.0924
	CH2	0.0091	0.0103	-0.0159	-0.1339	0.0251	0.0193	0.2564	**0.9565**
	CH3	-0.0091	0.0166	0.0043	-0.0924	0.0292	**0.9945**	-0.0334	-0.0063
	CH4	0.0086	0.0153	**0.9994**	0.0168	-0.0062	-0.0042	0.0136	0.0178
	CH5	0.0169	0.0265	-0.0839	0.0238	-0.1053	-0.0054	**-0.9374**	0.3186
	CH6	-0.0791	**0.9955**	0.0392	0.0206	-0.0073	-0.0055	0.0261	0.0013
	CH7	**0.9977**	0.0400	0.0056	-0.0341	0.0061	0.0176	-0.0392	0.0043
	CH8	-0.0095	-0.0002	-0.0013	0.0136	**-0.9757**	0.0397	-0.2131	0.0269

Table 3.1: *The Correlation coefficients between signals before and after ICA, for subject 2, repetition 1.*

It is clear that for each after-ICA channel, there exhibits one correlation that is highest. If we choose this highest correlation for each channel from all individuals and repetitions, it is possible to generate an errorbar plot (see Figure 3.5) with the variations of these highest correlations over time. It is now possible to see how well the before-ICA signals correlate with the after-ICA signals. Clearly these correlations vary only slightly.

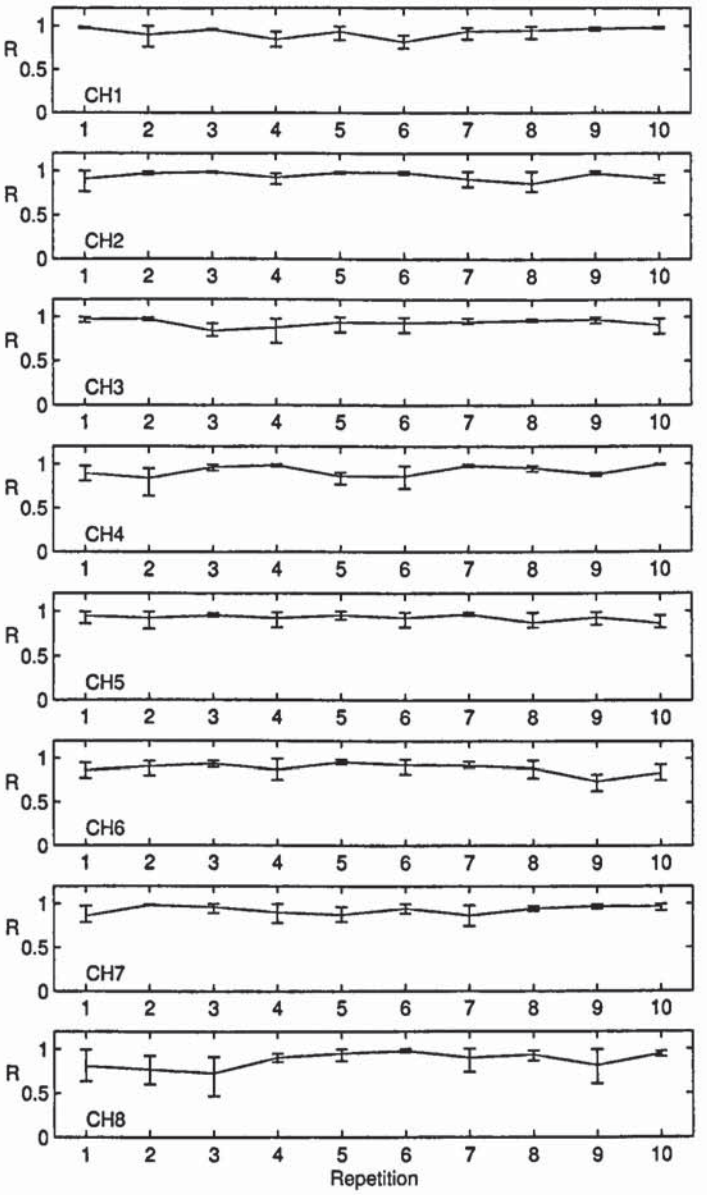

Figure 3.5: *Plots of the highest correlation coefficients between the X and Y ICA components, from all repetitions, all subjects, and for Channels 1 to 8.*

Another such method of determining independence would be to look at the correlation plots of the signals and determine if their structure shows dependency or independency. Subject 2's correlation plots for CH4 and all other channels are shown in Figure 3.6. It is apparent that each signal is already clearly defined and constrained to a specific direction, indicating that the signals are independent of one another [83]. This can be confirmed by calculating the correlation coefficient between the two signals in question. If these signals had been dependent, the plot would have a square shape, with one of the channel's pointing along the x-axis, and the other along the y-axis. However, by examining the dependency, we notice that there is little to no correlation between the signals.

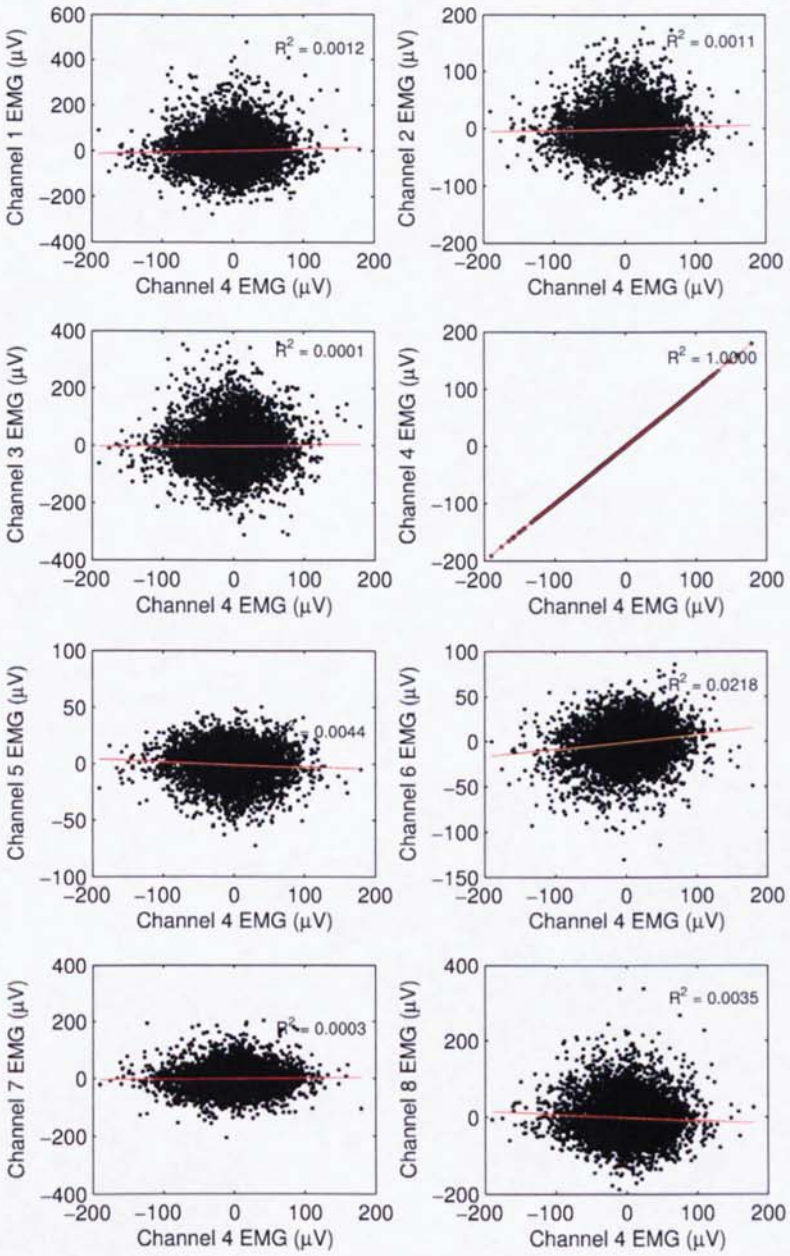

Figure 3.6: *Correlation plot of CH4 vs all other channels for subject 2, repetition 6, clearly indicating the independency between the channels.*

Finally, by considering the separation quality of the ICA process, we notice that the performance matrix, P, is essentially the identity matrix (see Table 3.2 and Figure 3.7). In addition, using equation 3.11 (Appendix A), PI found to be zero. Both results indicate that we have near perfect separation of the signals during the ICA process, and confirms once again that the unmixed signals are in fact almost identical to the original signals.

1	4.61E-17	0	2.71E-16	-8.84E-17	2.41E-16	-1.15E-16	-1.03E-16
4.52E-17	**1**	1.39E-17	-7.21E-18	4.17E-17	-2.51E-16	-1.04E-16	-3.95E-17
3.04E-18	-1.32E-16	**1**	-6.07E-18	1.58E-16	1.31E-16	-2.37E-16	1.04E-17
8.35E-17	2.45E-17	-6.94E-18	**1**	-1.11E-16	-5.18E-16	-5.06E-16	1.68E-16
-3.29E-17	1.58E-18	5.98E-17	-9.69E-17	**1**	2.62E-16	3.53E-16	-3.91E-17
3.59E-17	-4.37E-17	2.69E-17	-2.16E-16	1.53E-16	**1**	-2.35E-16	2.60E-16
-1.44E-17	-2.19E-18	-2.73E-17	-1.35E-16	1.34E-16	-1.05E-16	**1**	2.44E-17
-1.09E-16	6.86E-17	3.90E-17	3.48E-16	-9.69E-17	1.80E-15	4.97E-16	**1**

Table 3.2: *Performance matrix, P, for the FastICA algorithm, Subject 2, Repetition 6.*

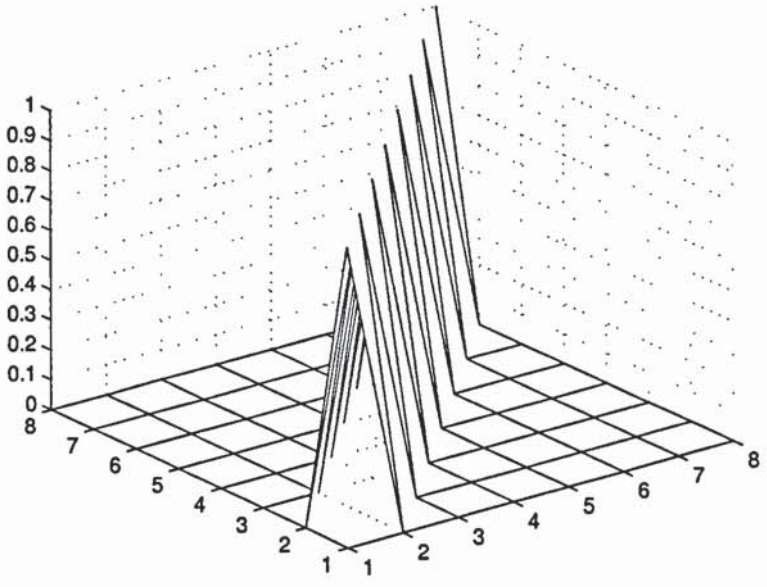

Figure 3.7: *Performance Matrix P for the separation of the 8 sources using the FastICA algorithm for subject 2, repetition 6.*

3.5 Conclusion

This chapter has applied several analysis methods on raw EMG data in an effort to determine channel dependency. Firstly, a distribution analysis was performed in an attempt to provide some insight into the statistical nature of the signal. The results demonstrated that EMG signals have a Super-Gaussian distribution and suggests that the raw signals are source signals, and do not consist of any mixtures. Secondly, a turns test was also performed to determine the randomness of the data set. The results demonstrated that the number of turning points within the specified windows were lower than the threshold value for randomness. This leads to the conclusion that EMG signals are not random, and can be considered once again as source signals.

Finally, ICA was used as a separation technique on the EMG signals for determining the independency of the EMG signals from different muscles. The relationship between the before and after signals was initially visually assessed, and then assessed by determining the correlation coefficient between all signal combinations. Although the channels before the ICA algorithm and after the ICA algorithm did not correspond exactly, it was shown that there existed always one combination that exhibited the strongest correlation. This indicated that for each before-ICA channel, there existed one after-ICA channel that it was linked with. The separation index of the algorithm was also assessed and was shown to be near perfect (PI = 0). Because the ICA algorithm separates signal mixtures into source signals using the principle of independence, and based on the findings of this chapter, we can therefore state that the simultaneous collection of EMG signals from different channels are independent of one another. This confirms that only single muscle analysis methods can be performed to determine muscular fatigue.

4

Complexity Analysis of Muscle Fatigue

4.1 Introduction

The previous chapter indicated that the EMG captured from different channels are independent of one another. This indicates that fatigue analyses must be performed on individual channels. Although the conventional method for detecting fatigue relies on shifts in the MF of the spectral density function, it is suggested that perhaps the complexity of the system could better represents the fatigue process. Because of the nonstationarity of the EMG signal, it is also very desirable to have the new representation provide better system robustness over different temporal window sizes. This chapter therefore presents a new fatigue index, which is found by dynamically embedding a single EMG channel's signal, and examining the changes in its complexity. The Hilbert Huang Transform (HHT) method presented by Xie *et al* [84] will also be applied to the EMG data, and will be compared with the conventional MF method and newly developed complexity method. This will ensure that a broader robustness comparison can be completed.

4.2 Methods

The traditional method of predicting muscle fatigue is by examining the changes of an EMG signal's Power Spectral Density (PSD). As time progresses, fatigue is usually demonstrated by a decrease in the mean frequency value on the PSD plots. These lower frequencies present themselves because of physiological tremors in the muscles, and as lower energy levels associated with the slowing muscle fibre activation [3, 52, 85].

4.2.1 Hilbert Huang Transform method of fatigue determination

Because of the non-stationarity nature and the length of the captured signals [86], the conventional Power Spectral Density (PSD) method for determining fatigue is generally not desired. The HHT technique, however, has been widely applied to study nonlinear and non-stationary time series signals [87]. This method calculates the MF within a time window by using the sum of the mean instantaneous frequencies from each empirical mode, and has demonstrated low MFs variances between different window sizes [84].

Empirical Mode Decomposition was introduced by Huang et al [87] as a method of representing the physical scale and frequency content of either nonstationary or stationary data sets. The method has been used in the decomposition of 2-D rainfall data into its high and low components [88]. It has also been used to analyze paleoclimatic data and the correlation between variables [89]. However, EMD has not been used in the detection of long term fatigue of surgeons while operating. The method decomposes a signal into different intrinsic modes of oscillation or Intrinsic

Mode Functions (IMF). Each of the IMFs must follow the following set of rules. That is:

- In the whole dataset, the number of extrema and the number of zero-crossings must either be equal or differ at most by one.
- At any point, the mean value defined by the envelopes of local maxima and local minima is zero.

The IMFs are found by an iterative process which derives a "local mean" m_1 by fitting upper and lower envelopes to the data. The upper envelope is found by fitting a cubic spline to the local maxima. Likewise a lower envelope is found by fitting a cubic spline to the local minima. Calculating the mean between these envelopes, provides us with a data set m_1. If we subtract the mean from the original data set, we are left with a non ideal IMF h_1.

$$h_1 = x(t) - m_1 \tag{4.1}$$

However, to ensure that both rules are met, a sifting process is performed. This process now treats h_1 as the original data, and the process from the beginning is performed again.

$$h_{1k} = h_{1(k-1)} - m_{1k} \tag{4.2}$$

The process is repeated k times until the extracted signal is reduced to an ideal IMF c_1.

$$c_1 = h_{1k} \tag{4.3}$$

according to the stopping criterion described in [90], where e_{max} and e_{min}, are the maximum and minimum amplitude envelopes respectively.

$$\left|\frac{0.5(e_{max}(t)+e_{min}(t))}{0.5(e_{max}(t)-e_{min}(t))}\right| < 0.05 \tag{4.4}$$

The IMF can then be subtracted from the original data and the process (1-3) can be repeated until we have determined all the ideal IMFs c_j.

$$r_1 = x(t)-c_1 \quad , \quad r_2 = r_1 - c_1 \quad , \quad \ldots \quad , \quad r_n = r_{n-1} - c_n \tag{4.5}$$

By summing all equations in (4.5), we get

$$x(t) = \sum_{j=1}^{n} c_j(t) + r_n(t) \tag{4.6}$$

We have thus reduced the original data series into n-implicit modes, with a residue r_n.

4.2.2 Determining the mean frequency using the Hilbert Huang Transform

After the signal has been decomposed into its IMFs, the next step to the HHT process calls for determining the instantaneous mean frequencies from the analytic signal.

$$z(t) = x(t) + iy(t) = A(t)e^{i\theta(t)} \tag{4.7}$$

Where $y(t)$ is found from the Hilbert transform

$$y(t) = \frac{1}{\pi} P \int \frac{x(\tau)}{t-\tau} d\tau \tag{4.8}$$

Where P is the Cauchy principle value, θ is the instantaneous phase, and $A(t)$ is the amplitude.

$$\theta(t) = arctan\left(\frac{y(t)}{x(t)}\right) \tag{4.9}$$

and

$$A(t) = \sqrt{x^2(t) + y^2(t)} \tag{4.10}$$

We can then define the instantaneous frequency of the Hilbert spectrum as

$$\omega(t) = \frac{d\theta(t)}{dt} \tag{4.11}$$

The weighted mean instantaneous frequency, or power of the signal $z(t)$, from each j IMF with k data points is calculated as follows.

$$\bar{f}_j = \frac{\sum_{i=1}^{k} A_j^2(i)\omega_j(i)}{\sum_{i=1}^{n} A_j^2(i)} \tag{4.12}$$

where A_j^2 is the weight

The combined mean frequency is then calculated using sum of the 2-norm of the amplitudes from each of the frequency bands.

$$\bar{f} = \frac{\sum_{j=1}^{n} \|A_j\| \bar{f}_j}{\sum_{i=1}^{n} \|A_j\|} \tag{4.13}$$

4.2.3 Entropy method of fatigue determination

Mean frequencies determined from the PSD plots provide a generalized quantitative measure of fatigue, but offer little knowledge about the dynamics of the system. We suggest an alternative for fatigue analysis by characterizing a system's dynamics and examining its complexity from signals measured at a single EMG electrode. It has been assumed that the complexity of the signal decreases as the muscle fatigue during a sustained isometric muscle contraction. This could be the result of the change in distribution of the active motor units. An increase in the number of slower twitching motor units would result in less of a spread between all units. This can be explained as a reduction in the frequency band. The variation between motor unit firings would be more uniform, more predictable and consequently less complex. A system's complexity is generally characterized by the Shannon entropy [91] and it is calculated using the probabilistic method [28]. This Chapter proposes to evaluate the Shannon entropy using a dynamical approach in order to provide a better representation of the dynamics of the system. Takens' theorem [30] presents a method of characterizing the dynamics of a system based on measured time series. It demonstrates that we can represent the unknown actual dynamical system by constructing a state space representation as a Dynamical Embedded (DE) matrix based on successive observations of the original time series. The information extracted from the embedded matrix is used to construct a new dynamical system model that is representative and invariant of the actual dynamical system.

This Chapter applies Taken' theorem to construct a DE matrix that represents adequately the dynamics of actual system using the EMG signals measured from

fatiguing muscles. The DE matrix is then decomposed to derive the singular values that can be used to calculate the Shannon entropy related to the complexity of the system.

The DE matrix can be constructed using a series of time delays taken from the original measurement. The unobservable system is defined as

$$X(t)=\left\{x_{t-\tau}, x_{t-2\tau}, \ldots, x_{t-(m-1)\tau}\right\} \tag{4.14}$$

where m is the number of time delays and τ is the time lag.

The number of lag vectors, N, can be chosen to produce the following DE matrix.

$$DE=\begin{bmatrix} x_t & x_{t+\tau} & \cdots & x_{t+N\tau} \\ x_{t+\tau} & x_{t+2\tau} & \cdots & x_{t+(N+1)\tau} \\ \vdots & \vdots & \ddots & \vdots \\ x_{t+(m-1)\tau} & x_{t+m\tau} & \cdots & x_{t+(m+N-1)\tau} \end{bmatrix} \tag{4.15}$$

The determination of time delay, m, is reliant on the convergence of the eigenvalues of the system. The larger the value m, the more converged the eigenvalues of the new embedded system will be. It was suggested in [29] as a practical "rule of thumb" that the number of time delays is

$$m \geq \frac{f_s}{f_L} \tag{4.16}$$

where f_s is the sampling frequency and f_L is the smallest frequency of interest.

The value m can be varied until the desired convergence is reached by setting the time lag τ to 1. To ensure that a sufficient amount of information about the time series is captured for the systems dynamics to be characterized adequately, N should be at least as large as m.

Each column in the embedded matrix represents a point on the Euclidean manifold. In essence all the columns together represent the path the system follows over this manifold. This manifold maps the dynamically embedded system, which is an invariant of the actual system.

The DE Matrix can be used next to characterize the complexity of the system. The Shannon entropy, as an estimate measure of system complexity, would be a useful tool to predict the onset of muscle fatigue, which is commonly demonstrated by a decrease in PSD mean frequency. The entropy is calculated by using a singular spectrum approach similar to that described in [29]. The Shannon Entropy (H fatigue index) and hence the complexity of the system is defined as

$$H = -\sum_{i=1}^{m} \hat{\sigma}_i \log \hat{\sigma}_i \tag{4.17}$$

Where $\hat{\sigma}$ is the normalized singular value described as follows:

$$\hat{\sigma}_i = \frac{\sigma_i}{\sum_{i=1}^{m} \sigma_i} \tag{4.18}$$

The singular values, σ_i, are calculated using singular value decomposition

$$DE = U\Sigma V^T \tag{4.19}$$

where Σ is the singular value matrix, U contains a set of orthonormal output basis vector directions for DE, and V contains a set of orthonormal input basis vector directions for DE. The values on its diagonal are the singular values of the system. The changes in singular values indicate the changes in system complexity and energy. For instance, a system with the first few singular values much larger than the rest indicates a system of low complexity. Conversely, a system with more than just the first few singular values similar to one another indicates a system with high complexity [29].

4.3 Measurements

The EMG data was collected as described in Section 3.3.1 – 3.3.3. The only difference is that the raw signals were inputted directly into the conventional MF, the HHT MF, and DE calculation algorithms by using a 500 ms time window. This window size was chosen so that small bursts of muscle activity during the operation could be captured. Before this was done, however, the Maximum Voluntary Contraction (MVC) of each muscle group was determined for each subject. The MVC determination tests consisted of 5 seconds long EMG recordings. An RMS envelope was fitted to the recordings, and the maximum RMS calculation was used as MVC. During each MVC, the subjects were exposed to a brief resting period during which the muscles were in a relaxed state of minimal electrical activity. The EMG test data was then normalized as a percentage of the MVC, so that it would be represented as the total effort in a percent of the maximum required to complete the task.

In this case, the purpose of performing the extension exercises was not only to mimic the posture and arm positioning of a surgeon, but to determine if measuring the complexity of an EMG signal could be a viable method of determining fatigue. If successful, the method could be applied to real-time surgically captured EMG. The method was also compared against the MF results from the conventional MF and HHT MF methods.

Muscle fatigue can, however, be reduced by allowing the muscles to recover during periods of rest and inactivity. Consequently, longer periods of overall activity can be achieved. During an operation, micro surgeons experience several of these recovery periods. In addition, they expose themselves to relatively high stress levels during which they are constantly concentrating on their performance. In order to simulate the

effect of stressful environments and rest periods during an operation, the subjects were asked to perform challenging micromanipulation tasks for a period of time between each weight extension set. The micromanipulation tasks involved holding between tweezers a 2mm pin, within a 4 mm pin hole. To make the tasks even more challenging, the volunteers were asked not to touch the sides of the hole. These tasks had the added challenge of being performed under a microscope. Each micromanipulation task lasted 30 seconds. These periods of high stress activity under the microscope not only allowed for a period of recovery, but also provided a stressful environment for future fatigue and tremor development. The tremor data captured during this period was not used for fatigue analysis discussed in this Chapter, however. The volunteer have been asked to repeat 10 times the 30 second extension exercise and 30 second micromanipulation task. During each repetition, EMG data was recorded for the muscles of interest when doing the extension exercise. Figure 4.1 shows a 0.5 second capture of the raw muscles EMG signals from volunteer 11.

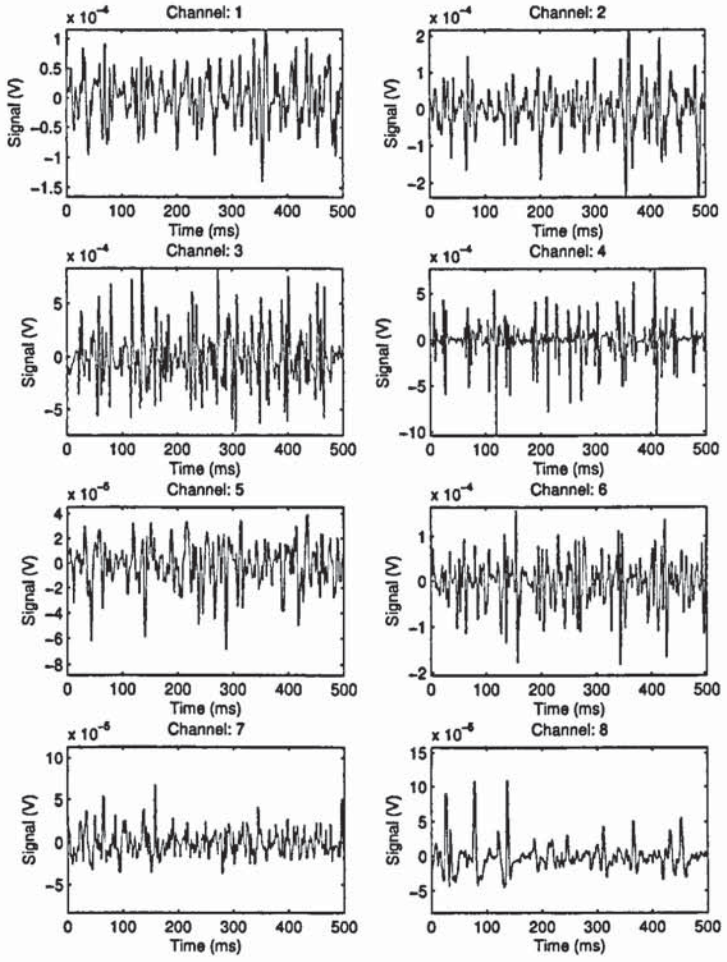

Figure 4.1: *0.5 second samples of the raw EMG signals collected from channels 1 through 8.*

4.4 Results and Discussion

4.4.1 Frequency Analysis

A PSD analysis was performed on the collected EMG signals to demonstrate increasing fatigue levels in the conventional fashion. The PSD plots were generated using Welch's averaged modified periodogram method of spectral estimation, using Hamming window lengths of 256, with 50% window overlap. The estimations were applied to specific window size and the MF were calculated for all windows. Figure 4.2 demonstrates volunteer 11's entropy and MF plots respectively for repetition 1 using a window size, N=1000. Although generally there are oscillations in the mean frequency curve, there is a decreasing trend over time that clearly indicates an increase in muscle fatigue.

4.4.2 Complexity Analysis

The original EMG signals were pre-processed accordingly, and the DE matrix was constructed using the time lag, τ = 1 ms and the chosen data window size, N. As the sampling frequency, f_s, was set as 1000 Hz, and the lowest frequency of interest, f_L, of 20 Hz, the number of time delays, m, was chosen as 50 to satisfy the rule of thumb previously discussed. This ensured the convergence of the singular values. The Shannon entropy was then calculated from the embedded matrix and the specified data window size. The complexity of the embedded signal has been normalized between 0

and 1. The maximum possible entropy is defined as *log m*, where *m* is the number of time delays, or the embedding dimension.

4.4.3 Frequency and complexity method Comparison

If we plot the time series of the calculated entropy values, we notice a clear trend in complexity of the EMG signal. The same is apparent for the MF time series. By fitting a linear regression curve (p1: slope parameter, p2: point of intercept parameter) to the entropy (coefficients p1 = -.001156, p2 = 0.8639 (with 95% confidence bounds), and R-square of 0.4965), MF (coefficients p1 = -1. 1100, p2 = 132.9562 (with 95% confidence bounds), and R-square of 0.6235), and HHT data (coefficients p1 = -0.5979, p2 = 108.8459 (with 95% confidence bounds), and R-square of 0.6393), we are provided with two parameters in which to compare against each other: the point of intercept and the slope. Figure 4.2 clearly shows a decrease in Entropy associated with the decrease in MF. It suggests that as the muscle fatigues, the complexity of its EMG signal does in fact decrease.

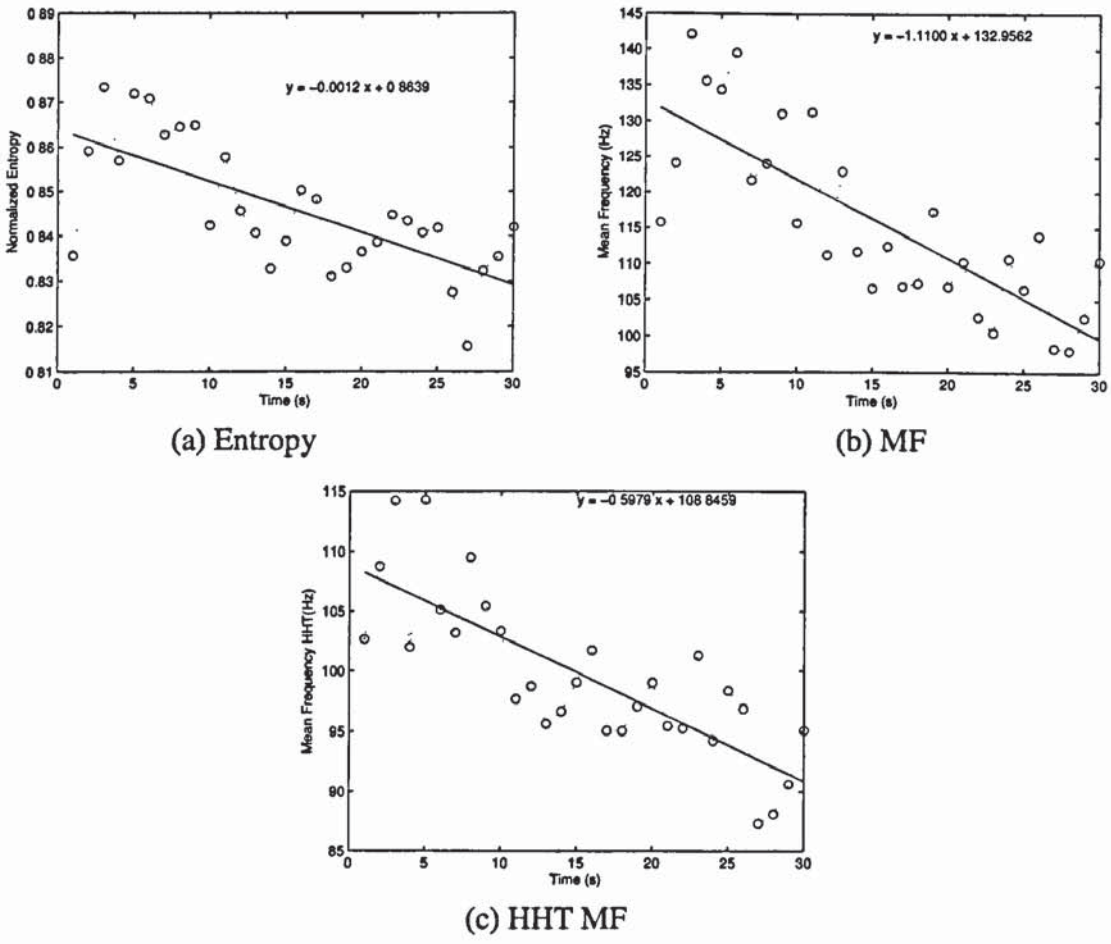

Figure 4.2: *The Analysis of the first repetition of Channel 3 of volunteer 11 with a window size N=1000.*

Examining the entropy over all repetitions (Figure 4.3a), and fitting a linear regression curve to the entropy data(coefficients p1 = -6.629e-5, p2 = 0.8384 (with 95% confidence bounds), and R-square of 0.1418), we notice that the overall entropy trend is not as steep as that of individual repetition. However, more importantly, the variation trend of entropy is similar to the trend of the MF (Figure 4.3b) (coefficients p1 = -0.03127, p2 = 110.7 (with 95% confidence bounds), and R-square of 0.08497) and HHT method (Figure 4.3c) (coefficients p1 = -0.0220, p2 = 96.4758 (with 95%

confidence bounds), and R-square of 0.09048). These observations validate the new method of using Shannon entropy of the DE matrix to determine the muscle fatigue in relation to the well established MF method.

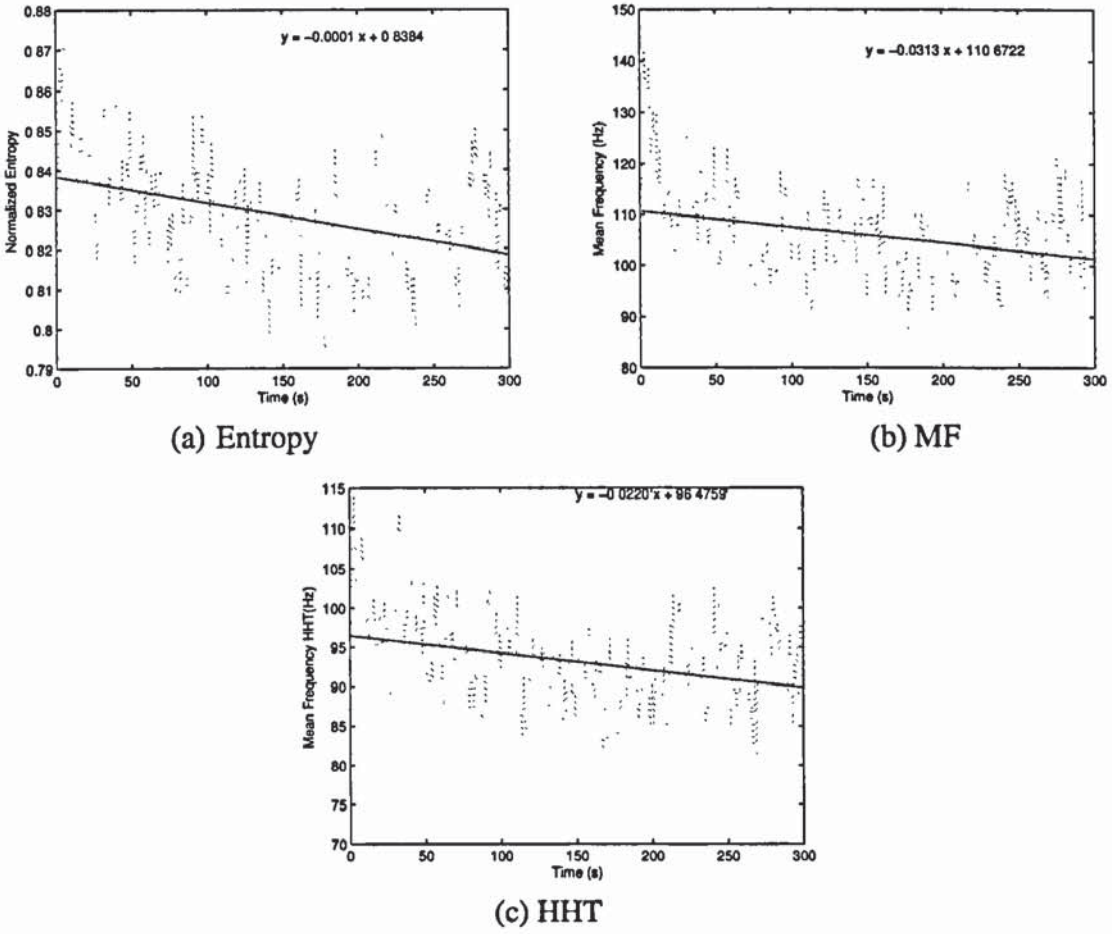

(a) Entropy

(b) MF

(c) HHT

Figure 4.3: *The Analysis of all 10 repetitions of Channel 3 of volunteer 11 with a window size N=1000.*

We can compare the complexity and frequency analysis methods by examining the variation between the regression parameters over different window sizes. In effect, this will provide us with a measure of robustness of the two methods. The slope and point of intercept from both methods using volunteer 11's repetition 3 data were calculated for window sizes of 250 to 5000. These parameters were plotted in Figure 4.4 and demonstrated the variance of slope and point of intercept for changing data window sizes. It is evident that the slope and point of intercept parameters for the Entropy, MF, and HHT-MF methods are fairly stable for the chosen window sizes. Therefore either one of them could considered as an alternative for determining fatigue.

Although in most studies the window sizes for the MF method have been chosen as being 1 s or less than 1 s long [4, 5, 19] because of the approximated stationarity of the signal within this time frame. Interestingly, Figure 4.4 indicates that the estimated parameters are consistent for windows sizes up to 5 s. This would support the use of the MF method for window sizes above 1 s stationarity threshold.

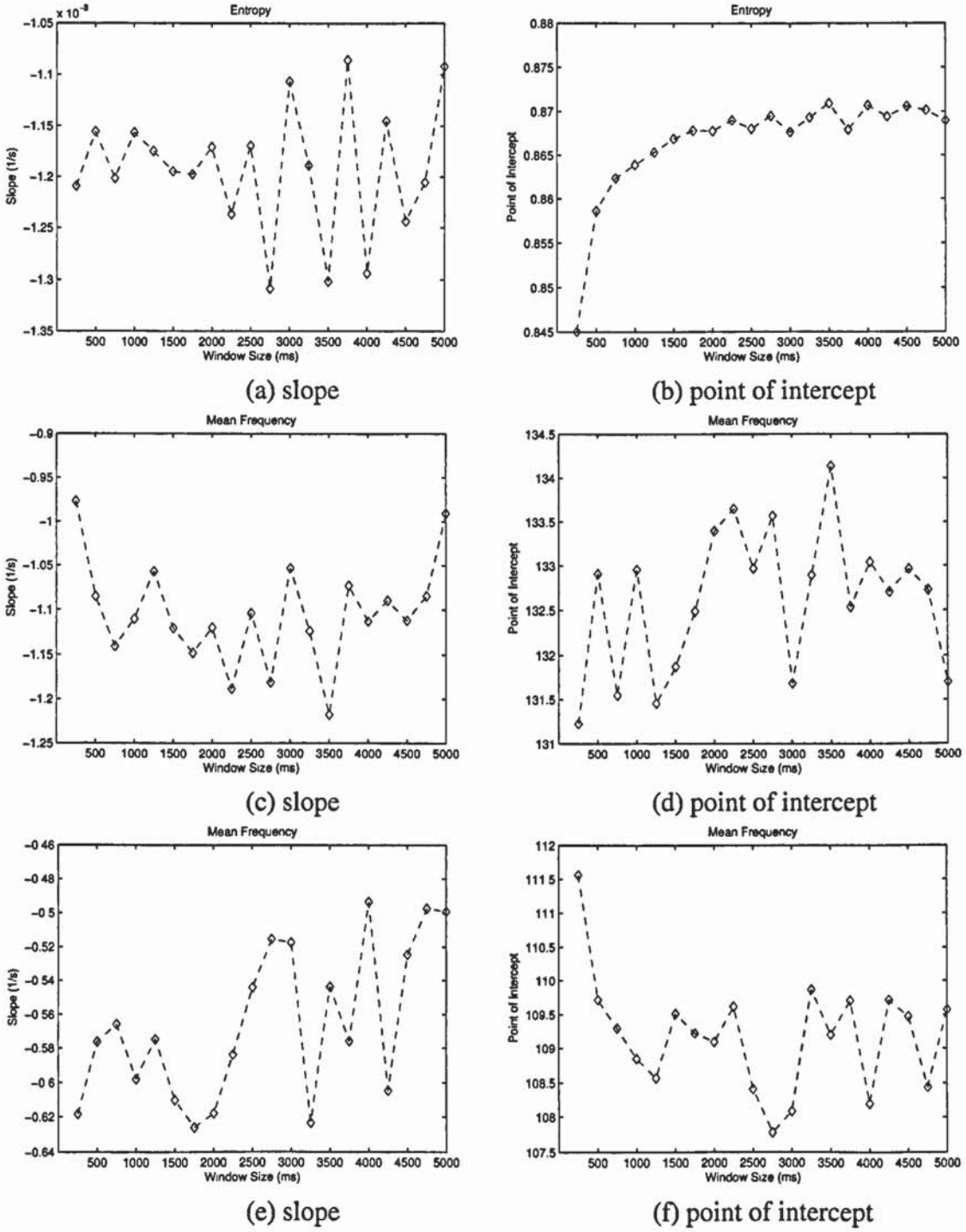

Figure 4.4: *The analysis of the 3rd repetition of Channel 3 of volunteer 11 by varying the window sizes between 250 and 5000; Entropy trend's parameters (a) & (b), MF trend's parameters (c) & (d), and HHT trend's parameters (e) & (f).*

The coefficient of variation (COV) is defined as the ratio between the standard deviation σ and the mean μ of a sample set, $COV = \sigma/\mu$. It is effectively a measure of the spread of a probability distribution. A distribution with COV < 1 is considered to have a low variance. Alternatively a distribution with COV > 1 is considered to have a high variance.

All three methods were compared in this fashion. The COV for both the slope and point of intercept regression parameters calculated from a variety of data window sizes (N=300-5000) and all EMG channels are shown in Figures 4.5 and 4.6. This included the data from all 12 subjects and each of their 10 repetitions. The upper lines of the box plots are the upper quartile values, the lines in the middle of the plots are the median, and the lower lines are the lower quartile values. The whiskers extending from each of the boxes demonstrate the extent of the rest of the data. The crosses on some of the box plots are the outliers, whose data values lie beyond the whisker.

It is apparent from Figure 4.5 that there is less of a variation between the slope and point of intercept regression parameters for the Entropy method. In addition, the COV medians for the Entropy method are generally less than those for the MF and HHT-MF method. The median differences between the two methods can also be confirmed by the p values in Table 4.1 for the null hypothesis. They represent the probability that all samples are drawn from the same population. It is apparent that when concerned with the slope parameter there are very little differences (large p values) between all methods indicating that the Entropy method is only fractionally more robust than the MF, and HHT-MF methods for window sizes of 1000 to 5000. However, when analyzing the differences in COV for window sizes under 1000 (Figure 4.6), there is a more pronounced difference between the slope and point of intercept regression parameters (smaller p values) (Table 4.2). The COV medians for the Entropy method

are much less than those for the MF method. This suggests that the Entropy method offers more robustness than the MF method of analysis as far as the point of intercept regression parameter is concerned. Thus it can be said that overall the complexity method offers slightly more robustness than the MF and HHT-MF methods irrespective of the chosen window size, and could be used as an alternative method of fatigue determination.

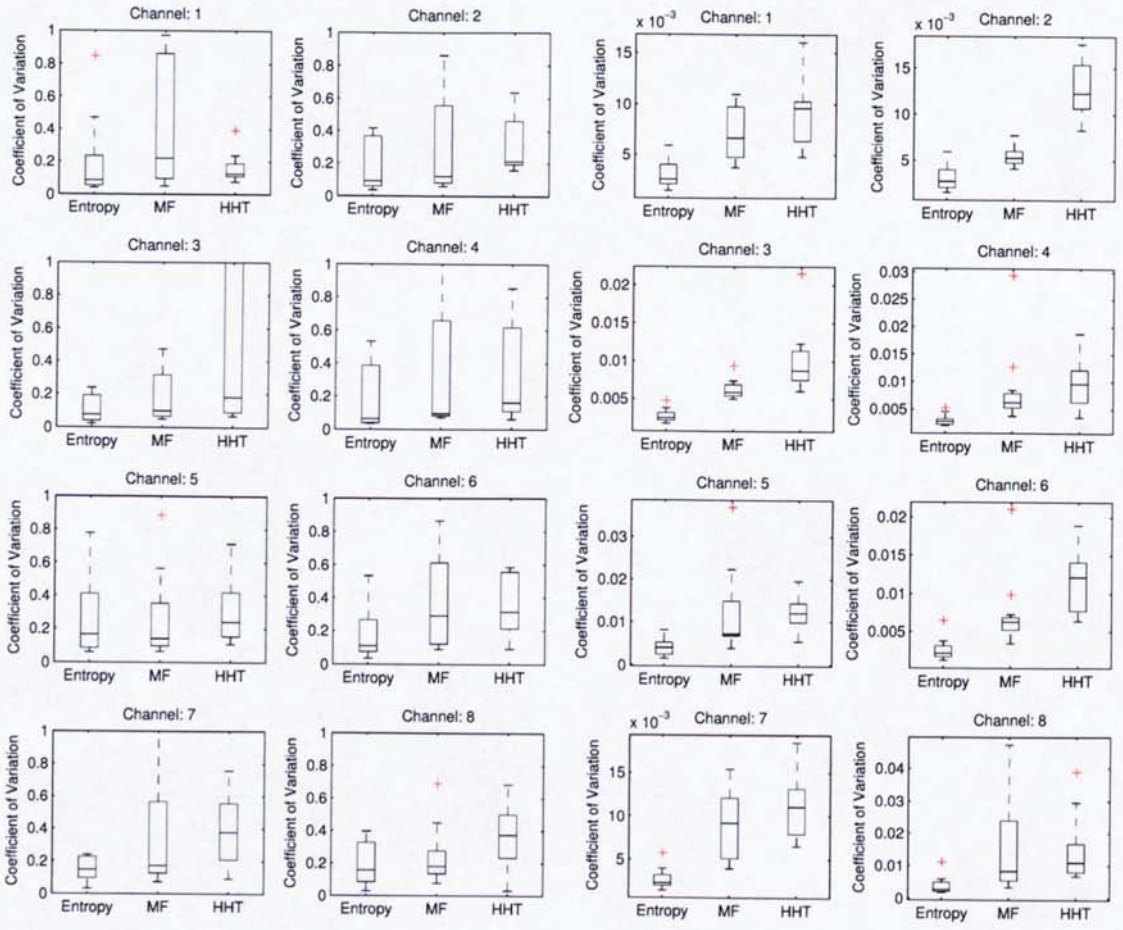

(a) slope (b) point of intercept

Figure 4.5: *Coefficient of Variation comparisons between the linear regression parameters of the Entropy, MF and HHT MF methods for channels 1 through 8. Each box plot includes data from all 12 subjects and all repetitions for window sizes between 1000 and 5000.*

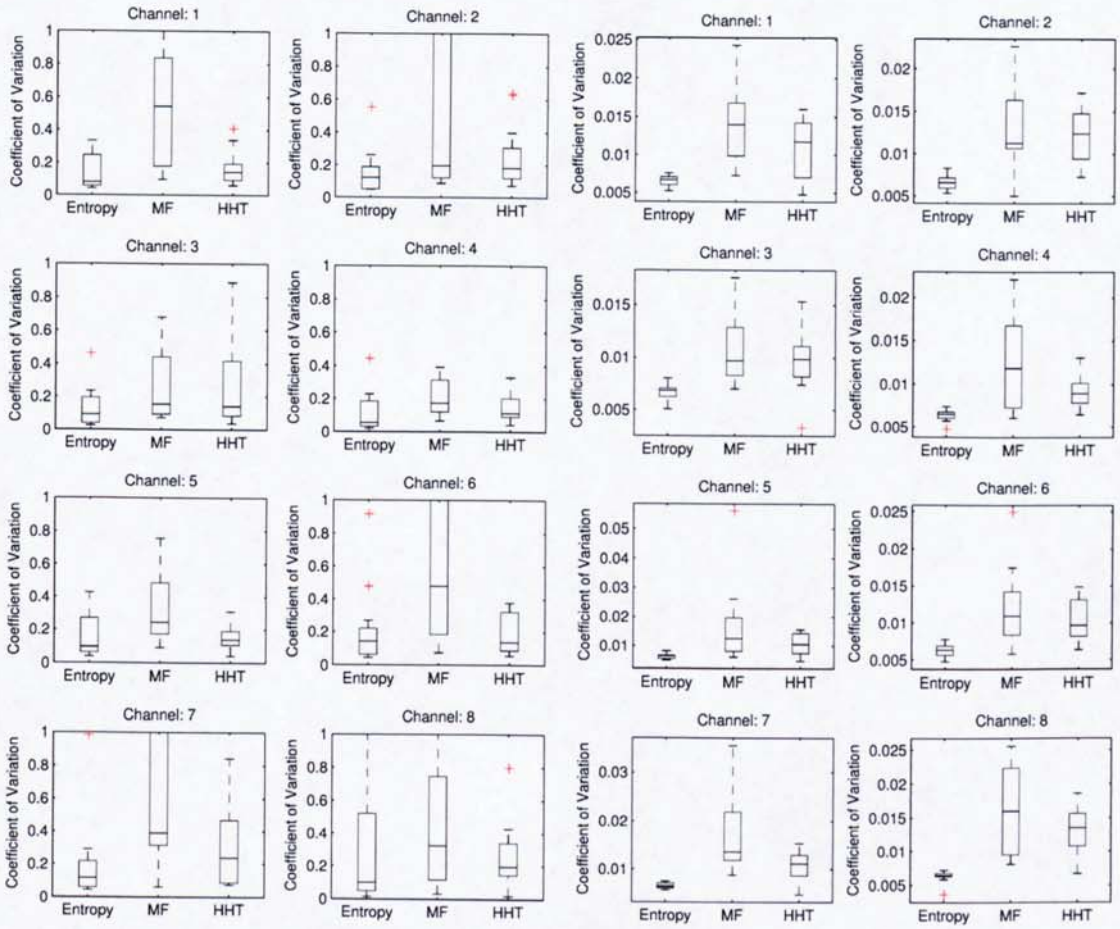

(a) slope (b) point of intercept

Figure 4.6: *Coefficient of Variation comparisons between the linear regression parameters of the Entropy, the MF, and HHT MF methods for channels 1 through 8. Each box plot includes data from all 12 subjects and all repetitions for window sizes between 300 and 1000.*

Regression Parameter	Channel	*p*
Slope	1	0.3714
	2	0.4734
	3	0.6788
	4	0.5094
	5	0.7274
	6	0.1841
	7	0.4830
	8	0.5375
Point of Intercept	1	$4.833\ e^{-06}$
	2	$3.128\ e^{-13}$
	3	$3.403\ e^{-07}$
	4	0.0029
	5	0.0042
	6	$4.256\ e^{-06}$
	7	$7.086\ e^{-07}$
	8	0.0156

Table 4.1: *p values of the median differences between the Entropy, the MF, and the HHT MF linear regression parameters (ANOVA). Window sizes 1000 to 5000.*

Regression Parameter	Channel	*p*
Slope	1	0.3670
	2	0.0655
	3	0.5118
	4	0.9125
	5	0.0066
	6	0.0868
	7	0.4878
	8	0.4377
Point of Intercept	1	0.0001
	2	$9.073\ e^{-05}$
	3	0.0002
	4	0.0004
	5	0.0137
	6	0.0012
	7	$9.188\ e^{-05}$
	8	$9.971\ e^{-06}$

Table 4.2: *p values of the median differences between the Entropy, the MF, and the HHT MF linear regression parameters (ANOVA). Window sizes 300 to 1000.*

The results from the HHT method appear to suggest that it offers the least amount of window sizes robustness of all three methods. One would assume that because the method is ideally suited for nonstationary and stationary data alike, that it would demonstrate the opposite. Although the results for the point of intercept parameter are inline with previously published results, the slope parameter are different by a factor of ten [84]. Perhaps the differences can be explained by the fact that Xie *et al* only examined the muscular fatigue for one repetition of 50s, whereas this chapter has repeated the process ten times and combined the results from each. In addition, the present research focuses on several muscles, whereas previous research only examined the bicep brachii.

4.5 Conclusion

This Chapter has demonstrated a relation between the muscle fatigue and the measure of signal complexity by using the Shannon entropy over a series of repetitive tasks. The signal complexity was compared against the method of mean frequency shift, which is widely considered as a method of determining muscle fatigue. The results from all subjects indicated a decrease in the acquired EMG signals complexity from the MD1, MD2, FD, FCU, TBLAH, ECU, BR, and BB muscles; muscles which are used extensively during lengthy microsurgical procedures. The system entropy in all cases indicated a decrease in the complexity as the muscles fatigued.

The complexity was analyzed by creating a DE matrix of the original time series. This matrix was constructed using successive observations from the original time series and provided a representative picture of the dynamics of the actual system. The singular values of the system were extracted from the embedded matrix, and the Shannon entropy was calculated over time. Trends in the data were illustrated by linear regressions which were fitted to the data.

The robustness of the Entropy, MF, and HHT-MF systems was evaluated by comparing the coefficients of variation of their linear regression parameters over a variety of window sizes. It was found that the complexity method is a fractionally more robust method of analyzing fatigue, and demonstrates that the choice in window size has little effect on the linear regression parameters. Within individual repetitions, each of the measured muscles demonstrated decreases in complexity, which not only indicates the possibility of repeatability of the results on individual subjects, but the potential of determining an overall method to predict fatigue level based on signal trends.

In conclusion, the findings suggest that we can therefore characterize fatigue during a sustained isometric contraction by a decrease in complexity. In addition, the results suggest a potentially more reliable and more robust method of describing fatigue over the existing MF. The results derived from the HHT-MF method also suggest that it can be used for fatigue analysis for different window sizes. As a result, this method will be used in future chapters for determining the fatigue trends in MF and as a comparison with the Entropy method.

5

Surgical Analysis of Fatigue and Tremor

5.1 Introduction

The previous chapters have focused on developing an algorithm which exhibits robustness over different window sizes, and that can be used to analyze fatiguing muscles from dynamic EMG measurements. These analyses have been until now, restricted to a controlled lab environment. However, the purpose of this thesis is to determine the changing body state of surgeons. Therefore, the methods will be applied to actual surgically collected data, in an attempt to predict the changing fatigue levels of surgeons throughout a day of operating.

This chapter will also introduce an alternate measure of fatigue which is more representative: the maximum tremor amplitude. This additional information will provide more insight into how a surgeon's tremor changes while operating, and will ultimately provide valuable information with regards to their accuracy and precision. The temporal trends of this new measure will therefore be evaluated, and be related to the changes in fatigue indices discussed previously.

The aim of this chapter is to try to determine whether or not a surgeon's fatigue level and hand tremor increase, decrease, or remain the same throughout a day of surgery, compared to controls performing desk work. If the fatigue level increases during the day, then perhaps another surgeon should perform the more challenging parts of a

single lengthy operation, or that the more difficult operations should be performed at the beginning of the day.

5.2 Methods

Positional information can be obtained from the acceleration measurements through double integration [92]. An appropriate method for integrating discrete time series is the cumulative trapezoidal algorithm. This method computes an approximate cumulative integral of the data with respect to time. Therefore the acceleration data can be first integrated using this method to obtain the velocity, and integrated again to obtain the desired position.

Integrated electronics piezoelectric (IEPE) accelerometers provide the desired characteristics for this type of application. They are reasonably small and very sensitive. Unfortunately, they are subject to drift. Drift is not a function of the measured variable and is typically defined as an undesirable change over time caused by either low insulation resistance, or leakage current from the input. The measured signal therefore tends to decay towards zero at the time constant's rate. The drift demonstrates itself as a low frequency trend in the signal and is usually minimized with signal conditioning. The suggested integration algorithm is highly susceptible to fluctuations within the accelerometer data, specifically the data trends. Therefore it is imperative that these trends be removed to accurately predict the position of an individual's hand. The following section presents the Empirical Mode Decomposition (EMD) algorithm as a method to remove drift in the acquired acceleration signals as its result preserves the nonlinearity and nonstationarity of the physical data. We also present a new method based on Proper Orthogonal Decomposition (POD) to calculate the maximum tremor amplitude.

5.2.1 Correction of the Accelerometer Drift Artifact

Pinzon et al [93] suggested that the trends of the signal are obtained from the last IMFs of the EMD approach, and can be used as time-space filters. With acceleration data, the trends emerge as low frequency components of the signal. It is therefore possible to apply a high pass filtering to the data or

$$x_k(t) = \sum_{j=1}^{k_1} c_j(t) \qquad \text{, where } 1 < k_1 < n \tag{5.1}$$

Removing the lower frequency empirical data from the accelerometer signal essentially removes the drift trends. However, it is crucial that the right amount of IMFs be extracted from the original signal. If too few are extracted, there is the possibility that the trend could still be retained. Too many could result in loss of data or accuracy of the predicted position. In essence, the correct number of retained IMF's is found by examining the standardized empirical mean, $\hat{x}_k(t)$, and determining where it departs significantly from zero. This is because according to the stopping criterion in Section 4.2.1, the standardized mean for the trend-free IMFs should be close to or equal to zero. In contrast, the standardized mean for any residue or trend would not. The index k is therefore increased from 1, until the mean of the $k+1$ IMF differs substantially from the previous IMFs. We then chose k as the number of indices to keep for the detrending process.

5.2.2 Amplitude Determination

It is possible to generate an enveloped manifold of the hand's global position after the acceleration signal has been detrended and double integrated (Figure 5.1). From this information one can determine the approximate maximum and average amplitudes of the tremor. The tremor information is important as it is directly linked to the performance of the surgeon, and could cause an operation to extend beyond the desired time frame.

Because the displacement measurements are in three dimensions, it would be necessary to retain this information when calculating the maximum amplitude. For instance, if we calculated the amplitudes at each point in time using the 2-norm, we would lose directional information, and the results would be inaccurate. The reason for these inaccuracies can be explained by the fact that the 3D values are rectified. For example, the actual distance between P_1 and P_2 is $\sqrt{\{[1-(-1)]^2+[1-(-1)]^2+[1-(-1)]^2\}}=\sqrt{12}$ (see Figure 5.1). However using the inaccurate rectified method this distance is 0. Hence it is required that an alternate method be found for determining the maximum amplitude; one that retains directional information.

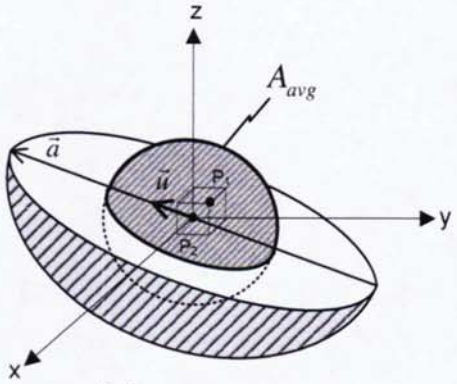

$$\|\vec{a}\| = A_{max}$$

$$P_1(x, y, z) = (1, 1, 1)$$

$$P_2(x, y, z) = (-1, -1, -1)$$

Figure 5.1: *Maximum and average tremor manifolds. As shown in the figure, the maximum manifold is not necessarily symmetrical to the axes, and its shape is not necessarily sphere. The maximum tremor calculated using the presented method is the maximum length of its principal axis.*

5.2.3 Maximum Tremor Amplitude

The maximum amplitude can be found by projecting all coordinate positions from the double integrated acceleration data onto a vector such that the greatest variance by any projection of the data comes to lie on this vector. This vector found using Proper Orthogonal Decomposition (POD), is essentially in the direction of the first Proper Orthogonal Mode (POM) and its length approximates the maximum tremor. Before projecting all coordinates in the direction of the POM, however, we must first define a unitary vector $\vec{u}$ and an elementary orthogonal projector of the form (Figure 5.2)

$$M = I - \vec{u}\vec{u}^T \tag{5.2}$$

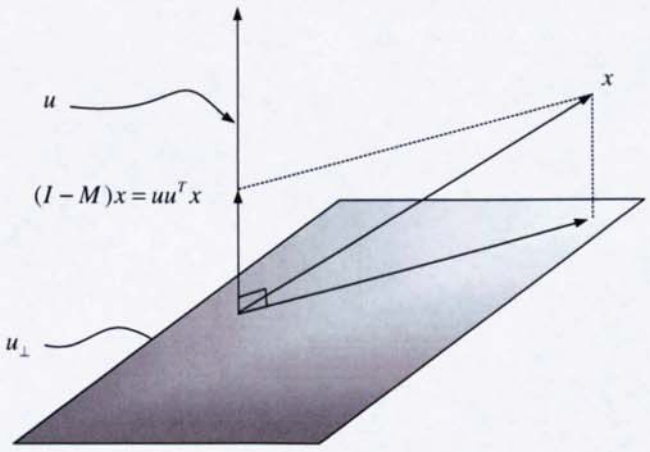

Figure 5.2: *Orthogonal Projector* M *and* $I-M$ *to project the elements of* x *onto* u *and* u^T.

The elementary direction $\vec{u}$ in our case is the dominant eigenvector that is calculated using POD.

$$PP^T = U\Sigma\Sigma^T U^T \tag{5.3}$$

P is defined as the matrix including all x, y, and z coordinates within the tremor manifold, and Σ is the singular value matrix.

$$P = \begin{bmatrix} x_1 & y_1 & z_1 \\ x_2 & y_2 & z_2 \\ \vdots & \vdots & \vdots \\ x_n & y_n & z_n \end{bmatrix} \tag{5.4}$$

Because it is not square, it is multiplied by its transpose to make the matrix square. U is defined as the matrix of all eigenvectors ($\in R^{3x3}$) of the P matrix, whose first eigenvector is $\vec{u}$. By projecting all points in the vector space $x \in R^{3x1}$ onto $\vec{u}$, a new vector, $\vec{a}$, is found that includes all the projected points. The length of the new vector, $\|\vec{a}\|$, is the maximum tremor (A_{max}).

5.2.4 Average Tremor Amplitude

Likewise, the average tremor amplitude provides an envelope which can be considered as a good indicator of an person's tremor. This parameter is determined by first calculating the centroid of all the points in the manifold.

$$x_c = \sum_{i=1}^{n} \frac{x_i}{n}, \qquad y_c = \sum_{i=1}^{n} \frac{y_i}{n}, \qquad z_c = \sum_{i=1}^{n} \frac{z_i}{n} \tag{5.5}$$

It is then possible to determine the average distance of all positions from this centroid. In essence, this is the radius of the average manifold for all hand positions. However, it is the diameter of this manifold, or the amplitude, which we are interested in. This is calculated as follows

$$A_{avg} = \frac{2\sum_{i=1}^{N} \|x_i - x_c, y_i - y_c, z_i - z_c\|}{N} \tag{5.6}$$

5.3 Measurement

5.3.1 Experimental Calibration

The aim of these experiments is to determine the combined accuracy of the integrated, detrended and maximum amplitude algorithms at a variety of frequencies. The maximum amplitudes calculated from each accelerometer's direction are to be compared against the measured signal.

5.3.2 Experimental Setup

The acceleration signals were collected from three tri-axial Delatron accelerometers (Bruel & Kjaer, type 4524B). The first accelerometer had sensitivities of 95.72, 98.18, and 95.26 mV/g in the X, Y, Z directions. The second accelerometer had sensitivities of 97.92, 100.7 and 97.72 mV/g in the X, Y, Z directions. The third accelerometer had sensitivities of 95.96, 95.07 and 101.8 mV/g in the X, Y, Z directions. All three accelerometer sensitivities were calibrated at the factory. The signals from the accelerometers were connected to an Endevco Isotron power supply (Model 2793) and signal conditioner. The signals from the signal conditioning unit were then attached to a Delsys Inc. Universal Input Unit, and finally to National instruments Data Acquisition card (DAQCard 6036E). The acquisition software used was the Delsys EMGWorks Acquisition 3.1.0.5. The data was acquired at a sampling rate of 1 kHz and 16-bit precision.

Three experiments were conducted in total to test separately the three accelerometers. Each comprised of mounting one of the three accelerometers to a permanent magnet vibration exciter (Bruel & Kjaer, Type 4808), which was excited to a variety of frequencies. A digital vernier caliper was mounted vertically as shown in (Figure 5.3) and was used to measure the displacement of the exciter. This displacement was used as the calibration data for the testing algorithms. A frequency generator (TTi, TG550) was attached to the power amplifier (Bruel & Kjaer, Type 2719) and provided the frequency input for the exciter The frequency of the sinusoidal input signal was varied from 25 to 5 Hz. This is around the human postural tremor range. The amplitude of the frequency generator was maintained throughout the experiment at 5.0 V peak to peak. The vernier caliper was zeroed to the center of the exciter, and the frequency was adjusted minutely throughout the experiment to ensure that the calipers did not encounter any excessive impact force. Ten seconds of data was recorded at each frequency.

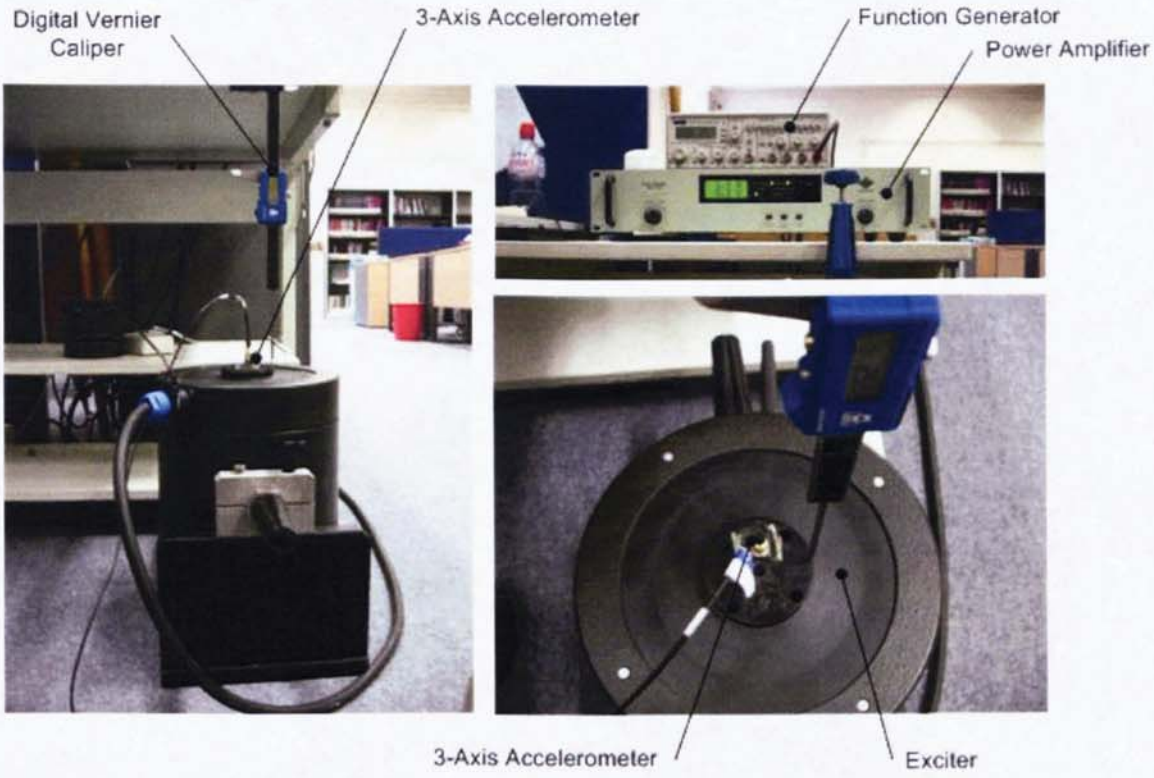

Figure 5.3: *Experimental Setup.*

5.3.3 Surgical Trials

The aim of these experiments is to apply the HHT-MF and Entropy (H) method discussed in Chapter 4, and the newly developed maximum amplitude monitoring method to EMG and acceleration signals captured from surgeons whilst performing their operations, and demonstrate a link between them. Similar to related research, the collection of data was limited to a small number of participants [47].

5.3.3.1 Subjects

Eight healthy surgeons, six male consultants, one male registrar, and one female registrar volunteered to participate in the surgical arm fatigue arm of the study. Twenty non-surgical measurements were taken during the fatigue control arm. The surgeon's ages varied between 31 and 47, with a mean age of 40.63. The non-surgeon's ages varied between 25 and 35, with a mean age of 32.35.

Twelve healthy surgeons, ten male consultants, one male registrar, and one female registrar volunteered to participate in the surgical tremor arm of the study. Nineteen non-surgical measurements were taken during the tremor control arm of the study. The surgeon's ages varied between 31 and 62, with a mean age of 42.17. The non-surgeon's ages varied between 27 and 35, with a mean age of 34.16. All the surgeons and all but one of the non-surgical controls were right handed. The surgical fatigue part of the study consisted of acquiring fatigue measurements whilst performing an operation, while surgical tremor part of the study consisted of acquiring tremor measurements before and after. Although eight of the surgeons had their EMG measured during the operations, the remaining four did not. The length of all the operations have been displayed in Table 5.1, and the four surgeons who did not participate in the fatigue study have been included as #9 to #12.

The control part of the study consisted of acquiring 60 second acceleration measurements before and after several hours of routine desk work, and 30 second EMG measurements at a variety of times throughout the day.

Table 5.1: *Surgery description, length of operation, and the time between sets*

Surgeon	Surgery Description	~ Length (mins)	~ Length between EMG readings (mins)
#1	i), j)	120	8
#2	a), b), c), d), e), g)	600	8
#3	k)	180	2.5
#4	l)	60	0.5
#5	m), n)	240	8
#6	h)	210	3
#7	a), b), c), d), e), g)	480	10.5
#8	f)	180	5.5
#9	a), b), c), d)	210	NA
#10	a), b), c), d)	270	NA
#11	a), b), c), d), e)	420	NA
#12	a), b), c), d), e)	420	NA

a) Tracheostomy
b) Left selective neck dissection
c) Mandibulotomy
d) Resection of tumor left tonsil
e) Left palate reconstruction with radial forearm flap
f) Cochlear Implantation
g) Abdominal skin graft
h) Right combined approach tympanoplasty (stage 2)
i) Panendoscopy
j) Excision biopsy (right brachial cyst)
k) Left Modified Radical Neck Dissection
l) Excision Left Submandibular Gland
m) Left Mastoid obliteration
n) Bone anchor hearing aid

5.3.3.2 Fatigue Measurement Techniques and Analysis

The EMG signals were collected using a Bagnioli-16 system, with a bandpass filter within the signal conditioning unit of 20-500 Hz, and preamplified with a system gain of 1000. The data was captured using the DE-2.1 electrodes, the Delsys EMGWorks Acquisition 3.1.0.5, and a National Instruments DAQ Card-6036E Data acquisition card sampled at a rate of 1000 Hz. The DE-2.1 electrodes are organized in a single differential configuration. It consists of two 10.0 x 1.0 mm Ag contacts separated by 10 mm. The contacts lie within a 41 x 20 x 5 mm casing. The data was acquired at a sampling rate of 1 kHz and 16-bit precision.

The electrodes were placed over the muscle belly of each subject's dominant arm. The deltoid lateral head (MD) and brachioradialis (BR) muscles were chosen for analysis to attempt to compare their fatigue levels, and how they are used throughout a day of operating. These two were chosen as they are used primarily for stabilizing both the arm and forearm, and would be the most likely muscles to fatigue. The skin was cleaned with alcohol and all hair shaved, an interfacing film was attached to each of the electrodes, and these films were then attached to the skin.

The raw EMG signals were analyzed off-line without any pre-processing other than the bandpass of the signal conditioning unit (20–500 Hz). Using the Hilbert Huang Transform [84] and Embedded methods discussed in Chapter 4, the MF and H were calculated respectively. As discussed previously, both methods have demonstrated low variances between different window sizes. A 500 ms window size was chosen so that small bursts of muscle activity during the operation could be captured. As it is impossible to keep each muscle contraction at a specific percent of their Maximum

Voluntary Contraction (MVC), each surgeon's 100% MVC was chosen as 607 μV for the MD and 345 μV for the BR. These were chosen as MVC as it correlated to the average MVC voltage for the controls part of the study. All portions of the EMG signals were scaled as a percent of this maximum. During the day, the collected EMG data was then normalized as a percentage of the MVC, so that it would be represented as the total effort in a percent of the maximum required to complete the task. The choice of 100 %MVC seemed reasonable as most of the signal amplitudes analyzed fell within the 5-30 %MVC. Using the Borg scale to calculate MVC, this is described as extremely weak to moderate muscular activity. Only contractions above 5 %MVC were used to determine the fatigue indices.

5.3.3.3 Tremor Measurement Techniques and Analysis

The tremor measurements were acquired using two triaxial Delatron piezoelectric accelerometers (Bruel and Kjaer Type 4524) attached to the back of the dominant hand on a mounting mechanism as shown in Figure 5.5. Two accelerometers were chosen so that the data from them could be averaged and a more accurate tremor measurement achieved. The mounting mechanism was manufactured from DSM 1770 plastic using a rapid prototype machine, and was positioned on the hand in such a way as to not impede the grip of the volunteers, nor affect the tremor measurements in any way. This enabled tremor measurements to be acquired directly above the hand. The first accelerometer had sensitivities of 95.72, 98.18, and 95.26 mV/g in the X, Y, Z directions. The second accelerometer had sensitivities of 97.92, 100.7 and 97.72 mV/g in the X, Y, Z directions. All three accelerometer sensitivities were calibrated at the factory. The signals from the accelerometers were connected to an Endevco Isotron power supply (Model 2793) and signal conditioner. The signals from the signal conditioning unit were then attached to a Delsys Inc. Universal Input Unit, and finally

to National instruments Data Acquisition card (DAQCard 6036E). The acquisition software used was the Delsys EMGWorks Acquisition 3.1.0.5. The data was acquired at a sampling rate of 1 kHz and 16-bit precision.

Each of the tremor readings were measured over a period of 60 seconds and were taken at the beginning and end of the surgeries. The non-surgical volunteer's tremor measurements were taken on separate working days at a variety of times. The volunteers were asked to perform a standing, dominant handed, micromanipulation task by holding a 2 mm diameter pin between tweezers and attempting to hold it steady within a 4 mm diameter hole as shown in Figure 5.5. Most surgical instruments are stabilized in the hand. The tremor exhibited at the instrument tip is related to the length of the instrument and will be proportional to the hand tremor. We have therefore used hand tremor as a measure of instrument tip tremor. The volunteers were also asked not to rest their arms at any time during the readings and remain standing.

5.3.3.4 Maximum Tremor Determination

As most of the position signals incorporate a small trend, the global position's maximum amplitudes for both the experimental and surgical data were calculated using the method described in Section 5.2.2.1. The raw piezoelectric accelerometer signals were detrended in order for the global position's maximum amplitude to be calculated. It was found that the mean of $\hat{x}_k(t)$ departed from zero at $k_1 = 1$ for the calibration data, and $k_1 = 7$ for the surgical data. k_1 is larger for the surgical data, as there exist more underlying frequencies within the signal. In contrast there exists only one for the experimental data. The acceleration signals from the three axes were integrated twice to give a displacement as shown in Figure 5.4. The direction of maximum variance was obtained from the first POM of the three dimensional displacement. All tremor

positions were then projected onto the POM. The maximum tremor amplitude was determined by the length (norm) of this line. This method was duplicated for each of the accelerometers, and the mean of these amplitudes was used as the maximum calculated tremor.

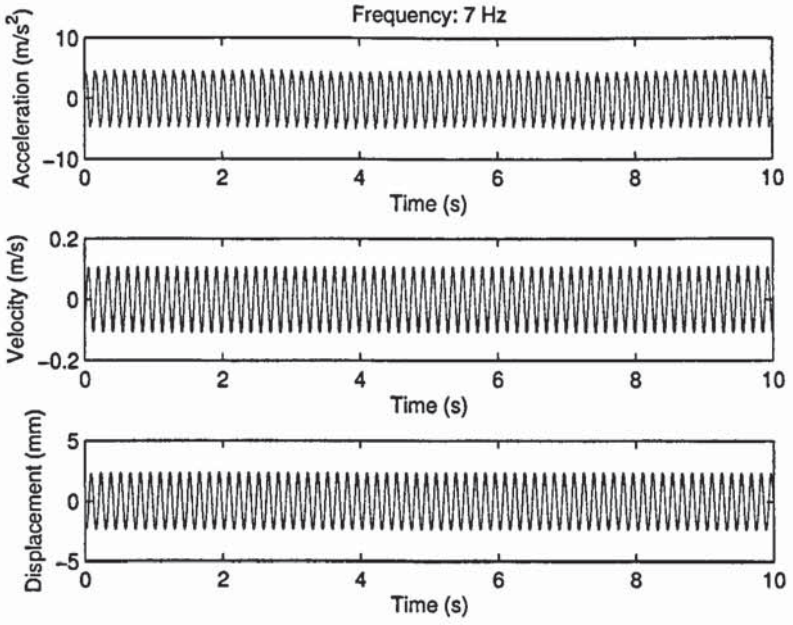

Figure 5.4: *Accelerometer 2, z-axis (top) Acceleration signal at 7 Hz, (middle) Velocity signal derived from the integration of the acceleration signal, (bottom), Displacement signal derived from the integration of the velocity signal.*

5.3.3.5 Average Tremor Determination

The average tremor was only determined for the calibration data using the same detrended data from each of the axes, and following the average tremor determination method described in section 5.2.2.2.

Statistical comparisons were performed on the fatigue and tremor data from all of the volunteers. All statistical and other analysis were performed using the Matlab R2006a Statistical and Frequency Analysis Toolboxes. Any significant differences were defined at ($p > 0.05$).

Figure 5.5: *Accelerometer Placement and demonstration of micro-manipulation task of holding within a 4 mm hold a 2mm pin grasped between tweezers. The surgeons were asked to remain standing during this operation.*

5.4 Results

5.4.1 Experimental Calibration

As expected the resulting position data from the calibration data is also sinusoidal, and 180° out of phase from the acceleration (Figure 5.4). The maximum calculated amplitude from the integrated signal was compared with the measured values. Figure 5.6 shows the experimental results from all accelerometers.

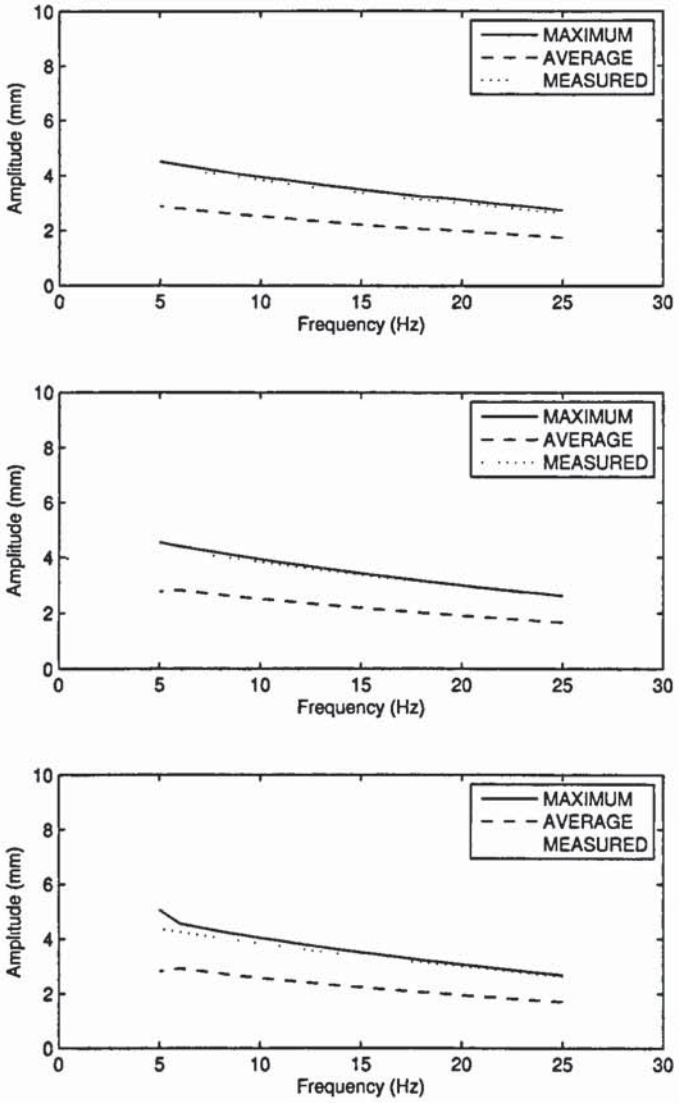

Figure 5.6: *The measured amplitude (small dashed), calculated average amplitude (large dashed), and the calculated maximum amplitude (solid) for accelerometer 1 (top), accelerometer 2 (middle), and accelerometer 3 (bottom).*

The difference between the maximum and measured values appears very small. This is confirmed with Figure 5.7, which shows the mean error between the measured and calculated maximum amplitudes for all accelerometers. It demonstrates that as the frequency is decreased, the error is slightly increased.

The difference between the maximum and measured values appears very small. This is confirmed with Figure 5.7 which shows the mean error between the measured and calculated maximum amplitudes for all accelerometers. The vernier calipers only provided accuracies up to 2 decimal places (mm). However, even with these accuracies, the difference between the measured and calculated is remarkably low. In effect there is a maximum error of less than 7% between the measured and calculated amplitudes at 5 Hz. One of the likely causes for this error could be in the reading of the vernier caliper. A 0.01mm deviation in the caliper reading on a 4 mm tremor would translate to a 0.25% error between the measured and the calculated. Another cause could be drift in the accelerometer's sensitivities, as it is possible that the sensitivities of the factory calibrated accelerometers might have drifted slightly over the time. However at all other frequencies and directions, and more important at the 8-12 Hz postural tremor range, the errors were typically less than 5%. This is reasonably small, and would only constitute a 0.2 mm error on a 4 mm tremor measurement; a very acceptable deviation for a surgeon [60]. It also suggests that this is a potentially viable method of determining the maximum tremor of an individual's hand.

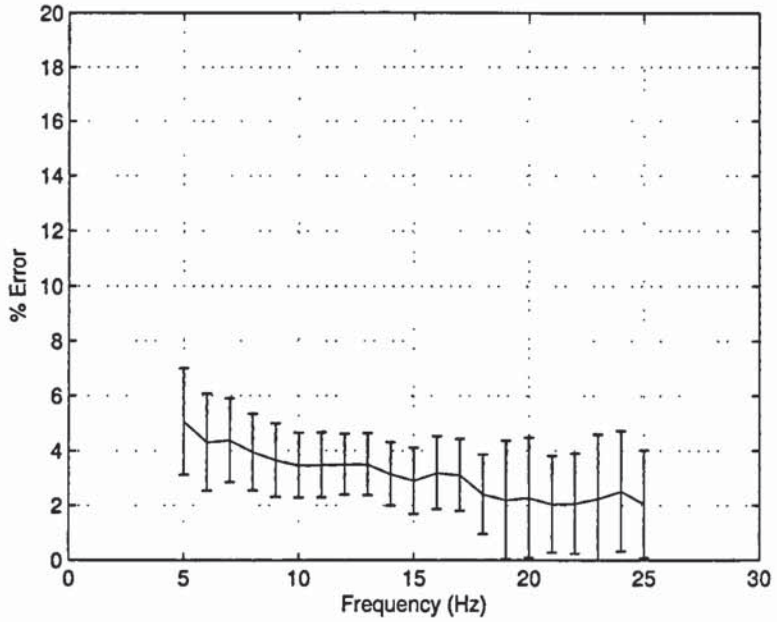

Figure 5.7: *The percentage error between the mean measured maximum amplitude (dashed) and the mean calculated maximum amplitude for all three accelerometers.*

The average amplitude has also been calculated for all sensors and compared with the maximum amplitude. The results indicate that all average amplitudes equate to 63.66 ± 0.55 % of the maximum value. This result is noteworthy as calculating the average displacement of a non experimental single axis sinusoidal signal, we would expect to see a displacement of 63.65 % of the maximum. This can be clarified by applying Equation (5.6) over a period of 1 second for a sinusoidal time series (in the x-direction) having an amplitude of 2mm, a frequency of 2π rad/s and a sampling rate of 1000Hz. This leads to:

$$A_{avg} = \frac{2\sum_{i=1}^{1000}\|x_i,0,0\|}{1000} = \frac{2\sum_{i=1}^{1000}\sqrt{x_i^2}}{1000} = \frac{2(1273)}{1000} = 2.5465mm \qquad (5.7)$$

This suggests that A_{avg} is 63.65% of the maximum displacement (2 times the sinusoidal amplitude or 4mm).

5.4.2 Surgical Fatigue

The results from all surgical EMG measurements indicate a decrease in the MF and H fatigue indices over the length of the operation for both the MD and the BR muscles. The MF analysis on operation #3's MD muscle has been used as an example. All calculated MFs are plotted in Figure 5.8a. A linear regression curve, with 95% confidence intervals, has been fitted to the data. Figure 5.8b demonstrates the mean %MVC (bar graph) for each repetition superimposed with the change in mean MF (line graph). This decrease in MF suggests an increase in muscular fatigue level.

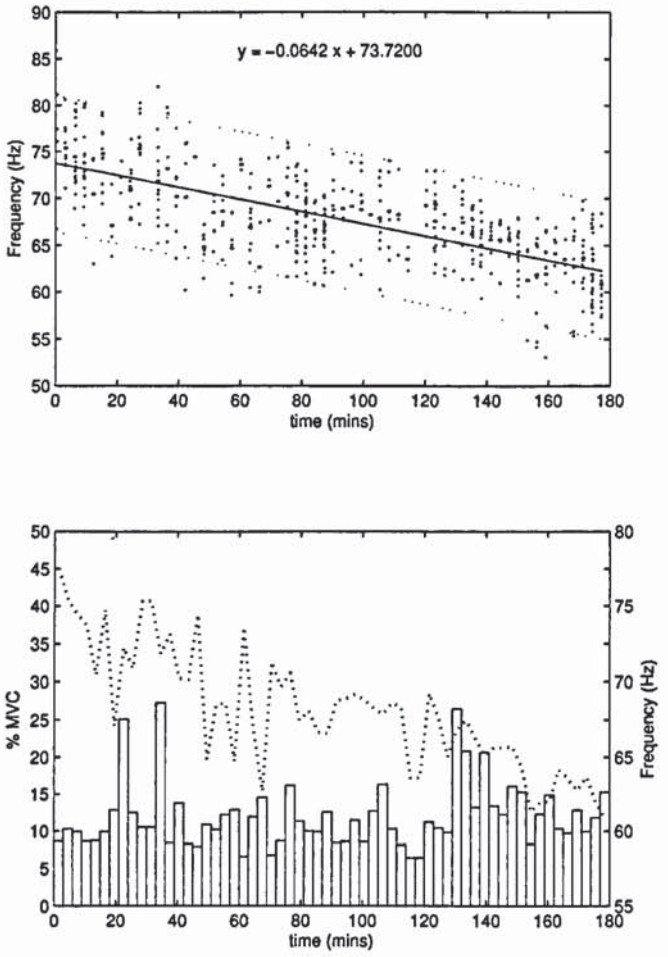

Figure 5.8: *(top) The Mean Frequencies (MF) for the Mid Deltoid (MD) muscle calculated throughout operation #3. The data has been fitted with a linear regression curve with 95% confidence intervals. (bottom) The mean Percent Maximum Voluntary Contraction (%MVC) for each repetition during operation #3 (bar graph). The superimposed dashed line represents the change in the mean of the Mean Frequencies (MF) during each repetition.*

Neither the MF nor the H readings taken at the beginning of the day showed any significant difference between the consultants (#1, #2, #3, #4, #7, and #8) and registrars (#5 and #6), (ANOVA, $p = 0.7193$ (MF:MD), $p = 0.3458$ (MF:BR), $p = 0.525$ (H:MD), $p = 0.4627$ (H:BR)).

By analyzing the percent change of the MF for each operation and correlating it with its length, we discover a linear relationship between the percent change in fatigue index and the length of the operation for both muscles. A linear regression with confidence bounds of 95% has been fitted to the data and is shown in Figures 5.9a and 5.10a. The same holds true for the percent change in H and is shown in Figures 5.9b and 5.10b.

These figures demonstrate the constant increase in fatigue based on the length of the operation. They also demonstrate that it would be possible to predict the change in a surgeon's muscular fatigue index during an operation given a baseline measurement. It is also apparent that the BR fatigues more than 1.5 times as fast as the MD muscle.

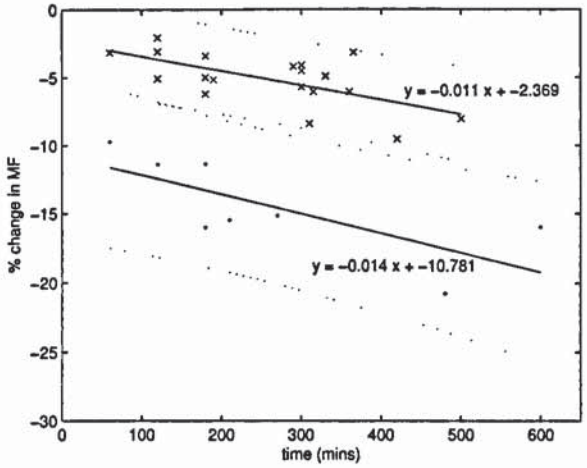

(a) Mean Frequency (MF)

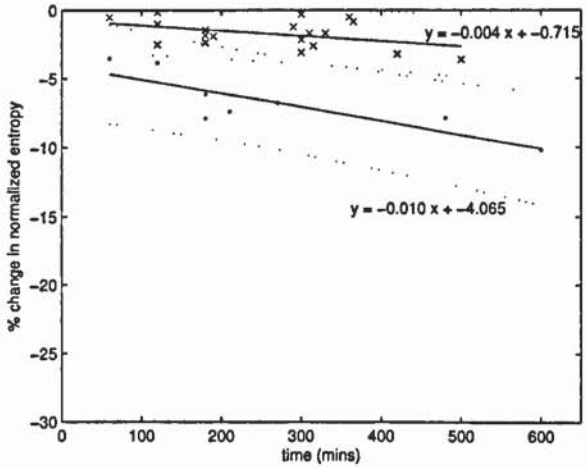

(b) Normalized Entropy (H)

Figure 5.9: *Percent change in fatigue index from baseline of the Mid Deltoid (MD) muscle. This is based on the length of operation and normal working day conditions. Points indicate the percent change of the surgical fatigue index; the solid line is the fitted linear regression to the data, and the dashed lines indicate the 95% confidence interval for the fitted data. . Crosses indicate the percent decrease of the non-operating fatigue index; the solid line is the fitted linear regression to the data, and the dashed lines indicate the 95% confidence interval for the fitted data.*

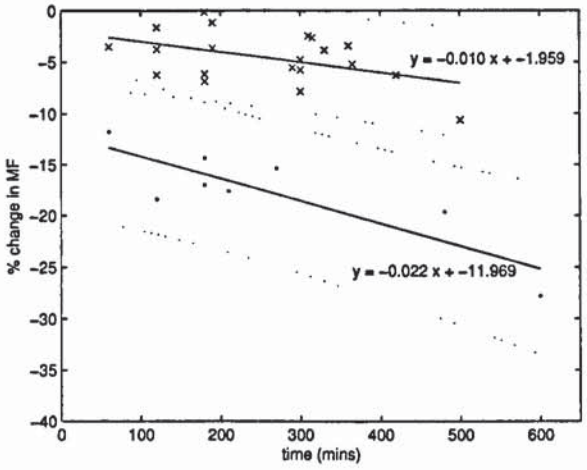

(a) Mean Frequency (MF)

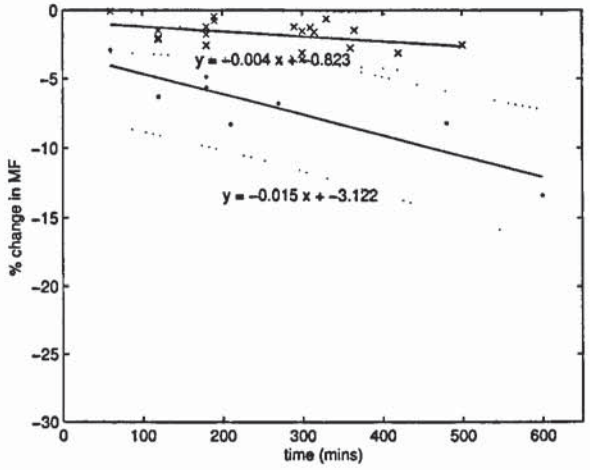

(b) Normalized Entropy (H)

Figure 5.10: *Percent change in fatigue index from baseline of the Brachioradialis (BR) muscle. This is based on the length of operation and normal working day conditions. Points indicate the percent decrease of the surgical fatigue index; the solid line is the fitted linear regression to the data, and the dashed lines indicate the 95% confidence interval for the fitted data. . Crosses indicate the percent decrease of the non-operating fatigue index; the solid line is the fitted linear regression to the data, and the dashed lines indicate the 95% confidence interval for the fitted data.*

In the control arm of the study, the volunteers fatigue index increased throughout the day, although only fractionally in comparison to the the surgical arm (controls (MF): 0.011%/minute (MD), 0.010%/per (BR); surgical (MF): 0.014%/minute (MD), 0.022%/per (BR); controls (H): 0.004%/minute (MD), 0.004%/per (BR); surgical (H): 0.010%/minute (MD), 0.015%/per (BR)). A linear regression with confidence bounds of 95% has also been fitted to the data.

The mean %MVC for both muscles has been averaged over all operations. Figure 5.11 shows that the mean %MVC of the BR muscles is roughly higher than that of the MD muscles. This suggests that the muscular activity of the BR muscle is greater and indicates that the BR muscles are used more than the MD during the operations.

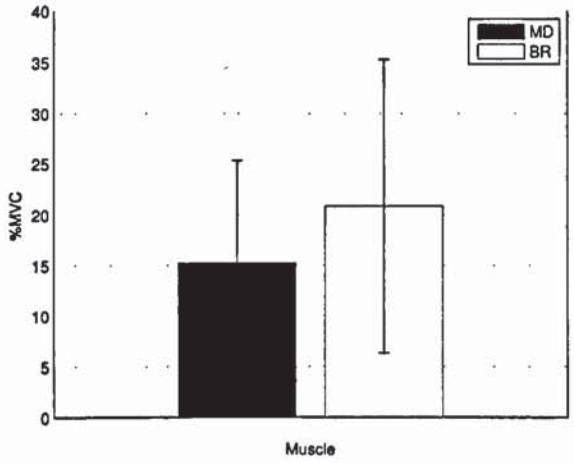

Figure 5.11: *The Percent Maximum Voluntary Contraction (%MVC) contribution of the Mid Deltoid (MD) and Brachioradialis (BR) muscles throughout all surgical operations.*

5.4.3 Surgical Tremor

There was no statistically significant difference between the pre-operative tremor level of the consultants (#1, #2, #3, #4, #7, #8, #9, #10, #11 and #12) and registrars (#5 and #6), (ANOVA, $p = 0.982$). Figure 5.12 demonstrates the pre and post-operative tremor readings from the specified surgeons in Table 1. Irrespective of experience level, there is a tremor increase in all surgical cases, with surgeons #1, #3, #4, #5, #6, #8, #9 being the lowest, and surgeons #2, #7, #10, #11 and #12 being the highest. The large variation between the tremors of the latter are typically indicative of the length of the operations carried out, which is a challenge for precise tool point control.

The results from the surgical tremor readings indicate an increase over the length of an operation at a rate of 0.1 % per minute (Figure 5.13) (Figure 5.12). A linear regression with confidence bounds of 95% has been fitted to the data. It demonstrates the constant tremor increase based on the length of the operation and that it would be possible to predict the change in tremor during an operation given a baseline measurement. It also demonstrates that for every hour of operating, there is a 6.7% increase in tremor.

In the control arm of the study, the volunteers tremor increased throughout the day, although only fractionally (0.8% per hour). A linear regression with confidence bounds of 95% has also been fitted to the data.

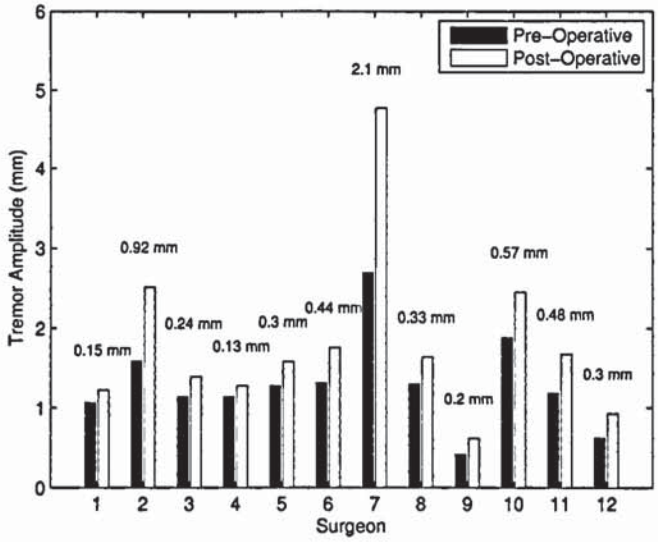

Figure 5.12: *Pre and post-operative tremor readings from each of the surgeons.*

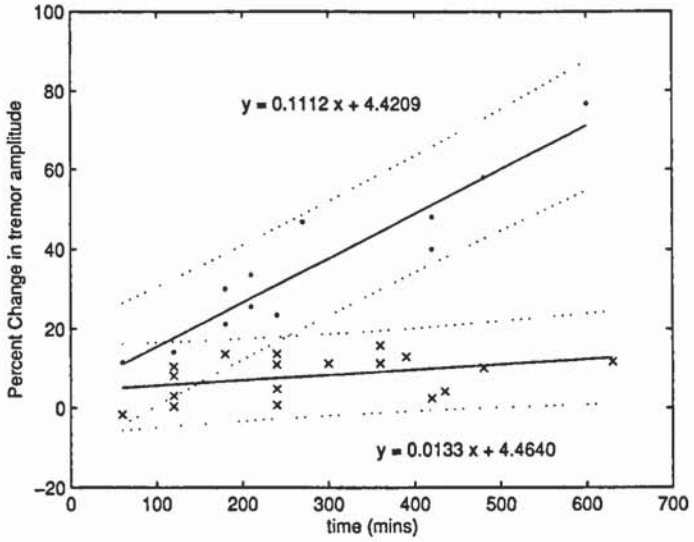

Figure 5.13: *Percent tremor increase from baseline based on the length of operation and normal working day conditions. Points indicate the percent increase of the surgical tremor, the solid line is the fitted linear regression to the data, and the dashed lines indicate the 95% confidence interval for the fitted data. Crosses indicate the percent increase of the non-operating daily tremor, the solid line is the fitted linear regression to the data, and the dashed lines indicate the 95% confidence interval for the fitted data.*

5.5 Discussion

5.5.1 Clinical applicability

This study focused on the development of fatigue and tremor by analyzing either the MF or H, and maximum amplitude shifts over the length of various operations, and correlating these trends with the level of expertise of the surgeon.

It has been demonstrated that there was no statistical difference in the pre operative fatigue indices and tremor amplitudes between the consultants and registrars. The decrease in fatigue index and maximum amplitude throughout the day irrespective of the level of muscular contraction (%MVC), suggests that surgeons fatigue throughout an operation. This suggests that baseline fatigue is not 'improved' with practice and it is likely that all people have different levels of muscular activation frequencies. It also suggests that hand tremor is not 'improved' with practice and it is likely that all people have an intrinsic level of tremor, over which they have little control.

By comparing the differences between the MF and H fatigue methods, we confirm the hypothesis from Chapter 4, that the MF method is more sensitive. This is apparent from figures 5.9 and 5.10, whereby the slope of the percent decrease MF curve is more substantial than that of the H (MF: -0.011, H: 0.004). Although a large difference in the two would make the MF method more able at discriminating fatigue, the actual difference between the two is only marginal (~1.45 times).

We have shown that there is a very little decrease in fatigue index, and a very little increase in tremor amplitude while performing desk work. This leads us to deduce that

the decrease in fatigue index and the increase in tremor during an operation are solely due to the operating.

As is shown from the %MVC, each of the surgeons used their BR muscles at a higher level than they used their MD muscles throughout the operations. Because of this, it stands to reason that both MD and BR muscles should fatigue at different rates. The rate at which the BR muscle fatigued was approximately 1.57 times (MF) and 1.5 times (H) more than the MD as shown in Figures 5.9 and 5.10. This suggests that this muscle is being used more during the operations. This could be due to the fact that most of the actions performed during the operations use the forearms, and that they are continuously lifting the forearms and hands against gravity, and they are not being rested on supports for much of the operation. This correlates with all surgeons reporting that their forearms felt fatigued after a long operation. The linear relationship between the percent change in fatigue index and time allows us to predict the fatigue index of both the MD and BR at the end of an operation based on an initial MF or H measurement.

More interestingly, the percentage change in tremor caused by operating was not significantly different between the trainees and consultants. We would have assumed that as the operations reached a stage of complexity which the trainee had encountered infrequently, their tremor would have increased much more than a consultant who is likely to have performed the operation many times before. This unexpected result may be due to the fact that the consultant took over for the complex part of the operation for both trainees, leading to the trainee not experiencing any additional mental fatigue that could have increased their tremor.

Looking at the overall change in tremor over a day, and taking the controls initially, we demonstrated that there is a gradual, although very small, increase in hand tremor throughout the day, even when not performing physically or mentally demanding tasks. When this is compared to the change in hand tremor induced by operating, the difference is stark. Operating as opposed to performing routine desk work leads to an increase in tremor by a factor of 8.4. The increase in operative tremor is likely to be due to combination of the additional physical and mental fatigue induced by operating. However, it is very difficult to assess which of these two components is responsible for the increase in tremor.

The amplitude of hand tremor is only small even after many hours operating (1.305 ± 0.581 mm pre-operative, 1.818 ±1.078 mm post-operative). However, when a surgeon is holding an instrument, the tremor at the tip will be proportionally greater than the hand tremor, depending on the instrument's length. Therefore the effects of the hand tremor will have a more pronounced effect on accuracy.

These results confirm the hypotheses that there is an increase in tremor caused by operating. The results demonstrate that the decrease in fatigue index is associated with an increase in tremor. This will have an impact on long operations, as often the most technically difficult section, a vascularized free flap reconstruction, takes place at the end of the procedure. Surgeons should therefore be aware that their muscles will be fatigued by this stage and it may be worth a fresh surgeon performing this section of the operation. Short operations can also be very technically demanding. Excessive hand tremor caused by muscular fatigue would therefore decrease the surgeon's accuracy and subsequently the outcome of this operation. Operations requiring high degrees of accuracy should therefore be performed early on in the day. This is unlikely to affect the outcome of the majority of operations. However, if a particularly exacting

step is needed towards the end of a long operation, the surgeon should be aware their tremor will be greater than their baseline tremor and may make this step more difficult.

5.5.2 Limitations

It is very difficult to apply this practically, as there is no specific point at which and individual is fatigued. All that we can determine is that a person does fatigue during an operation. And that the longer the operation, the more fatigued they will be.

5.6 Conclusion

The purpose of this investigation was to quantify surgeon's fatigue level, tremor amplitudes, their level of expertise, and to assess their tremor amplitude changes after performing an operation. This has been compared to the change in tremor and fatigue throughout a day's desk work of healthy control subjects.

Displacement or positional information has been suggested as a more representative method of quantifying an individual's tremor. This Chapter presented a technique that can derive global positional information from accelerometer signals acquired from tri-axial accelerometers. The technique includes novel methods that detrend the original signal, and calculate the maximum and average tremor amplitudes.

This Chapter presents the first evidence of using the EMD method to detrend accelerometer data by breaking down the signal into different intrinsic modes related to frequency information of the data. The drift has been eliminated by removing the lower frequency intrinsic modes functions and residual that contribute to its signal. It has also been demonstrated that manifolds for both an average and maximum tremors can be generated, and directional information about the tremor retained using POD.

The experimental results demonstrate that it is possible to determine tremor amplitude and positional information about an object from its acceleration data by combining new techniques of drift removal, integration and maximum amplitude determination. Consequently, the presented method is particularly valuable within environments which require minimum instrument setup and where positional information is needed,

as was shown with the monitoring of surgeons tremor amplitudes during an operating day.

It was also demonstrated that muscular fatigue and maximum hand tremor increases throughout a day of operating directly proportional to time. No evidence was found to support differences in muscular fatigue between the consultants and registrars. Neither was there any difference in the pre operative hand tremor levels of registrars compared to consultants. The amount of muscular usage correlates with the level of muscular fatigue, with the brachioradialis muscle being used more than the mid deltoid and it fatigues more rapidly. In addition the results demonstrate that there is an increase in hand tremor, induced by operating of 0.1% per minute (6.7%per hour).

Surgeons should be aware that their fatigue levels and tremor will increase as an operation progresses. Therefore, if possible, the more complex parts should be performed as early as possible, or, in the case of very long operation, a change in surgeons may be necessary.

6

Tremor Prediction Analysis

6.1 Introduction

The following Chapter describes a method of using fatigue data captured from the EMG to predict an individual's tremor information. Because of the restriction associated with attaching devices to the hand while performing a surgery, this relatively non-invasive measure could ultimately be quite useful for providing a surgeon's hand positional information. There are several ways of predicting these characteristics on systems such as this. One such method, and the one used for in this Chapter, is by using an Artificial Neural Network (ANN).

ANNs can be considered imitations of neural systems. They allow us to infer information from a series of inputs, and predict an outcome based on a training regime. They do so by mathematical modeling a system based on biological neural model made up of interconnected artificial neurons. They are comprised of weights and biases, which are combined within the network, and optimized to suit a specific application. Similar to biological systems, these networks need to be trained for a specific application, and retrained should the system change. One of the benefits of using neural networks is that they allow us to explore independent functions within a system, or a combination of systems, and optimize them to work as a single unit. In essence, little understanding about the desired system is required for the network to make its prediction. This makes them ideal for predicting the outcomes of biological systems,

which comprise from the cell level a hierarchy of systems that work together to perform specific tasks.

Neural networks have proven themselves in a variety of fields as satisfactory prediction methods. Applications have included load position and weight predictions along a beam embedded with Fibre-Bragg sensors [62], as well as the estimation of high precision temperature measurement [63] . Although neural networks have been typically adapted to nonlinear dynamic systems, they have also been utilized with EMG and accelerometer measurements to predict specific underlying parameters of many biological systems. Some neural network EMG research has been completed in the determination of muscle fatigue [64, 65], however, most of the efforts have been directed towards the recognition of limb motion [66-69], filtering [70], and control [71]. In addition, they have been used in tremor classification [73, 74], and involuntary motion cancellation which could be applied to microsurgery using telerobotics or handheld instruments [75, 94]. However, none of these studies have used a fatigue index from EMG measurements to predict the outcome of an individual's tremor amplitude.

It is proposed that by collecting EMG and acceleration measurements from various muscles during muscular activity, it should be possible to train a dynamic neural network capable of predicting an individual's tremor amplitude from their fatigue index.

6.2 Methods

6.2.1 NARX Neural Network

Although there are various types of dynamic networks, the Nonlinear AutoRegressive with eXogenous inputs (NARX) type, is preferred for this application [95]. The reason is that it is a recurrent network with sequential data and feedback connections within its structure, thus making it ideal for time series modeling [96]. The equation that defines the NARX model is:

$$y(t) = f\{y(t-1), y(t-2), \ldots, y(t-n_A), u(t-1), u(t-2), \ldots, u(t-n_u)\} \quad (6.1)$$

where $y(t)$ is the dependent output,

$u(t)$ is the independent exogenous input or fatigue index (MF or H),

n_A represents the output order,

n_u represents the input order,

The predicted data is therefore dependent on previous predictions, and the input data.

NARX networks have been used as predictors [97, 98], for nonlinear filtering and control [99], and more importantly, for modeling of nonlinear dynamic systems [100]. NARX networks typically take on a parallel configuration for their operation form (Figure 6.1b). However, for training purposes, they can take on the series-parallel configuration (Figure 6.1a). The benefit of using this type of configuration during the training stage is that it is possible to use the actual data as training input, resulting in a

better approximation of the trained function. As well, because the network has a pure feedforward configuration, a static backpropagation can be used for training. Following this step, the trained network can then be converted to a parallel configuration for the prediction purpose.

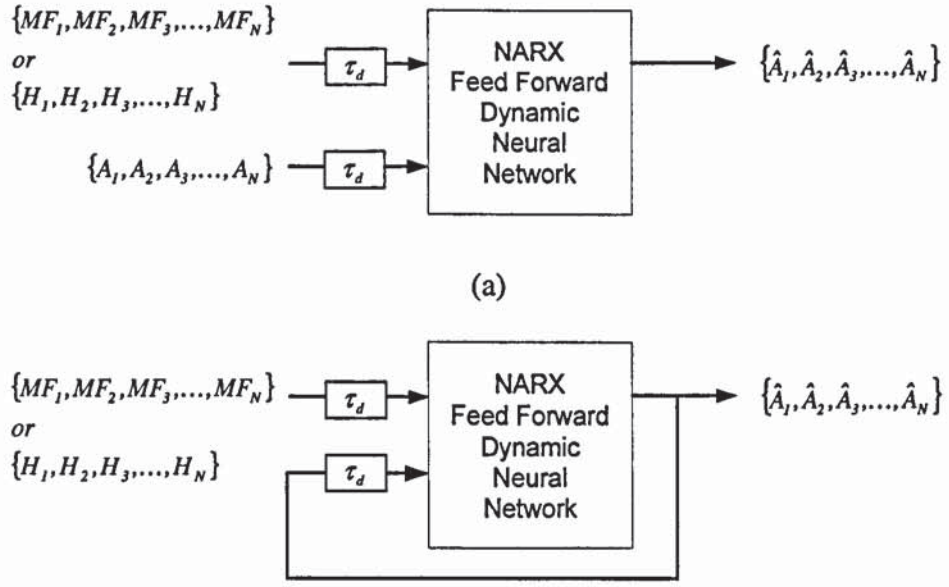

Figure 6.1: *a) Series-Parallel configuration for training of the NARX neural network using a tapped delay. b) Parallel configuration of the predictive NARX neural network using a tapped delay.*

6.2.2 Network Normalization

The normalization of the data ensures that all the network weights are closest to their optimum values. The data is normalized by setting the maximum value to 1, and the minimum value to -1. All other values are scaled with respect to these limits as follows:

$$A\{t\} = \frac{(A_{max} - A_{min})(u\{t\} - u_{min})}{(u_{max} - u_{min})} + A_{min} \tag{6.2}$$

6.2.3 Network Initialization

Once initialized, the fatigue data in the form of entropy or MF shifts can then be used to predict the maximum tremor amplitudes, as shown in Figure 6.2. A generalized model can be produced using a single layer feed-forward neural network and an activation function that depends on the modeled data and the desired result. Essentially for back-propagation learning, it is desirable to have the activation function differentiable and bounded [101]. The most common choices are the Gaussian functions, and sigmoidal functions, such as logistic and hyperbolic tangent. The hyperbolic tangent activation function, however, is ideally suited for the predictive application as it produces negative and positive values, {-1, 1}. Better numerical conditioning allows it to achieve faster training than a function that only produces positive values, such as the logistic functions, [102]. Ideally, a hyperbolic tangent activation function is applied to the inputs, and a pure line function to the outputs. The pure line ensures the output values extend beyond the normalized initial trained limits.

This proves beneficial, as the tremor values lay above the original limits as the individual fatigues.

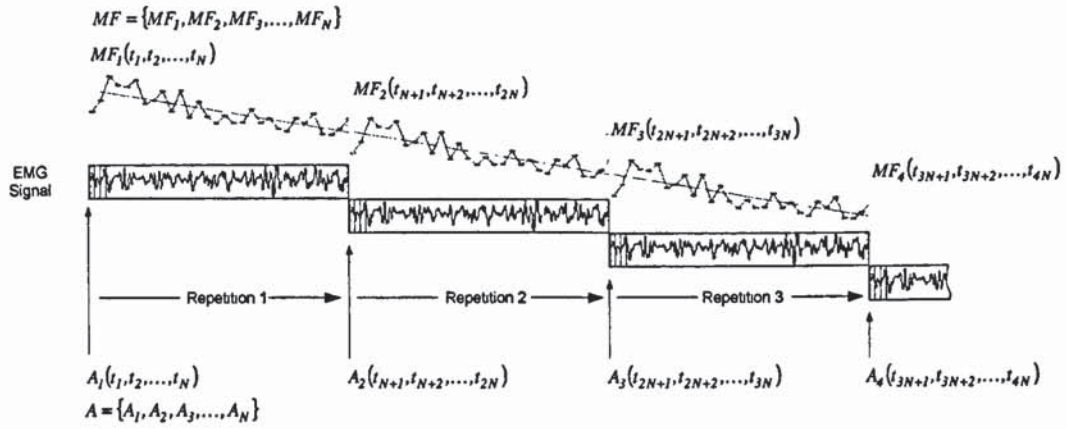

Figure 6.2: *Initialization configuration for the data used in the predictive NARX neural network.*

6.2.4 Training the Neural Network

Training of the neural network is the stage in which the training inputs are fed into an initialized neural network. Weights and biases of the neural network are trained to fit the desired function by using the backpropagation algorithm depicted in Figure 6.3. The training algorithm is an iterative process, whereby the Mean sum of the Squared Error (MSE) cost function between the target and predicted values is minimized according to either a regularization or early stopping limit. These limits ensure that the neural network is not over trained.

$$x_{k+1} = x_k + g_k \alpha_k \tag{6.3}$$

Where x_k, is the vector of current weights and biases,

g_k is the current gradient function

α_k is the current learning rate

Bayesian Regularization (BRN) is one such training algorithm that performs regularization, whereas early stopping can be performed with Resilient backPropagation (RP). The performance of these two training methods can be compared by examining their MSE, as was done by Danesman *et al* in the nonlinearity estimation of different thermocouple types [63].

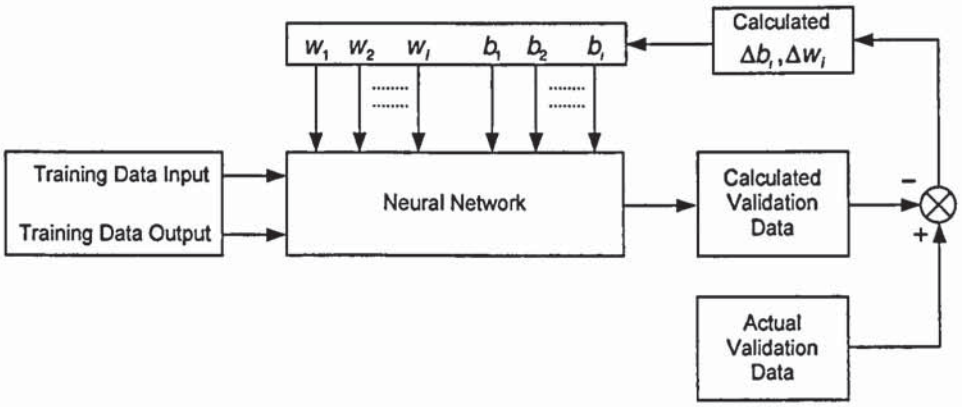

Figure 6.3: *Neural Network Back Propagation Training Scheme.*

6.2.5 Early stopping technique

The network is optimized by examining the validation error between the calculated validation output and the experimental output. As expected, in non-linear networks, the fitted function should reach a local minimum and then diverge, as the data is over-trained, or over-fitted. Essentially, this is because the more you train the data, the more the network will try to fit the training curve, thus increasing the error between the two predictions. Early stopping gets its name from the point at which the validation error reaches a minimum, and where training should be stopped to minimize any noise from the data. The Resilient Backpropogation algorithm, which has been proposed as an early stopping method for this study, tracks sign of the derivative of the error with respect to the weights rather than its magnitude [103].

6.2.6 Regularization technique

Bayesian Regularization is a modification of the Levenberg-Marquardt algorithm [104]. It improves the generalization by modifying the cost function, or the MSE [105, 106]. The new function ensures that the weights and biases are smaller, thereby reducing the likelihood that the network will over fit the data. It modifies the function by adding a term that tracks the Mean sum of the Square of the Weights (MSW). Essentially, the algorithm converges to a solution when the MSE and MSW remain constant over several iterations.

$$\varphi_{MSER} = \gamma\varphi_{MSE} + (1-\gamma)\varphi_{MSW} \tag{6.4}$$

$$\text{Where } \varphi_{MSE} = \frac{1}{N}\sum_{i=1}^{N}(e_i)^2, \tag{6.5}$$

$$\varphi_{MSW} = \frac{1}{M}\sum_{k=1}^{M}(w_k)^2 \tag{6.6}$$

e_i are the errors between the target and predicted values,

and w_k is the weights of the system

and γ is the performance ratio.

6.2.7 Assessing the quality of the fit

Following the training stage, the neural network's predicted outputs can then be compared with the real outputs to assess the network's quality. This is accomplished by examining the Root Mean sum of the Square of the Error (RMSE). A small RMSE designates a small error between the two data sets. This error is calculated as follows:

$$\varphi_{RMSE} = \sqrt{\frac{1}{N}\sum_{i=1}^{N}(A_i - \hat{A}_i)^2} \tag{6.7}$$

where φ is the RMSE,

A is the target output,

$\hat{A}$ is the predicted output from the Neural Network,

N is the number of data points.

6.3 Measurements

The following section will outline the procedures followed to create the neural network that predicts the maximum tremor amplitude from the fatigue index of captured EMG signals. The EMG data was collected as described in Section 3.3.1 – 3.3.3.

6.3.1 Tremor measurement techniques and analysis

The tremor measurements were acquired using two triaxial Delatron piezoelectric accelerometers (Bruel and Kjaer Type 4524) attached to the back of the dominant hand on a mounting mechanism as shown in (Figure 5.5). Two accelerometers were chosen so that the data from them could be averaged and a more accurate tremor measurement achieved. The mounting mechanism was manufactured from DSM 1770 plastic using a rapid prototype machine, and was positioned on the hand in such a way as to not impede the grip of the volunteers. The first accelerometer had sensitivities of 95.72, 98.18, and 95.26 mV/g in the X, Y, Z directions. The second accelerometer had sensitivities of 97.92, 100.7 and 97.72 mV/g in the X, Y, Z directions. Both accelerometers had their sensitivities calibrated at the factory. The signals from the accelerometers were connected to an Endevco Isotron power supply (Model 2793) and signal conditioner. The signals from the signal conditioning unit were then attached to a Delsys Inc. Universal Input Unit, and finally to National instruments Data Acquisition card (DAQCard 6036E). The acquisition software used was the Delsys EMGWorks Acquisition 3.1.0.5. The data was acquired at a sampling rate of 1 kHz and 16-bit precision.

The volunteers were asked to perform standing, dominant handed, micromanipulation tasks for a period of time between each weight extension set. The micromanipulation tasks involved holding between tweezers a 2mm pin, within a 4 mm pin hole as shown in (Figure 5.5). To make the tasks even more challenging, the volunteers were asked not to touch the sides of the hole. These tasks had the added challenge of being performed under a microscope. Each micromanipulation task lasted 30 seconds. In addition, a tremor reading was obtained as a baseline before the arm extension exercises. The volunteers were also asked not to rest their arms at any time during the readings and remain standing.

The maximum amplitude for each volunteer was calculated from the raw piezoelectric accelerometer signals using the method described in Section 5.2.3. This method was duplicated for each of the accelerometers, and the mean of these amplitudes was used as the volunteer's tremor.

6.3.2 Neural Network description

Following the methods discussed in Section 4.2, the MF and Entropy data from the EMG signals were calculated using the HHT and Entropy methods respectively at intervals of 500 ms. It should be noted that neural networks require large amounts in order to train and predict results accurately. For this reason, the surgical data was not chosen because it provided only two tremor amplitudes measurements (pre and post operative) for each individual. Instead, the equivalent experimental tremor data from the laboratory was chosen for this application as it provided eleven such amplitude measurements. Consequently, this supplied 600 points of input data from each channel. Although this is still considered a relatively low number of training points,

the purpose of this chapter is to demonstrate the predictive ability of the NARX networks.

Two laboratory trials were conducted for each of the fatigue methods: the first with all EMG channels used, and the second with only CH 2 and CH 4. Eleven amplitudes were calculated. This included one tremor reading taken as a baseline before any exercise, nine between each exercise set, and one after all the sets were completed. Because a maximum amplitude calculation was determined for each of the micromanipulation repetitions, it was assumed that the tremor remained the same over those periods. The amplitude data was then offset by 2 ms so that the baseline and final amplitudes could be predicted by the network, and so the network incorporated 600 data points to match the MF and H data. In essence, had this not been performed, only ten tremor measurements could have been examined, rather than the eleven.

All neural networks were designed using the MatLAB R2006a Neural Network toolbox. Preliminary tests were performed on the BRN and RP trained networks in an attempt to determine the number of neurons in the hidden layers. It was decided that good prediction accuracy would be more desired than faster training times. Consequently, after several trials with different number of neurons it is found that 20 neurons in the hidden layers achieved the desirable results (RMSE < 0.1). The BRN and RP neural networks were trained in a series-parallel configuration using a two sample delay, 20 neurons in the hidden layers, and all 600 original data points from the MF / H and actual tremor data. This process was repeated 30 times for each of the network scenarios, and the mean training time and RMSE for each network were calculated. Once trained, however, the networks were then converted to a parallel configuration using the *sp2narx* command in MatLAB. Once again, all 600 points were used during this stage. Although this new parallel network was validated using

all the original MF or Entropy data, the second input was provided by the predicted amplitude. The predictions from the parallel network were then compared against the target data using once again the RMSE between the two.

The above procedure was duplicated using a linear regression of the MF/ H as input for subject 2's data in an all channel configuration. The same number of points were used as inputs and outputs as before, however, each data point was now a point on the linear regression curve.

6.4 Results and Discussion

The accuracy for each of the trained networks is demonstrated by comparing the RMSE for the parallel configuration using both the BRN and RP training algorithms. The predictive ability of the created neural networks was assessed by comparing the results from the Entropy and MF data, in the all-channel and two-channel configurations. Both the time to complete the network training, and the average RMSE from 30 trials for each of the individuals have been tabulated in Tables 6.1 through 6.4. Although the accuracy of the fitted data is much better for the BRN networks (RP min: RMSE = 0.16 mm ; BRN min: RMSE = 0.012 mm), the network training times appear to always be lower for the RP algorithm (RP: time < 11.38 s ; BRN: time < 315 s). This was the case whether the networks had been trained with either of the fatigue indices, in a two-channel or all-channel configuration. Although the training times of the BRN and RP networks are more similar in the two-channel configuration, the BRN training times extended up to and beyond five times the training times for the RP networks. These lower training times are the result of the early stopping algorithm used, which prevents the network from over fitting the data. In fact, because the RP networks train much faster, it makes them very suitable for a real time training application. However, because of the nature of the desired application, and that the network would have to be trained offline before any prediction could be performed, these training times are essentially inconsequential. The BRN algorithm would therefore be the most appropriate choice of training algorithm for the required application, as it produces the best accuracies.

Additionally, the overall results clearly demonstrate that the RMSE, which is generally lower for the BRN training algorithm in the two-channel configuration, is even more pronounced in the all-channel configuration (BRN-2 min: RMSE = 0.11 mm ; BRN-8

min: RMSE = 0.012 mm). This result is true whether the Entropy or the MF data had been used as input. The reason for the lower RMSE in the BRN training is due to the regularization technique, whereby the extra training epochs provide an even closer fit to the desired function.

As an example, the various trained network configurations for individual 2 have been determined. The results, which demonstrate the differences between the actual vs predicted data, are displayed in Figure 6.4. It shows the closeness of the fit to the real data for all configurations. The errors, although occasionally at around 20%, are reasonably accurate. For example, on a 4 mm tremor, this would correspond to an error of only 0.8mm. In general, however, the errors lie below 5%, and much less than this for the BRN method, whose maximum errors are less than 2%. In essence, the trend of the individual amplitude predictions follows the actual data extremely well.

The same procedure has been applied to the other individuals and displayed in Figure 6.5. Clearly, the results demonstrate the prediction errors of BRN trained networks in the all-channel configurations are much lower than all other configurations. In addition, the choice of fatigue index does not appear to have much of an effect on the RMSE, other than with the RP trained, all-channel configurations. These results confirm that the BRN trained networks provide the best prediction accuracies.

	2 Channel		All Channels	
Individual	BRN	RP	BRN	RP
1	0.279403	0.665673	0.0502	0.297597
2	0.992547	0.888676	0.54814	0.848022
3	0.648272	0.780883	0.012989	0.462385
4	1.049437	0.676295	0.020853	0.40776
5	0.692879	0.641286	0.739009	0.537544
6	0.765186	0.614016	0.017794	0.763308
7	0.113459	0.3148	0.009786	0.156983
8	0.542623	0.713358	0.198789	0.466299
9	0.504696	0.587514	0.123223	0.625167
10	0.553358	0.74843	0.376367	0.682157
11	0.586304	0.642312	0.057477	0.604888
12	0.443433	0.701922	0.153676	0.363085

Table 6.1: *Root Mean Square Error (RMSE) (mm) of the BRN and RP algorithms between the predicted and real tremor amplitude, using the MF data as input data for all subjects.*

	2 Channel		All Channels	
Individual	BRN	RP	BRN	RP
1	11.6023	8.494714	210.2723	11.37704
2	38.28113	8.282215	315.0743	9.801138
3	34.95427	8.245952	289.3569	9.376849
4	17.39431	8.274401	263.2259	9.685439
5	9.676334	8.310152	203.1873	9.798204
6	56.26958	8.28008	215.0942	9.333735
7	51.86663	8.514876	315.6996	9.34302
8	11.85428	8.277426	235.36	9.379464
9	9.324921	8.333179	207.2166	9.418797
10	10.04144	8.30384	198.505	9.392336
11	19.00886	8.35658	287.5753	9.355251
12	6.407174	8.543231	225.4356	9.42863

Table 6.2: *Time to train (sec) MF data using the BRN and RP algorithms for all subjects.*

	2 Channel		All Channels	
Individual	BRN	RP	BRN	RP
1	1.450584	0.923424	0.046725	0.772221
2	0.831053	0.659838	0.051949	0.786539
3	1.031036	0.686803	0.088875	0.471297
4	1.923409	0.697363	0.038385	0.592914
5	1.145964	0.843334	1.046155	1.250057
6	1.020878	0.81816	0.011596	0.51683
7	0.946898	0.461436	0.026471	1.025816
8	0.988672	0.567852	0.068853	0.400176
9	0.934146	1.078784	0.093631	0.496632
10	1.02081	0.622619	0.038304	0.350867
11	1.046528	0.628243	0.14856	0.463813
12	1.086071	1.058219	0.049089	0.481329

Table 6.3: *Root Mean Square Error (RMSE) (mm) of the BRN and RP algorithms between the predicted and real tremor amplitude, using the Entropy data as input for all subjects.*

	2 Channel		All Channels	
Individual	BRN	RP	BRN	RP
1	50.07104	9.960761	241.2036	10.30634
2	40.96885	9.527616	352.9644	10.41199
3	26.08048	9.671134	243.3078	10.52834
4	52.60241	9.675444	232.0238	10.55788
5	28.83118	9.713516	237.9347	10.58495
6	39.46535	9.664217	261.773	10.4819
7	53.65632	9.563824	289.653	10.50902
8	27.20148	9.740185	249.9135	10.44494
9	25.71538	9.47465	191.6706	10.27183
10	28.74208	9.67139	264.9664	10.54945
11	25.89765	9.534198	230.3786	10.47693
12	25.03465	9.74548	181.3349	10.49796

Table 6.4: *Time to train (sec) Entropy data using the BRN and RP algorithms for all subjects.*

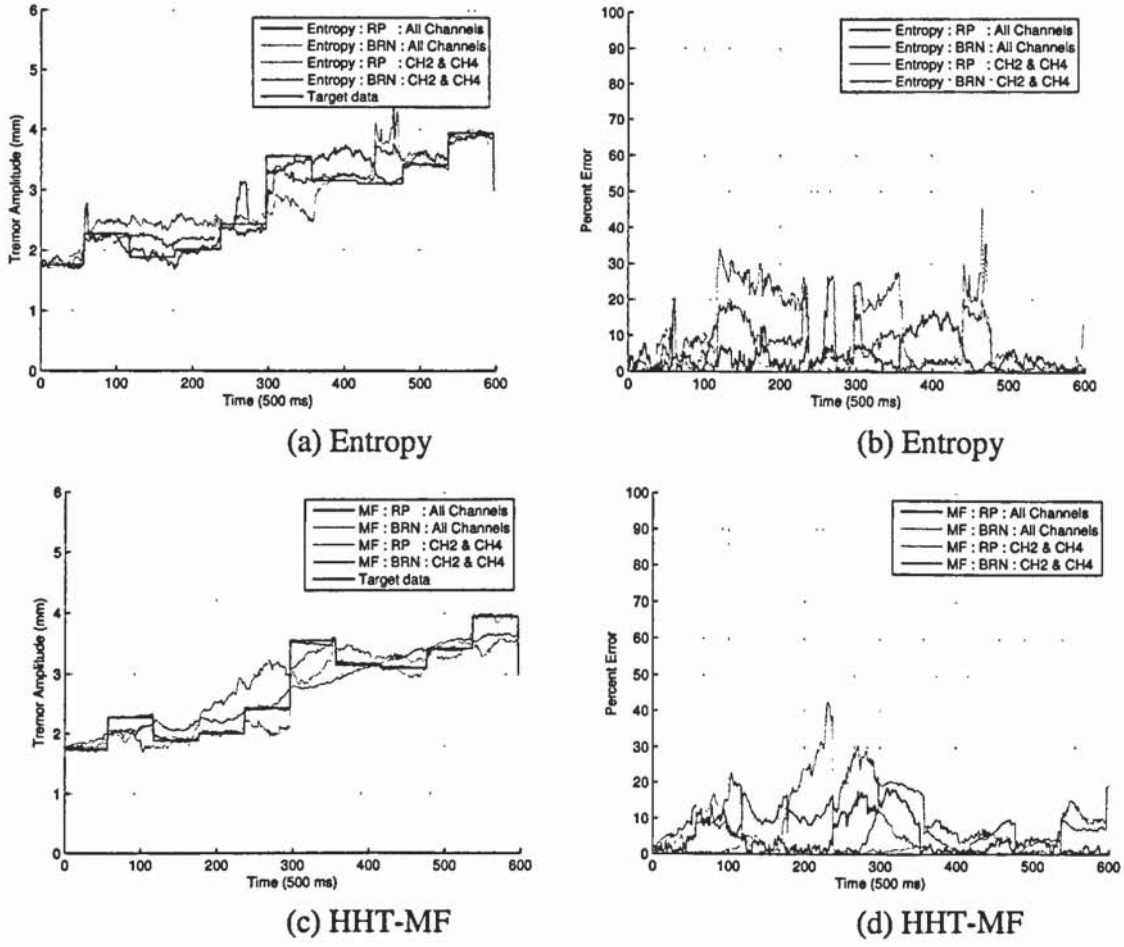

Figure 6.4: *Subject 2's tremor amplitude scenarios predictions. a) Tremor amplitude approximation for the different training scenarios using (a) Entropy & (c) MF data as input. Percent error between measured and predicted tremor amplitudes for the different training scenarios using (b) Entropy & (d) MF data as input.*

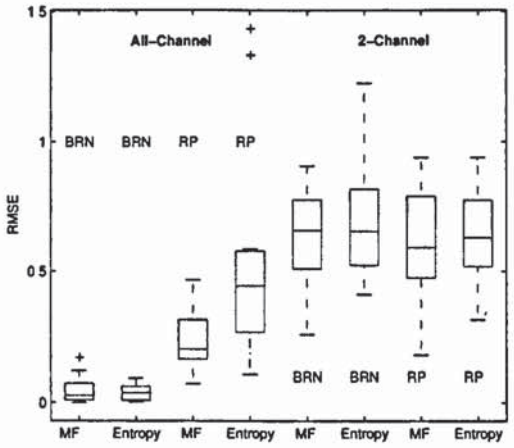

Figure 6.5: *Range of the RMSE values (mm) between the predicted and real data for the various trained network configurations.*

In general, the predicted output appears to fluctuate a great deal. This is the result of the actual mean frequency rather than the linear regression curve being used as input. Consequently, the data fluctuates substantially as is shown in Figure 4.2. It would be assumed that if the linear regression curve was used instead as input, that any fluctuations between sequential data points would be smoothed out in the prediction. Figure 6.6 demonstrates that this is in fact true. In addition, the predicted data is shown to be only fractionally less accurate (BRN/All Channel-RMSE: 0.2506 mm, RP/All Channel-RMSE: 0.2483 mm) for this method than by using the non-regressed MF as input data (BRN/All Channel-RMSE: 0.1601 mm, RP/All Channel-RMSE: 0.2245 mm).

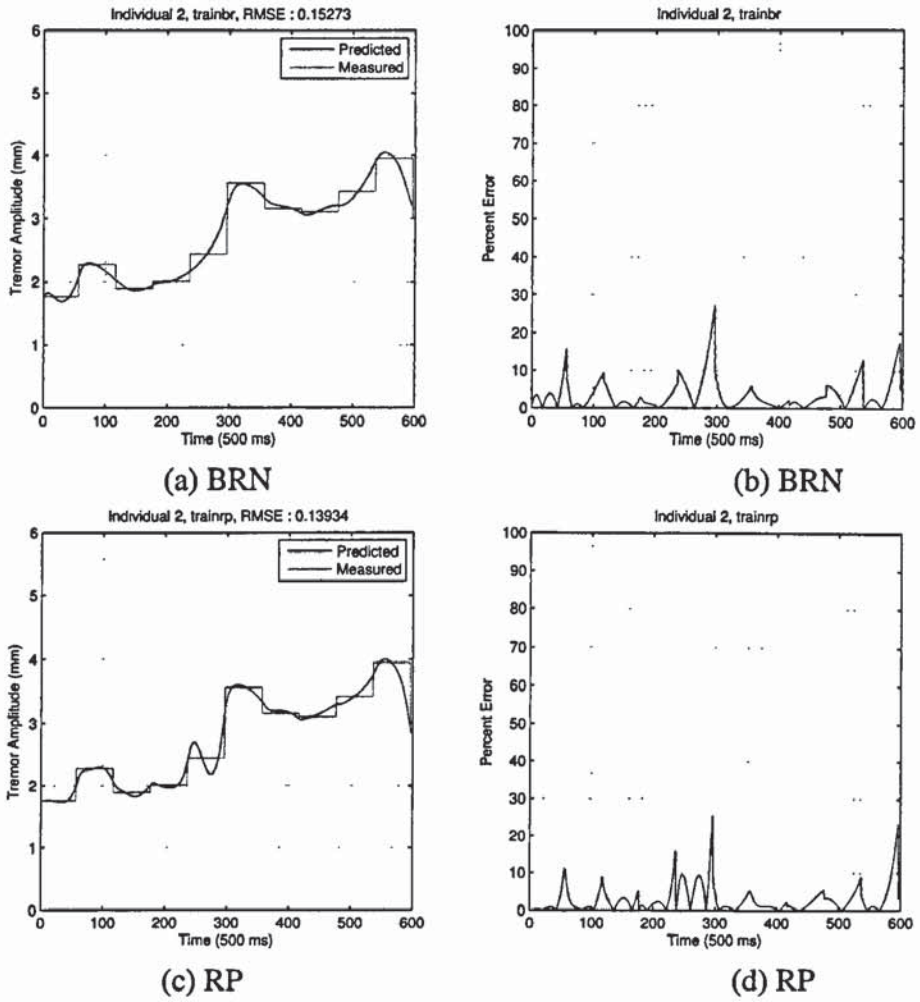

Figure 6.6: *Subject 2's, all-channel, tremor amplitude scenarios predictions. Tremor amplitude approximation for the different training scenarios using linear regression of the MF data as input and the (a) BRN & (c) RP training algorithms. Percent error between measured and predicted tremor amplitudes for the (b) BRN (d) RP training algorithms.*

It must also be clarified that although the MF and H data were used as input for training and testing, the amplitude data used in the two stages was different. Essentially, the actual amplitude data is only employed during the training procedure for defining the full range of the data (Figure 6.1a), whereas a predicted amplitude is used during the testing procedure (Figure 6.1b). Therefore, as the network has essentially been trained with different amplitude inputs, it is reasonable to use the original fatigue data for validation purposes.

Although both Entropy and MF trained neural networks appear to be very effective at predicting the tremor amplitudes, the HHT method offers marginally faster but less consistent training times than the H method. However, because the Entropy method is overall less computationally demanding, than the HHT method, it most certainly is the preferred choice for prediction of the real-time tremor amplitude.

6.5 Conclusion

It has been shown that it is possible for a NARX neural network to predict an individual's maximum tremor amplitude, based solely on their fatigue index. This determination could be particularly useful in surgical environments for determining when and if a surgeon has reached the limit of their ability.

Several training algorithms , and several network input configurations were assessed by their RMSE. These included entropy and mean frequency fatigue indices from 2 and 8 EMG channels, and using the BRN and RP training algorithms. It was found that although most of the network configurations provided reasonable accuracy, the BRN trained networks using the MF or Entropy data from all channels as input, provided the best accuracies (RMSE 0.011 mm). However, because the Entropy method is computationally less demanding, and provides more consistent training times, its data would be considered the preferred choice for input into the prediction system (RMSE = 0.013).

The results have also been limited by the amount of experimentally collected data. As mentioned previously, neural networks require large amounts of training data to represent a system appropriately. Therefore, improved accuracy could most certainly be achieved by providing more data for training and validation. However, that being said, the results from this Chapter have clearly shown that it is possible to predict an individual's tremor with reasonable accuracy.

7

Conclusion

7.1 Concluding Remarks

This thesis has demonstrated that it is possible to predict the level of a surgeon's muscular fatigue and hand tremor during lengthy surgical procedures. Tremor, which is typically in the range of 8-12 Hz, has been analyzed independently from the EMG signals, as the EMG equipment operates in the 20-500 Hz range. Consequently, novel methods for separately analyzing muscular fatigue from EMG and accelerometer signals have been developed and implemented to both non-surgical and surgical captured data. Ultimately, this led to the development of a maximum tremor amplitude prediction system which is based solely on captured EMG data, and which could be developed into a real time prediction surgical system.

Chapter 3 determined the independence of EMG captured signals by using ICA, the Turns randomness test, and its own distribution. It was noted that the EMG signals had a Super-Gaussian distribution, which indicated according to the limit value theorem, that the signals were not composed of signal mixtures and could be considered independent deterministic source signals. This was also confirmed with the results of the Turns test, which demonstrated that the number of turning points within a length of signal was less than the threshold value of $\frac{2}{3}(N-2)=132$, once again proving that the signal is deterministic and not random. Finally, after applying the FastICA

algorithm to the EMG signals, it was determined that the signal sources determined from the ICA algorithm were strongly correlated ($R > 0.94$) with the original signal mixture. Because ICA separates signal mixtures into their independent source components, and because the results demonstrated that the EMG signals entering and leaving the ICA algorithm were the same, we can state that the original signals are already independent of one another. In fact, by examining the EMG signals and performing a correlation analysis of the individual channels, it was found that their was little correlation between them ($R < 0.0044$). It can therefore be concluded that although there might exist coupling of the muscles between various muscular actions, there is no coupling between the EMG signals. In addition, this enforced the reasoning behind developing the univariate analysis method for determining fatigue of Chapter 4.

In Chapter 4, a novel single channel algorithm for determining muscular fatigue was developed, which suggested that the complexity within an EMG signal decreases as an individual fatigues. The complexity of signal was examined by dynamical embedding the signal, and defining its temporal Shannon entropy. The new fatigue index exhibited a decrease with an increase in fatigue, similar to the conventional MF method. This suggests that it could accurately monitor fatiguing trends. In addition, an extension of the HHT method was proposed for monitoring the EMG signal's frequency shifts. The difference between this method, and the conventional MF method, is that HHT method is ideally suited for analyzing stationary and non-stationary signals alike, whereas the MF method is typically published as being a stationary method suited for signal window sizes less than 1 s. Linear regressions were fitted to the data, and the robustness of all methods were compared by examining the coefficient of variation of their linear regression parameters over a variety of window sizes. It was found that the newly developed method provided marginally more consistent results over a variety of window sizes than the MF and HHT methods. This suggests that the choice in window size has little effect on the linear regression

estimation parameters, and that the complexity method offers slightly more reliable results over the other two methods. However, because the difference was only marginal (ANOVA, < 1 s: $Slope - p_{max}$: 0.9125, $Slope - p_{min}$: 0.0655, 1 s - 5 s : $Slope - p_{max}$: 0.7274, $Slope - p_{min}$: 0.1841), all three methods are acceptable choices for predicting fatigue. The results for the MF method also suggest it demonstrates good robustness for not only window sizes less than 1 s, but for window sizes up to 5 s, which is contrary to previously documented results.

A novel algorithm was developed in Chapter 5, and which could be used to determine maximum tremor amplitude during surgical procedures from acceleration signals. It comprised of using EMD to remove the drift from the signals, and through integration determine the position of the hand. The maximum amplitude was then determined from the position signal by applying PCA to ascertain the direction of maximum tremor. The algorithm was first calibrated on experimental data at a range of frequencies, and it was found that the errors within the postural tremor range (8-12 Hz) between the calculated and measured displacement, were less than 5%.

The HHT-MF and Entropy methods of fatigue analysis described in Chapter 4, were then applied to actual surgical EMG data collected the BR and MD muscles from 8 surgeons, while performing operations ranging from 90 mins to 10 hours in length. The results were compared with the fatigue trends of subjects performing regular desk work (the controls). It was found that all surgeons, irrespective of their experience levels, fatigued at a greater rate than the controls (controls-MF: 0.7%/hour (MD), 0.6%/per (BR); surgical-MF: 0.8%/hour (MD), 1.3 %/per (BR)). This is quite important, as it allows us to predict the surgeon's fatigue index based solely on their initial levels. Likewise, it was found that the BR muscle fatigued more than the MD muscle (1.57 times), which was suggestive that it is being used more during the

operations. This was confirmed through discussions with the surgeons, who suggested that their BR muscle was more fatigued after the operations.

The maximum tremor amplitude method was then applied to actual surgical acceleration data, which had been collected from surgeons before and after the operations. Similar to the fatigue analysis of the data, the amplitude results were also compared to those of subjects performing regular desk work. This increase in tremor was associated with an increase in the surgeon's muscular fatigue. The results concluded that neither the level of tremor or fatigue was improved with training or expertise, and that the increases were substantially larger with operating as opposed to performing desk work. In fact, from the results, it was possible to determine a surgeons tremor at any point during the operation from a baseline measurement, which was found to increase at a rate of 6.7%/hour. This is quite interesting from a surgeon's point of view, as the most challenging parts of the operations, such as the palate reconstructions, are typically performed at the end. Although this has been discussed with the surgeons who participated in the study, through ongoing discussions, other surgeons should be made aware of these increases as they can affect their performance.

In Chapter 6, a predictive tremor amplitude neural network was developed that uses only an EMG fatigue index as input. This could be advantageous for a couple of reason. Firstly, because tremor amplitude, rather than fatigue, is better understood as an index. Secondly, because it is far less invasive to attach EMG electrodes under the clothing than attaching accelerometer devices to the surgeon's hand. Several configurations of NARX Neural Networks were compared by analyzing their RMSE. This included a comparison between BRN and RP trained networks, 2-Channel and 8-Channel EMG, and HHT-MF and H input data configurations. The results demonstrated that although the BRN trained networks produced the lowest RMSE

(0.011 mm), they took upwards of 350 seconds in some cases to train. However, since training would be performed offline, the accuracy of the predictions would be a more important parameter to consider.

While the networks were trained in a series-parallel configuration, however, they were tested in a parallel configuration. The results suggested that it was possible to predict tremor amplitude using only the fatigue index from the BR and MD muscles as inputs (RMSE-BRN-MF:0.6572 mm, RMSE-BRN-H:0.6535 mm) , although better accuracy could be achieved using all eight muscular channels (RMSE-BRN-MF:0.0285 mm, RMSE-BRN-H:0.0377 mm). This shows that the BRN trained HHT-MF method marginally produces the best results, although it was not much different from the complexity method. Despite of the networks ability to predict an individual's tremor accurately, it would be necessary to train the network for each individual. While this could take some time, the developed network could be used as a valuable tool for real time prediction of a surgeon's hand steadiness, or when they have reached the limit of their ability.

7.2 Limitations

Because of sterilization and movement constraints imposed on surgeons during procedures, it is sometimes challenging to attach cabled EMG electrodes to their muscles. Although the electrodes are not felt during the procedures, the difficulties in attaching the cables to their body, and the cumbersome nature of having cables dragging throughout the operating room, makes them in the very least a challenge for the operating staff to deal with, and difficult to have them attached without becoming detached from the muscles during the operation. In fact, it would far more acceptable to have the information from the electrodes transferred wirelessly to the data caption

system. This would certainly resolve some of the cumbersome issues of the existing system.

Probably the most important limitation with the research is convincing surgeons that their tremor could truly affect the outcome of an operation. It is doubtful that any surgeon wants to be informed that they are going to be relieved because their tremor has increased to an unacceptable level. Therefore, convincing them could pose a serious challenge for the operating staff and hospitals. However, if explained correctly and emphasizing the crucial benefits of the system, this issue could be avoided.

7.3 Future Work

The prediction methods could be further developed by taking the existing work's current foundation and designing surgical integration procedures for the application. This would include designing initialization procedures for individual network training, as well as a real-time stand-alone system which would contain the trained prediction system for a multitude of users. Ultimately, the system could be developed to determine when or if a surgeon should be relieved from surgery, so that potential for patient or surgeon injury be reduced.

Future work could also investigate other factors which might improve an individual's operating tremor. These could include administering relaxants taken before and during an operation, imposing regulations that limit a surgeon's caffeine intake, or supporting arms or wrists during the more challenging parts of the operation. Once again, the main challenge for suggesting any of these procedures would be convincing surgeons of their importance.

Finally, future work could also include deriving information from the surgeon's tremor index and be used to develop a control algorithm that could reduce or eliminate undesired physiological tremor or tremor caused by fatigue. This could have significant advantages within the fields of microsurgery and telerobotic surgery by improving accuracy during the most critical surgical tasks.

Bibliography

1. Rothbaum, D., et al., *Robot-assisted stapedotomy: Micropick fenestration of the stapes footplate.* Otolaryngology—Head & Neck Surgery, 2002. **127**(5): p. 418-426.

2. Sherman, K.M., *An evaluation of fatigue and performance changes during intermittent overhead work*, in *Industrial and Systems Engineering*. 2003, Virginia Polytechnic Institute and State University: Blacksburg, Va. : University Libraries.

3. Smaga, S., *Problem-Oriented Diagnosis: Tremor.* American Family Physician, 2003. **68**(8): p. 1545–1552.

4. Oda, S. and N. Kida, *Neuromuscular fatigue during maximal concurrent hand grip and elbow flexion or extension.* J Electromyogr Kinesiol, 2001. **11**(4): p. 281-9.

5. Potvin, J.R. and L.R. Bent, *A Validation of Techniques Using Surface EMG Signals from Dynamic Contractions to Quantify Muscle Fatigue During Repetitive Tasks.* Journal of Electromyography and Kinesiology, 1997. **7**: p. 131-139.

6. Liu, J.Z., et al., *Nonlinear cortical modulation of muscle fatigue: a functional MRI study.* Brain Res, 2002. **957**(2): p. 320-9.

7. Garfield, R.E., et al., *Comparing uterine electromyography activity of antepartum patients versus term labor patients.* American Journal of Obstetrics and Gynecology, 2005. **193**(1): p. 23-29.

8. Gaudreault, N., et al., *Assessment of the paraspinal muscles of subjects presenting an idiopathic scoliosis: an EMG pilot study.* BMC Musculoskelet Disord, 2005. **6**: p. 14.

9. Lariviere, C., et al., *Biomechanical assessment of gloves. A study of the sensitivity and reliability of electromyographic parameters used to measure the activation and fatigue of different forearm muscles.* International Journal of Industrial Ergonomics, 2004. **34**(2): p. 101-116.

10. Berguer, R., *Surgical technology and the ergonomics of laparoscopic instruments.* Surgical Endoscopy, 1998. **12**(5): p. 458-462.

11. Boiley, B.J. and K.H. Calhoun, *Atlas of Head and Neck Surgery – Otolaryngology.* 2nd ed. 2001, Philadelphia: Lippincott Williams and Wilkins.

12. Snell, R.S., *Clinical Anatomy for Medical Students.* 5th ed. 1995, Boston: Little Brown and Company.

13. El ahrache, K., D. Imbeau, and B. Farbos, *Percentile values for determining maximum endurance times for static muscular work.* International Journal of Industrial Ergonomics, 2006. **36**(2): p. 99-108.

14. Enoka, R.M., *Mechanisms of Muscle Fatigue: Central Factors and Task Dependency.* Journal of Electromyography and Kinesiology, 1995. **5**(3): p. 141-149.

15. Rangayyan, R.M., *Biomedical Signal Analysis: A Case-Study Approach.* IEEE Press Series in Biomedical Engineering. 2001, New York: Wiley-IEEE Press. 556 pp.

16. Dimitrova, N.A. and G.V. Dimitrov, *Interpretation of EMG changes with fatigue: facts, pitfalls, and fallacies.* J Electromyogr Kinesiol, 2003. **13**(1): p. 13-36.

17. Chabran, E., B. Maton, and A. Fourment, *Effects of postural muscle fatigue on the relation between segmental posture and movement.* J Electromyogr Kinesiol, 2002. **12**(1): p. 67-79.

18. Roman-Liu, D., T. Tokarski, and K. Wojcik, *Quantitative assessment of upper limb muscle fatigue depending on the conditions of repetitive task load.* J Electromyogr Kinesiol, 2004. **14**(6): p. 671-82.

19. Farina, D., M. Gazzoni, and R. Merletti, *Assessment of low back muscle fatigue by surface EMG signal analysis: methodological aspects.* J Electromyogr Kinesiol, 2003. **13**(4): p. 319-32.

20. Ebaugh, D.D., P.W. McClure, and A.R. Karduna, *Effects of shoulder muscle fatigue caused by repetitive overhead activities on scapulothoracic and glenohumeral kinematics.* J Electromyogr Kinesiol, 2006. **16**(3): p. 224-35.

21. Sogaard, K., et al., *Evidence of long term muscle fatigue following prolonged intermittent contractions based on mechano- and electromyograms.* J Electromyogr Kinesiol, 2003. **13**(5): p. 441-50.

22. Lin, M.I., et al., *Electromyographical assessment on muscular fatigue--an elaboration upon repetitive typing activity.* J Electromyogr Kinesiol, 2004. **14**(6): p. 661-9.

23. Bacher, M., E. Scholz, and H.C. Diener, *24 hour continuous tremor quantification based on EMG recording.* Electroencephalogr Clin Neurophysiol, 1989. **72**(2): p. 176-83.

24. Boose, A., et al., *Wrist tremor: investigation of agonist-antagonist interaction by means of long-term EMG recording and cross-spectral analysis.* Electroencephalogr Clin Neurophysiol, 1996. **101**(4): p. 355-63.

25. Christensen, H., *Muscle activity and fatigue in the shoulder muscles during repetitive work.* European Journal of Applied Physiology, 1986. **V54**(6): p. 596-601.

26. Yang, H.-c., D.-m. Wang, and J. Wang. *Linear and Non-Linear Features of Surface EMG during Fatigue and Recovery Period.* in *Engineering in Medicine and Biology Society, 2005. IEEE-EMBS 2005. 27th Annual International Conference of the.* 2005.

27. Wei, Y., W. Jian, and L. Jiahai, *The sEMG Signal Complexity Changes during and following Local Muscle Fatigue Induced by Isometric Loading.* Sport Science, 2004. **24**(9): p. 19-23.

28. Sung, P.S., U. Zurcher, and M. Kaufman, *Nonlinear analysis of electromyography time series as a diagnostic tool for low back pain.* Med Sci Monit, 2005. **11**(1): p. CS1-5.

29. James, C.J. and D. Lowe, *Extracting multisource brain activity from a single electromagnetic channel.* Artificial Intelligence in Medicine, 2003. **28**(1): p. 89-104.

30. Takens, F., *Detecting strange actuators in turbulence.* In: Rand DA, Young LS, editors, Lecture notes in mathematics (Dynamical systems and turbulence, Warwick, 1980). 1981, Berlin: Springer. 898:366-81.

31. Kilner, J.M., S.N. Baker, and R.N. Lemon, *A novel algorithm to remove electrical cross-talk between surface EMG recordings and its application to the measurement of short-term synchronisation in humans.* J Physiol, 2002. **538**(Pt 3): p. 919-30.

32. Farina, D., R. Merletti, and R.M. Enoka, *The extraction of neural strategies from the surface EMG.* J Appl Physiol, 2004. **96**(4): p. 1486-95.

33. Liyu, C., W. Zhizhong, and Z. Haihong. *Classifying EMG signals using T-F representation and SVD [for artificial limb control].* in *[Engineering in Medicine and Biology, 1999. 21st Annual Conf. and the 1999 Annual Fall Meeting of the Biomedical Engineering Soc.] BMES/EMBS Conference, 1999. Proceedings of the First Joint.* 1999.

34. Khalil, M., et al. *Detection and classification in uterine electromyography by multiscale representation.* in *Engineering in Medicine and Biology society, 1997. Proceedings of the 19th Annual International Conference of the IEEE.* 1997.

35. Khalil, M. and J. Duchene, *Uterine EMG analysis: a dynamic approach for change detection and classification.* Biomedical Engineering, IEEE Transactions on, 2000. **47**(6): p. 748-756.

36. Kwon, O.-W. and T.W.T.-W. Lee, *Phoneme recognition using ICA-based feature extraction and transformation.* Signal Processing, 2004. **84**(6): p. 1005-1019.

37. Calhoun, V.D., et al. *ICA of Functional MRI Data: an Overview.* in *Proceedings, ICA2003, Fourth International Symposium on Independent Component Analysis and Blind Source Separation.* 2003. Nara , Japan.

38. Ristaniemi, T. and J. Joutsensalo. *Independent component analysis with code information utilization in.* in *Global Telecommunications Conference, 1999. GLOBECOM '99.* 1999.

39. Fung, Y. and X. Lei. *An application of independent component analysis in the arbitrage pricing theory.* in *Neural Networks, 2000. IJCNN 2000, Proceedings of the IEEE-INNS-ENNS International Joint Conference on.* 2000.

40. Calhoun, V.D., et al., *Spatial and temporal independent component analysis of functional MRI data containing a pair of task-related waveforms.* Human Brain Mapping, 2001. **13**(1): p. 43-53.

41. Srivastava, G., et al., *ICA-based procedures for removing ballistocardiogram artifacts from EEG data acquired in the MRI scanner.* NeuroImage, 2005. **24**(1): p. 50-60.

42. Makeig S, et al. *Moving-Window ICA Decomposition of EEG data reveals event-related changes in oscillatory brain activity.* in *Proceedings, ICA2000, the 2nd Int'l Workshop on Indeppendent Component Analysis and Signal Separation.* 2000. Helsinki, Finland.

43. Manduchi, R. and J. Portilla. *Independent component analysis of textures.* in *Computer Vision, 1999. The Proceedings of the Seventh IEEE International Conference on.* 1999.

44. Bartlett, M.S., J.R. Movellan, and T.J. Sejnowski, *Face recognition by independent component analysis.* Neural Networks, IEEE Transactions on, 2002. **13**(6): p. 1450-1464.

45. Elble, R.J., *Characteristics of physiologic tremor in young and elderly adults.* Clin Neurophysiol, 2003. **114**(4): p. 624-35.

46. Kalisch, T., et al., *Age-related attenuation of dominant hand superiority.* PLoS ONE, 2006. **1**: p. e90.

47. Raethjen, J., et al., *Amitriptyline enhances the central component of physiological tremor.* J Neurol Neurosurg Psychiatry, 2001. **70**(1): p. 78-82.

48. Abila, B., et al., *Exercise-induced hand tremor: a possible test for beta 2-adrenoceptor selectivity in man?* Br J Clin Pharmacol, 1986. **22**(1): p. 104-7.

49. Wharrad, H.J., et al., *The influence of fasting and of caffeine intake on finger tremor.* Eur J Clin Pharmacol, 1985. **29**(1): p. 37-43.

50. Humayun, M.U., et al., *Quantitative measurement of the effects of caffeine and propranolol on surgeon hand tremor.* Arch Ophthalmol, 1997. **115**(3): p. 371-4.

51. Viitasalo, J.T., J. Gajewski, and A. Wit, *Forearm tremor during three different isometric loadings.* Electromyogr Clin Neurophysiol, 1994. **34**(3): p. 131-6.

52. Morrison, S. and J. Keogh, *Changes in the dynamics of tremor during goal-directed pointing.* Hum Mov Sci, 2001. **20**(4-5): p. 675-93.

53. Uhrich, M.L., et al., *Assessment of fatigue, monitor placement, and surgical experience during simulated laparoscopic surgery.* Surg Endosc, 2002. **16**(4): p. 635-9.

54. Quick, N.E., et al., *The effect of using laparoscopic instruments on muscle activation patterns during minimally invasive surgical training procedures.* Surg Endosc, 2003. **17**(3): p. 462-5.

55. Wade, P., M.A. Gresty, and L.J. Findley, *A normative study of postural tremor of the hand.* Arch Neurol, 1982. **39**(6): p. 358-62.

56. Murbe, D., et al., *Tremor in otosurgery: influence of physical strain on hand steadiness.* Otol Neurotol, 2001. **22**(5): p. 672-7.

57. Patkin, M., *Ergonomics applied to the practice of microsurgery.* Aust N Z J Surg, 1977. **47**(3): p. 320-9.

58. Brommeland, T. and R. Hennig, *Mechanical accuracy of a new stereotactic guide.* Acta Neurochir (Wien), 2000. **142**(4): p. 449-54.

59. Hsu, P.A. and B.C. Cooley, *Effect of exercise on microsurgical hand tremor.* Microsurgery, 2003. **23**(4): p. 323-7.

60. Hughes, G.B., *The learning curve in stapes surgery.* Laryngoscope, 1991. **101**(12 Pt 1): p. 1280-4.

61. Braido, P. and X. Zhang, *Quantitative analysis of finger motion coordination in hand manipulative and gestic acts.* Hum Mov Sci, 2004. **22**(6): p. 661-78.

62. Cowie, B.M., et al., *Fibre Bragg grating sensors for distributive tactile sensing.* Measurement Science and Technology, 2007. **18**(1): p. 138-146.

63. Danisman, K., I. Dalkiran, and F.V. Celebi, *Design of a high precision temperature measurement system based on artificial neural network for different thermocouple types.* Measurement, 2006. **39**(8): p. 695-700.

64. Moshou, D., et al., *Dynamic muscle fatigue detection using self-organizing maps.* Applied Soft Computing, 2005. **5**(4): p. 391-398.

65. Azzerboni, B., et al. *Time-frequency characterization of multi-channel dynamic sEMG recordings by neural networks.* in *Proceedings of the International Joint Conference on Neural Networks.* 2003.

66. Matsumura, Y., et al., *Recognition of EMG Signal Patterns by Neural Networks*, in *Knowledge-Based Intelligent Information and Engineering Systems.* 2003. p. 623-630.

67. Matsumura, Y., et al. *Recognition of EMG signal patterns by neural networks.* in *ICONIP '02. Proceedings of the 9th International Conference on Neural Information Processing.* 2002.

68. Hope, W.P. and H. Rassoulian. *Modular neural networks applied to surface EMG signals for limb function identification.* 1999.

69. Matheson Rittenhouse, D., et al., *A neural network model for reconstructing EMG signals from eight shoulder muscles: consequences for rehabilitation robotics and biofeedback.* J Biomech, 2006. **39**(10): p. 1924-32.

70. Greco, A., et al. *A Morlet wavelet classification technique for ICA filtered sEMG experimental data.* 2003.

71. Au, S.K., P. Bonato, and H. Herr. *An EMG-position controlled system for an active ankle-foot prosthesis: an initial experimental study.* 2005.

72. Karlsson, J.S., et al., *An estimation of the influence of force decrease on the mean power spectral frequency shift of the EMG during repetitive maximum dynamic knee extensions.* Journal of Electromyography and Kinesiology, 2003. **13**(5): p. 461-468.

73. Jakubowski, J., et al., *Higher order statistics and neural network for tremor recognition.* Biomedical Engineering, IEEE Transactions on, 2002. **49**(2): p. 152-159.

74. Engin, M., et al., *The classification of human tremor signals using artificial neural network.* Expert Systems with Applications, 2007. **33**(3): p. 754-761.

75. Riviere, C.N. and P.K. Khosla. *Augmenting the human-machine interface: improving manual accuracy.* 1997.

76. Stone, J.V., *Independent Component Analysis: A Tutorial Introduction*, ed. B. Books. 2004: MIT Press.

77. Sanmiguel, C.P., M.P. Mintchev, and K.L. Bowes, *Dynamics of Level of Randomness of Electrogastrograms Can Be Indicative of Gastric Electrical Uncoupling in Dogs.* Digestive Diseases and Sciences, 1999. **44**(3): p. 523-528.

78. Challis, R. and R. Kitney, *Biomedical signal processing (in four parts).* Medical and Biological Engineering and Computing, 1990. **28**(6): p. 509-524.

79. Giannakopoulos, X., J. Karhunen, and E. Oja. *Experimental comparison of neural ICA algorithms.* in *In Proc. Int. Conf. on Artificial Neural Networks, (ICANN'98).* 1998. Skovde, Sweden.

80. Mantini, D., et al., *Performance comparison of independent component analysis algorithms for fetal cardiac signal reconstruction: a study on synthetic fMCG data.* Physics in Medicine and Biology, 2006. **51**(4): p. 1033-1046.

81. Hyvarinen, A., J. Karhunen, and E. Oja, *Independent Component Analysis.* Wiley, ed. S. Haykin. Vol. Adoptive and Learning Systems for Signal Processing, Communication, and Control. 2001: John Wiley & Sons, Inc.

82. Potter, M., N. Gadhok, and W. Kinsner. *Separation performance of ICA on simulated EEG and ECG signals contaminated by noise.* in *Electrical and Computer Engineering, 2002. IEEE CCECE 2002. Canadian Conference on.* 2002.

83. Stone, J.V., *Independent component analysis: an introduction.* Trends in Cognitive Sciences, 2002. **6**(2): p. 59-64.

84. Xie, H. and Z. Wang, *Mean frequency derived via Hilbert-Huang transform with application to fatigue EMG signal analysis.* Comput Methods Programs Biomed, 2006. **82**(2): p. 114-20.

85. Caviness, J.N., et al., *Electrophysiological observations in hereditary parkinsonism-dementia with Lewy body pathology.* Mov Disord, 2000. **15**(1): p. 140-5.

86. Knaflitz, M. and P. Bonato, *Time-frequency methods applied to muscle fatigue assessment during dynamic contractions.* J Electromyogr Kinesiol, 1999. **9**(5): p. 337-50.

87. Huang, N.E. and S.S.P. Shen, *Hilbert-Huang transform and its applications.* Interdisciplinary mathematical sciences Vol. 5. 2005 Singapore: World Scientific.

88. Sinclair, S. and G.G.S. Pegram, *Empirical Mode Decomposition in 2-D space and time: a tool for space-time rainfall analysis and nowcasting.* Hydrol. Earth Syst. Sci., 2005. **9**(3): p. 127-137.

89. Solé, J., A. Turiel, and J.E. Llebot, *Using empirical mode decomposition to correlate paleoclimatic time-series.* Nat. Hazards Earth Syst. Sci., 2007. **7**(2): p. 299-307.

90. Rilling, G., P. Flandrin, and P. Gonçalves. *On Empirical Mode Decomposition and its algorithms.* in *IEEE-EURASIP Workshop on Nonlinear Signal and Image Processing NSIP-03.* 2003. Grado (I).

91. Pincus, S.M., *Approximate entropy as a measure of system complexity.* Proc Natl Acad Sci U S A, 1991. **88**(6): p. 2297-301.

92. Kreyszig, E., *Advanced Engineering Mathematics.* 8th Edition ed. 1999, New York: John Wiley and Sons, Inc.

93. Pinzon, J.E., M.E. Brown, and C.J. Tucker, *EMD correction of orbital drift artifacts in satellite data stream,* in *Hilbert-Huang transform and its applications,* N.E. Huang and S.S.P. Shen, Editors. 2005, World Scientific: Singapore. p. 167-186.

94. Wei Tech, A. and C.N. Riviere. *Neural network methods for error canceling in human-machine manipulation.* in *Engineering in Medicine and Biology Society, 2001. Proceedings of the 23rd Annual International Conference of the IEEE.* 2001.

95. Siegelmann, H.T., B.G. Horne, and C.L. Giles, *Computational capabilities of recurrent NARX neural networks.* Systems, Man and Cybernetics, Part B, IEEE Transactions on, 1997. **27**(2): p. 208-215.

96. Tsung-Nan, L., et al., *A delay damage model selection algorithm for NARX neural networks.* Signal Processing, IEEE Transactions on [see also Acoustics, Speech, and Signal Processing, IEEE Transactions on], 1997. **45**(11): p. 2719-2730.

97. Parlos, A.G., O.T. Rais, and A.F. Atiya, *Multi-step-ahead prediction using dynamic recurrent neural networks.* Neural Networks, 2000. **13**(7): p. 765-786.

98. Gao, Y. and M.J. Er, *NARMAX time series model prediction: feedforward and recurrent fuzzy neural network approaches.* Fuzzy Sets and Systems, 2005. **150**(2): p. 331-350.

99. Plett, G.L., *Adaptive inverse control of linear and nonlinear systems using dynamic neural networks.* Neural Networks, IEEE Transactions on, 2003. **14**(2): p. 360-376.

100. Patel, A. and J.F. Dunne, *NARX Neural Network Modelling of Hydraulic Suspension Dampers for Steady-state and Variable Temperature Operation.* Vehicle System Dynamics, 2003. **40**(5): p. 285 - 328.

101. Kim, T. and T. Adali. *Complex backpropagation neural network using elementary transcendental activation functions*. 2001.

102. Sarle, W.S. *Neural Network FAQ, part 1 of 7: Introduction*. periodic posting to the Usenet newsgroup comp.ai.neural-nets 2002 [cited; Available from: ftp://ftp.sas.com/pub/neural/FAQ.html.

103. Baykal, N. and A.M. Erkmen. *Resilient backpropagation for RBF networks*. in *Fourth International Conference on Knowledge-Based Intelligent Engineering Systems and Allied Technologies*. 2000. Brighton, UK.

104. More, J.J., *The Levenberg-Marquardt Algorithm: Implementation and Theory. Numerical Analysis*, in *Lecture Notes in Mathematics 630*, G.A. Watson, Editor. 1977. p. 105-116.

105. Dan Foresee, F. and M.T. Hagan. *Gauss-Newton approximation to Bayesian learning*. in *International Conference on Neural Networks*. 1997. Houston, TX, USA.

106. MacKay, D.J.C., *A practical Bayesian framework for backpropagation networks* Neural Comput., 1992. **4**(3): p. 448-472

Appendix A

A.1 DVD Request

Appendix A is available on DVD/CD format only. Copies of the disc are available through Dr. Xianghong Ma at Aston University. Please send requests to:

Dr. Xianghong Ma
Bio-Medical Engineering Research Group
School of Engineering and Applied Science
Aston University, Aston Street
Birmingham, UK
B4 7ET
Or email: x.ma@aston.ac.uk

A.2 DVD/CD Contents

The DVD/CD contains the following files:

Table A.1, *List of files used to perform the analysis in the thesis*

EMBDH.m	Function that determines the entropy fatigue index from a set of data.
EMG_FISHENTR.m	Determines the COV parameters for the H,MF, and HHT-MF methods.
FastICA_2.5.zip	All files relating to the FastICA algorithm. Version 2.5, October 19 2005. Copyright (c) Hugo Gävert, Jarmo Hurri, Jaakko Särelä, and Aapo Hyvärinen.
HHTMF.m	Function that determines the HHT-MF fatigue index from a set of data.
NN_initialization2.m	NN network training and validation file.
SetAnalysis	GUI that determines the HHT-MF, MF, and H from a set of data.
turnstest.m	Determines the number of turning points, compares it with the threshold, and plots the results.
AmplitudeFinder.m	Determines the Maximum tremor amplitude based on the position data.
Acceleration_to_Position	Removes the drift from the signal using Empirical Mode Decomposition, and generates the position data by integrating the acceleration signal.